SEQUENCE BASED RECEIVERS

FOR

BANDLIMITED NONLINEAR CHANNELS

by

VIMAL KISHORE DUBEY, B.Sc. (Hons.), B.E., M.E.

A Thesis

Submitted to the School of Graduate Studies

in Partial Fulfilment of the Requirements

for the Degree

Doctor of Philosophy

McMaster University

 June, 1986

SEQUENCE BASED RECEIVERS

DOCTOR OF PHILOSOPHY (1986) McMASTER UNIVERSITY
(Electrical Engineering) Hamilton, Ontario, Canada

TITLE: Sequence Based Receivers for Bandlimited Nonlinear Channels

AUTHOR: VIMAL KISHORE DUBEY
B.Sc. (Hons.) (University of Rajasthan, India)
B.E. (Indian Institute of Science, Bangalore)
M.E. (Indian Institute of Science, Bangalore)

SUPERVISOR: Professor D.P. Taylor

NUMBER OF PAGES: xv, 145

ABSTRACT

This thesis examines receiver structures based on maximum likelihood sequence estimation (MLSE) for receiving quaternary phase-shift-keyed (QPSK) signals over bandlimited, non-linear satellite channels, in the presence of additive down link gaussian noise. Two satellite channel models are considered. In the first channel model, the effects of intersymbol interference caused by filtering followed by AM/AM and AM/PM conversions are taken into account while the second channel model includes a post-nonlinearity filter.

An explicit expression for the output of the bandpass nonlinearity (BPNL) for a QPSK signal is obtained in terms of an inphase (I)-quadrature (Q) path memory parameter p_k. The computation of the output of the BPNL requires a knowledge of its transfer characteristic. The transfer characteristics may be specified either analytically or through experimental measurements.

An optimum MLSE receiver structure for bandlimited, non-linear satellite channel is derived and its performance evaluated using computer simulation. Simulating the MLSE receiver in optimum form is too time consuming, so we estimated the I-Q path history parameter p_k's by using a simple procedure analogous to decision feedback processing. Although this method is not theoretically equivalent to an optimum computation, our results show that it performs essentially as well as an optimum computation. For moderate to high SNR, an upperbound on the probability of symbol error is obtained, using the concept of error events. A simplified expression for an upperbound on probability of symbol error, for the case when single-error error events are dominant, is also obtained. A sub-optimum receiver structure is then derived using average matched filter responses. The sub-optimum receiver which turns out to be a complex filter followed by a decision device, is a relatively simple

structure. The performance of the sub-optimum receiver was estimated for two different uplink filters. The effect of varying the BPNL input drive level was also studied. Our simulation results indicate that the performance of both the MLSE and the sub-optimum receivers approach asymptotically the same optimum performance band.

Finally, we extend our results on an optimum receiver structure for receiving QPSK signals over a digital satellite communications channel, to include the effects of filtering following the non-linear satellite transponder. It is shown that the complexity of the MLSE receiver is primarily determined by the uplink channel memory. The error performance of the receiver at low signal-to-noise ratios is evaluated by computer simulation. An upperbound on the probability of symbol error at moderate to high SNR is also obtained. A sub-optimum receiver similar to the uplink channel filtering case is developed and its performance evaluated using computer simulation. The degradation in performance of the sub-optimum receiver compared to the optimum receiver is found to be small.

ACKNOWLEDGEMENTS

I would like to express my sincere gratitude to my supervisor, Professor D.P. Taylor for his assistance and guidance during the course of my studies and preparation of this thesis.

I would also like to thank Professors C.R. Carter and W.F.S. Poehlman for serving on the Supervisory Committee. Thanks are also due to the Engineering Word Processing Centre for their excellent work in typing this thesis.

I am also grateful to the Canadian Commonwealth Scholarship and Fellowship Administration for the support provided during the course of this research.

Last but not least, I would like to express my deepest thanks and appreciation to my wife Archana, for the innumerable sacrifices she made during the course of this investigation, and to my son, Abhinav and my daughter, Richa, for the sacrifices they made unknowingly.

DEDICATED

TO

MY PARENTS

TABLE OF CONTENTS

TABLE OF CONTENTS

TABLE OF CONTENTS

LIST OF ILLUSTRATIONS

LIST OF ILLUSTRATIONS (continued)

LIST OF ILLUSTRATIONS (continued)

LIST OF ILLUSTRATIONS (continued)

LIST OF PRINCIPAL SYMBOLS

Symbol	Representation
AM-AM	Amplitude modulation to amplitude modulation
AM-PM	Amplitude modulation to phase modulation
BW	Bandwidth
BPNL	Bandpass nonlinearity
BPSK	Binary phase shift keying
CDMA	Code-division multiple acess
DSI	Digital speech interpolation
$E(\cdot)$	Error function
E_b/N_o	Bit energy to noise density ratio
EIRP	Effective isotropic radiated power
FM	Frequency Modulation
FDM	Frequency division multiplex
FDMA	Frequency division multiple access
F(Z)	defined on page 21
$f_n(t)$	interpulse product defined on page 24
$f_q^{(1)}\{(t-kT), p_k\}$	defined on page 25
$f_{q,r,s,}^{(3)}\{(t-kT), p_k\}$	defined on page 26
$f^{(1)}$, $f^{(31)}$, $f^{(32)}$, $f^{(33)}$	defined on page 28
FSM	Finite state machine
G(v)	AM/AM characteristic of BPNL
$\alpha(v)$	AM/PM characteristic of BPNL

LIST OF PRINCIPAL SYMBOLS (continued)

Symbol	Representation
$H_1[\cdot]$	Hankel transform of order 1
ISI	Intersymbol Interference
IF	Intermediate frequency
$J_1(\cdot)$	Bessel function of order one
J_I	Metric in MLSE
MLSE	Maximum likelihood sequence estimation
MSK	Minimum shift keying
MLSR	Maximum likelihood sequence receiver
N_s	Number of possible states of FSM
n(t)	Noise
p_k	I-Q phase history
I	Inphase component
Q	Quadrature Component
QPSK	Quarternary phase-shift-keyed signals
RF	Radio frequency
OQPSK	Offset QPSK
SPADE	Single channel per carrier, pulse code modulation, multiple access, demand assignment equipment
SNR	Signal-to-noise ratio
TDMA	Time division multiple access
TWTA	Travelling wave tube amplifier
U/C	Up-converter
VA	Viterbi Algorithm

LIST OF PRINCIPAL SYMBOLS (continued)

Symbol	Representation
ν	Channel memory
HPA	High power amplifier
FFSK	Fast frequency shift keying
h(t)	Unit pulse response of the bandlimiting filter
S_k	State of the channel at t = KT
$S_{i-j}^{k,\ell}$	Defined on page 36
T	Data pulse duration
$Y_i^1, Y_i^2, Y_i^3, Y_i^4,$	defined on page 136
ε	Error event
n_ε	Length of error event
S_ε	Set of allowable state sequence segments
ξ_k	State transition
Λ	Likelihood ratio
$\in$	Element of
$\supset$	Super set of
$\subset$	Subset of
$\|\|$	Norm
Re [ ]	Real part of
$\|\ \|$	Magnitude
ϕ_i	Phase of the ith transmitted pulse
N_o	One-sided white spectral density
B_i	Input back-off of TWTA
ν^1	Down-link channel memory

CHAPTER 1

INTRODUCTION

Modern satellite communications systems suffer from both power and bandwidth limitations. Because of the power limitation, digital satellite communication systems are normally operated with a non-linear amplifier, usually a travelling wave tube amplifier (TWTA), in the satellite transponder. In the non-linear region of operation, a TWTA exhibits both a non-linear input amplitude to output amplitude (AM-AM conversion) characteristic and a non-linear input amplitude to output phase (AM-PM conversion) characteristic. In addition, because of the limited availability of satellite bandwidth, the transmitted signals must be tightly band-limited, and this introduces intersymbol interference (ISI). The ISI combined with non-linear amplification causes significant degradation of system performance.

In this thesis we are concerned with the problem of developing an optimum receiver structure and estimating its performance for quarternary phase-shift keyed (QPSK) signalling over bandlimited, nonlinear satellite channels. In deriving the receiver, the maximum likelihood sequence estimation (MLSE) approach will be used, so that the receiver is optimum in the sense of minimizing sequence error probability on the bandlimited non-linear channel.

A satellite must share its capacity among a large number of earth terminals. This sharing is achieved by some form of multiple-access technique. The multiple-access problem is fundamental to satellite communications, because it is by this means that the wide, geographic coverage capability of the satellite channel is exploited. The satellite channel model in this thesis assumes in particular Time Division Multiple Accessing (TDMA). In

order for us to bring out the point that current trends are toward using TDMA, we briefly describe several basic multiple access techniques.

1.1 A Brief Review of Multiple Access Techniques for Satellite Communication Systems

Commercial Communications by satellite began officially in April 1965, when the world's first Communication Satellite INTELSAT I (known as "Early Bird"), was launched. The fully mature phase of satellite communications probably began with the installation of the INTELSAT IV into the global system starting in 1971. The INTELSAT system serves most of the countries of the world and has satellites over the Atlantic, Pacific and Indian Oceans.

Frequency-Division Multiple Access (FDMA), is one widely used multiple access technique. In FDMA, different carrier frequencies are used for each transmitting station. This allows use of the same transponder amplifier until finally the overall noise level limits the capacity of the amplifier. The presence of multiple carriers in any non-linear amplifier produce intermodulation products which raise the apparent noise level. To reduce intermodulation noise, the TWT drive level should be "backed-off" to avoid non-linear operation. The carrier received power level now is less and thus the effect of thermal noise generated in the earth station receiver is increased. This reduction in input drive level must thus be optimized. Even after optimization, the effect is not trivial and the reduction in capability of a transponder over what it would have if all the available information was multiplexed on a single carrier frequency can be as much as 6 dB. Nevertheless, FDMA remains a very popular technique for high capacity transmission commercial communication satellites. It is efficient if one is not power limited, and it is the natural expansion of terrestrial communications methods.

FDMA can be implemented in two ways. One is to multiplex, in the conventional terrestrial manner, many channels on each carrier that is transmitted through the satellite. Another is to use a separate carrier frequency for each telephone or baseband channel within the satellite. If many carriers are used, the intermodulation problem is still more serious. On the other hand, it does approach, asymptotically a limiting level that is usually acceptable. This single-channel per-carrier approach has particular advantages in systems where there are many links to be made, each one having only a few circuits to be handled at any one time. Normal multiplexing is very convenient terrestrially but may be economical only if each carrier has traffic, for example, in a group of 12 channels or more.

Both systems are in extensive use today. INTELSAT uses both systems, the SPADE (Single Channel per Carrier, Pulse Code modulation, multiple Access, Demand assignment Equipment) being a single channel per carrier modulation-access system. Canada, Indonesia and Algeria, to mention a few, countries who use single-channel-per-carrier systems.

Time-Division Multiple Access (TDMA) is the next basic technique of multiple access. Here each earth station is assigned a periodic time slot for its transmission, and all the earth stations use the same carrier frequency within a periodic particular transponder. In terms of the total satellite performance, this is the superior method because the intermodulation noise is eliminated and there is an increase in capacity. The required transponder back-off is much less, just that required to achieve acceptable spectrum spreading. The price paid is an increase in complexity of the ground equipment. It does seem as if the long term trend will be toward more and more TDMA since it fits naturally with the digital communications systems that are rapidly proliferating terrestrially, not only for data transmision but more and more for digitized voice.

Various experimental TDMA systems have been built and tested by INTELSAT and others. Their efficiency advantage over FDMA can be illustrated by comparing the approximate channel capacities of an INTELSAT IV global beam transponder operating with standard INTELSAT 30 metre earth stations, using TDMA and FDMA. Assuming 10 accesses, the typical capacity using FM/FMDA is about 450 one-way voice channels [1]. With TDMA, using standard 64 kb/s voice frequency PCM encoding, the capacity of the same transponder is approximately 900 channels. If Digital Speech Interpolation (DSI) is used to process the PCM bit streams, the capacity is further increased to about 1800 channels.

A TDMA system went into commercial operation on Telesat, Canada's system, starting in May 1976. INTELSAT is going to use the TDMA digital communication method for most of its voice circuits. Similar trends are present in North America, Europe, and Japan for domestic satellite systems requirements.

This trend to digital systems both terrestrially and via satellite is reinforced by the ease with which the TDMA methods can be combined with SDMA (Space Division Multiple Access) by switching transmission bursts from one antenna beam to another depending on their ultimate destination. The concept of time-division switching, seems very promising, as it is efficient in its exploitation of both the satellite power and the frequency spectrum. The price paid is increasing complexity. Time-division switching will be a major factor in communication satellite technology. A satellite-switch TDMA system (SS-TDMA) using a microwave switch matrix shows an increase of over 30 percent in available capacity over FDMA/TDMA [2] (separate frequency bands, each carrying TDMA).

The final basic method of multiple access is Code-Division Multiple Access (CDMA), called occasionally "spread-spectrum multiple access". The transmission from each earth station is combined with a pseudo-random code so as to cause the transmission to occupy the entire bandwidth of the transponder. The station for whom the transmission is intended

has a duplicate of this pseudo-random code and by cross-correlation techniques can extract it from the "noise level" created by the simultaneous signals of many other stations. It has considerable advantages in military systems because the spread-spectrum technique must be used anyway to protect satellite receivers against possible jamming and the pseudo-random sequences are necessary to provide cryptographic security.

The use of such crypto and antijam systems provides automatic multiple access. In a sense, it is free. However, the difficulty is that it is not nearly so efficient an exploitation of the resources of power and frequency spectrum as is even the FDMA system, not to mention TDMA. Nevertheless, it is used and will continue to be used for military systems. The possibility of its limited use in commercial systems may appear as satellite users become increasingly concerned with the possibilities of both malicious interference and unauthorized listening.

1.2 Digital Modulation Techniques

Digital Modulation Techniques have received considerable attention for use in satellite communications systems, in the last decade, because of increased demand for data communications. In addition, digital transmission offers options and flexibility not available with analog modulation. Most current satellite systems are bandwidth-limited, unlike early satellite communication systems which were power limited. A capacity comparison for FM/FDMA and PCM/PSK/TDMA [5], shows that PCM/PSK/TDMA is preferable to FM/FDMA for the bandwidth-limited satellite systems.

A comparison of digital modulation techniques based on average power is shown in Fig. 1.1 (reproduced from [4]). It is seen that, for a given information rate, PSK has a better performance compared to other modulation techniques except for combined amplitude and phase keying (APK). However, APK cannot be used over satellite channel, because of the

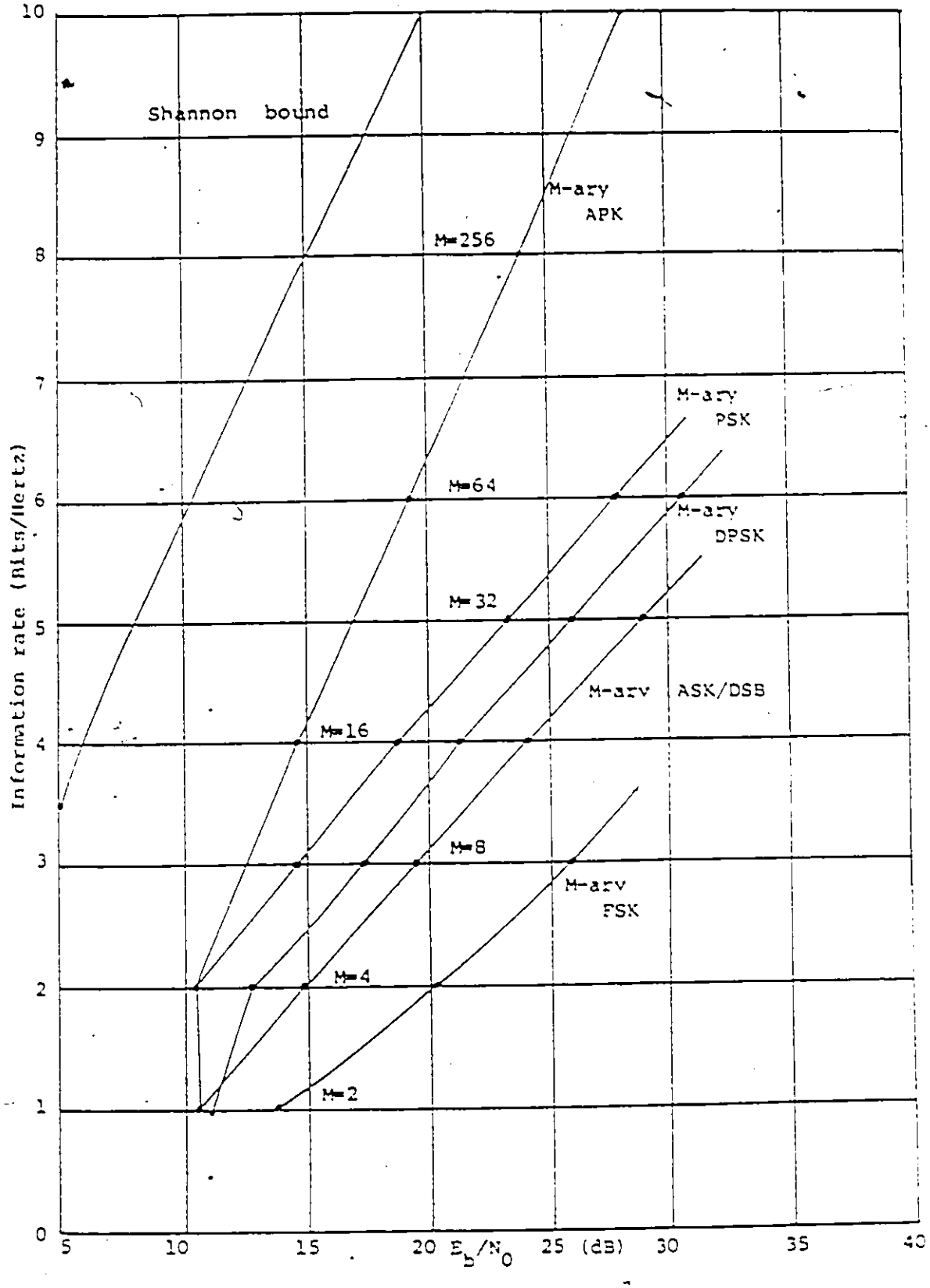

Fig. 1.1 Comparison of digital modulation systems based on average power [4].

nonlinear characteristic of the satellite transponder. Another advantage of PSK signalling is that by increasing the number of levels from two to four, the channel capacity can be approximately doubled without any expense of bandwidth.

The three digital modulation techniques QPSK, OQPSK (offset QPSK) and MSK (minimum shift keying) have received significant attention because of their properties, which are well suited to satellite communications systems. These characteristics include power and bandwidth efficiency as well as constant envelope. The performance of QPSK, OQPSK and MSK, over bandlimited, non-linear satellite channel has been investigated in [6,7]. The results of these simulations show that for a tightly band-limited channel, QPSK has better performance than the both MSK and OQPSK modulation. The poor performance of MSK and OQPSK on tightly bandwidth-limited channels is explained as follows. Although the overall envelope fluctuations are reduced for these two techniques, the enlarged scattering at the critical sampling point degrades the MSK and OQPSK channel performance in comparison to that of the QPSK channel. In wide-band satellite channels, where adjacent channel interference can be a limiting factor, the reduced spectrum spreading characteristic of OQPSK and MSK makes these formats more attractive.

Since most of the operational and planned digital satellite communication systems use QPSK modulation techniques, we will assume QPSK signalling throughout this thesis.

1.3 Sources of Impairments in Digital Satellite Systems

1.3.1 The Satellite Channel

A satellite communications system can take on several different forms. Typically it consists of two earth stations separated by a space segment (a satellite repeater) as shown in Fig. 1.2. The signals are transmitted from station A to B via the satellite repeater. The communication link from repeater to earth station is called the downlink path. The RF

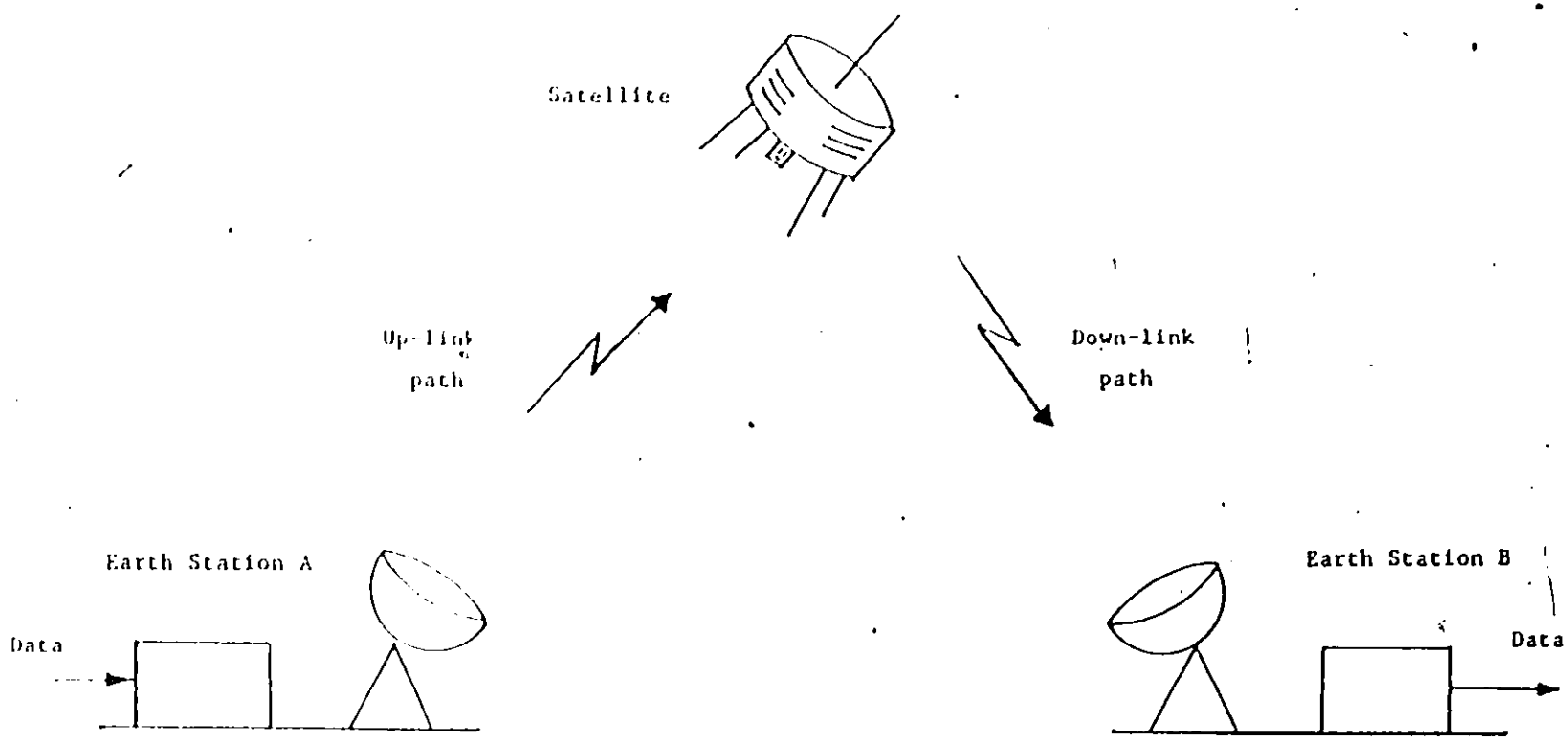

Fig. 1.2 Typical satellite communications system.

carrier frequencies for commercial communications satellites, for uplink and downlink channels are 6 and 4 GHz respectively. The bandwidth is limited to 500 MHz for 4/6 GHz band. These frequency bands are shared with many congested analog and digital line-of-sight microwave systems, and therefore siting an earth station can pose a major problem. In the time-frame 1980-2000, increasing demand for international and domestic satellite circuits will outstrip the capacity of the geostationary orbit for 4/6 GHz systems, even with the application of frequency reuse, TDMA, DSI, and more efficient modulation techniques. For these reasons the satellite systems of the 1980's and 1990's will have to employ higher radio frequencies. Satellite systems are already operational in the 12/14 GHz band. This band is reserved for satellite communications, so there is no interference with terrestrial line-of-sight microwave systems.

The satellite repeater basically consists of a low-noise receiver-converter and TWT high power amplifier (HPA). We now examine the sources of noise and interference in each of the sub-systems.

1.3.2 Transmitting Earth Station

Figure 1.3 shows the basic stages of a transmitting earthstation. The modulator transforms digital information into a form suitable for transmission. The modulator output spectrum is centered around some intermediate frequency (IF) and has a bandwidth related to the transmission rate. In the earth station context, this IF is usually 70 or 140 MHz. The modulator output at IF is translated to the earth station output RF by means of an upconverter (U/C). The U/C output is amplified by the HPA according to the power requirement in the up-link. For low power, solid state amplifiers are becoming available, for medium power, a TWT driver and a klystron amplifier are often used.

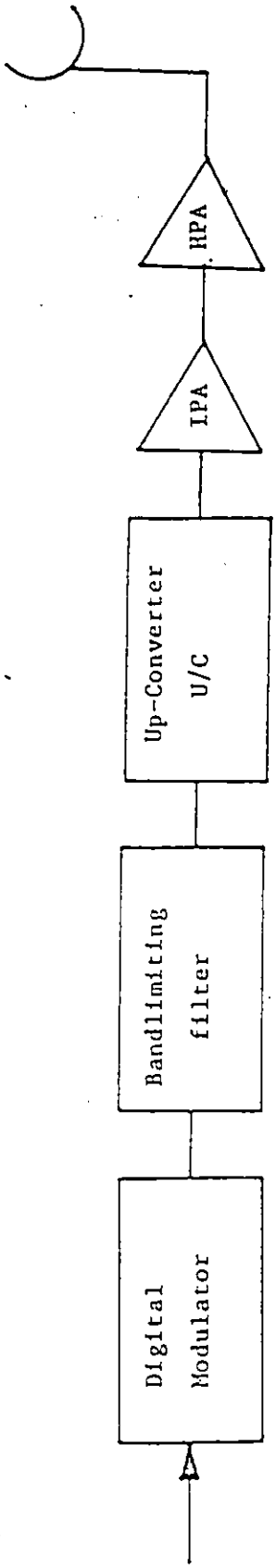

Fig. 1.3 Basic stages of a earth station

The bandlimiting filter is required to avoid adjacent channel interference. After bandlimitation, the pulses do not remain restricted to their time interval, but spread in time causing interference with adjacent pulses. The smearing of pulses due to band-limitation is known as intersymbol interference and is one of the major causes of system degradation.

The pulse spreading usually diminishes with time and in most digital satellite systems, there is no significant contribution beyond a couple of adjacent signalling intervals. There are other types of distortion introduced due to filtering in IF stages such as pulse shape distortion and phase distortion due to the non-uniform amplitude characteristics of the filters, but we are not concerned with these distortions. Usually, these types of distortion can be equalized by phase and amplitude equalizers in the transmission equipment.

As far as this thesis is concerned, the main source of interference in the system is ISI. Further, it is assumed that the high power amplification at the transmitter is essentially linear.

1.3.3 Satellite Repeater

The signal received by the satellite is fed to a bandpass filter and a low-noise amplifier, frequency translated to the downlink carrier frequency and transmitted back to the earth. For a large satellite communication system, the uplink thermal noise generated by the transmitting earth station electronic equipment and the equipment on board the satellite up to the input of TWTA, is assumed to be negligible.

The bandlimited signal is amplified by the TWTA without regeneration, i.e. we assume that there is no processing capacity on board the satellite. The TWTA is being exclusively used as a power amplifier. In INTELSAT IV, there are 12 such transponders each with 36 MHz BW. Satellite power amplifiers provide the primary amplification for the retransmitted carrier, and are one of the key elements in a communication satellite. Power

amplifiers, besides having to generate sufficient power levels and amplification, have additional requirements for reliability, long life, and suitability for the space environment. These requirements have been sufficiently met by the use of travelling wave tube amplifiers (TWTA).

In spite of all these advantages, the TWTA has one major disadvantage as far as communications systems are concerned, it is that it exhibits a non-linear input power to output signal phase transfer characteristic. The transfer characteristics of the Hughes 261-H (used in Intelsat IV) are shown in Fig. 1.4. In single carrier operation, the power transfer characteristics cause amplitude compression or soft-limiting of any input amplitude modulation (known as AM-AM conversion), and in addition, convert input signal amplitude variations to output signal phase modulation (known as AM-PM conversion). For low power amplification the TWT can be considered approximately as a linear device, but in high power amplification as used in satellites the transfer characteristics exhibit severe nonlinear behaviour. In multi-carrier operation such as FDMA, the effect of the non-linear characteristic of TWTA is to produce intermodulation distortion. In this thesis, we are primarily concerned with the AM-AM conversion and the AM-PM conversion effects in single carrier operation.

1.3.4 Receiving Earth Station

The signals received by the antenna of the receiving earth station are bandpass filtered to reduce out-of-band noise, amplified by a low noise amplifier, coherently demodulated, and then processed to recover the transmitted data. Thermal noise is generated in electronic equipment on the downlink path, primarily in the input stage of the earth station receiver which is considered as the main source of noise, and has the power spectral density N_0 defined as KT watts/Hz, where K is Boltzmann's constant and T is the equivalent

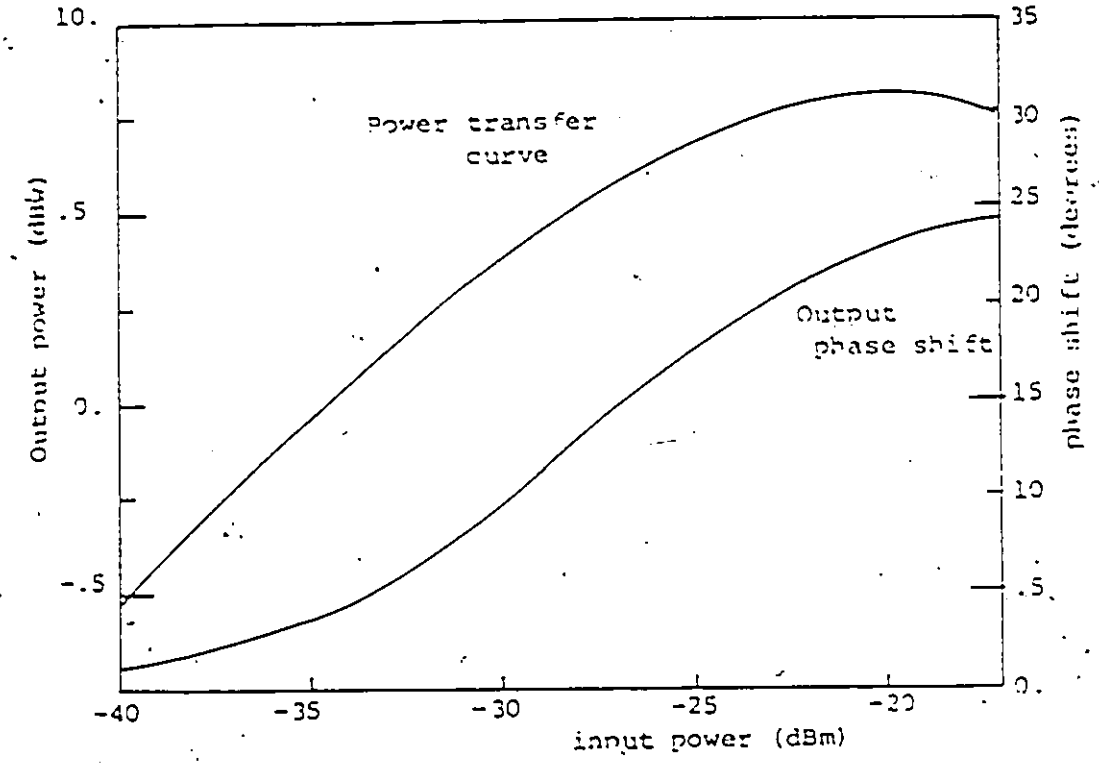

Fig. 1.4 Transfer characteristics of Hughes 261-H TWT.

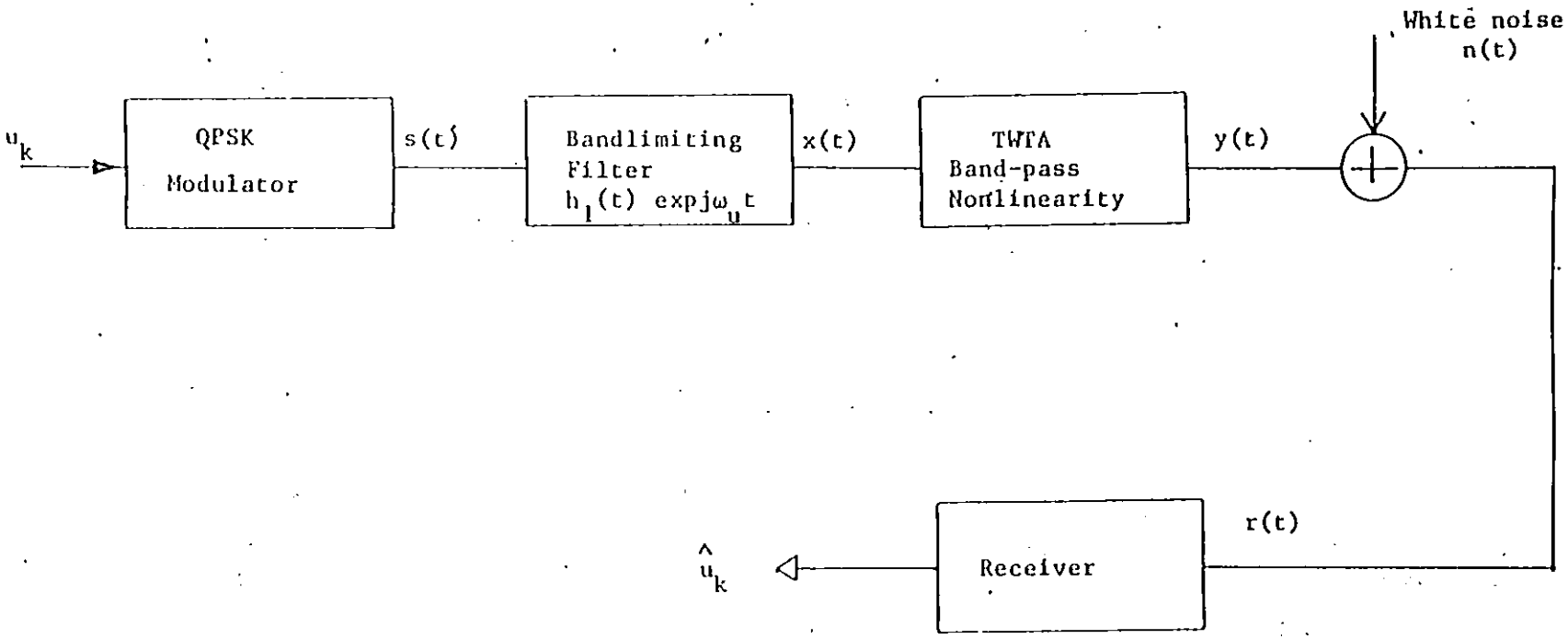

Fig. 1.5 The satellite channel model.

noise temperature of the receiver system in degrees Kelvin. The downlink thermal noise normally has a white frequency spectrum and Gaussianly distributed amplitude values. Since the effective isotropic radiated power (EIRP) of the satellite is comparatively much lower than the transmitting earth power station, the down-link thermal noise tends to be a significant factor in degrading system performance. Again, we will ignore adjacent and cochannel interferences which normally tend to be second order effects in well-designed satellite systems.

Figure 1.5 is a simplified channel model, and indicates the main sources of impairments mentioned so far and of primary concern to us in this thesis. We will refer to this as our communication system model except in Chapter 5, where the effects of downlink filtering are also included.

1.4 Scope of the Thesis

In this thesis, we address the problems of developing a maximum likelihood sequence receiver structure and estimating its performance for QPSK signalling over bandlimited, nonlinear satellite channels. Throughout the thesis we shall consider QPSK signalling. It is assumed that ideal carrier phase recovery is available at the receiver.

In Chapter 2, an explicit expression for the output of the bandpass nonlinearity (BPNL) for a QPSK signal is obtained as a function of inphase (I)−quadrature (Q) path history. The BPNL includes both AM-AM and AM-PM conversion. A maximum likelihood sequence receiver (MLSR) structure is then developed.

An upperbound on the probability of symbol error of the MLSR, at moderate to high signal-to-noise ratios, is obtained in Chapter 3. A simple expression for an upperbound on probability of symbol error is also obtained, for the case when single-error error events are dominant.

Error performance of the MLSR at low to moderate signal-to-noise ratios is estimated using computer simulation in Chapter 4. Considerable simplification in terms of memory requirement and computation is achieved by using a procedure analogous to decision feedback processing. At moderate to high SNR, upperbounds as developed in Chapter 3 are computed and shown to be consistent with the simulated results. A sub-optimum receiver based on the idea of an "average matched filter" is then developed and its performance evaluated using computer simulation. Although the sub-optimum receiver exhibits some sensitivity to the TWTA operating point, it appears to be a relatively robust structure.

Most real satellite systems have significant filtering on the downlink path, and considerable effort is spent on experimentally adjusting these filters for best performance. In Chapter 5, we address the problems of designing an MLSR and estimating its performance for QPSK signalling over a bandlimited, non-linear satellite channel which includes downlink filtering. The performance of the MLSR is evaluated using computer simulation and an upperbound on its probability of symbol error at moderate to high SNR is also obtained. A sub-optimum receiver is also developed and its performance evaluated using computer simulation.

Finally in Chapter 6, we briefly discuss the important results of the thesis. A few suggestions as to where this research can lead to in future, are also given.

CHAPTER 2

MAXIMUM LIKELIHOOD SEQUENCE RECEIVER FOR NONLINEAR BANDLIMITED QPSK CHANNELS

2.1 Introduction

The problem of ISI dates back to Nyquist [10], where he recognized the speed limitation in transmission of signals through band-limited channels. Since then, the problem of minimizing the effects of ISI on the performance of data communication systems has received considerable attention. In general, one can minimize ISI by shaping the transmitter pulse or can minimize its effects through equalization at the receiver [11,12].

There are two types of receivers to combat ISI, linear and nonlinear receivers. The linear receivers are called equalizers and consist of a matched filter followed by a sampler and tapped delay line [13-16]. Nonlinear receivers can be further classified into two broad categories, decision feedback receivers and maximum likelihood sequence receivers (MLSR) which are the type of interest in this investigation. Various decision feedback equalizers [17-19] to compensate for ISI effects in linear channels have been investigated. In [20], a decision feedback receiver structure for receiving binary phase-shift keyed (BPSK) signal over bandlimited, nonlinear channel is developed.

The Viterbi Algorithm (VA), originally introduced [21] for decoding convolutional codes, was first applied to the ISI problem by Forney [22], Kobayashi [23,24] and Omura [25] on linear channels. Forney has shown the VA to be a maximum likelihood sequence estimator. Therefore, it has the best possible block error probability. Although this approach does not optimize the symbol error rate, in practice these two criteria are almost equivalent.

Adaptive versions of MLSE receivers have been developed by Magee and Proakis [26]. Omura considered the VA over convolutionally coded information sequences transmitted over ISI channels. Falconer [27], Quershi and Newhall [28] considered linear adaptive filters before the maximum likelihood receiver to limit the time spread of the channel so as to reduce the complexity of the receiver.

As mentioned in Chapter 1, the ISI combined with nonlinear amplification causes significant degradation of system performance. To combat this distortion, receivers that take into account the non-linear characteristic of the channel have been investigated. In particular, Lawless [29] has applied a Volterra series approach to find maximum likelihood (ML) receivers for channels that include power law distortion, ISI and downlink noise. Mesiya, Mclane and Campbell [30], proposed using MLSE receivers over bandlimited nonlinear channels. They extended Forney's work, on the application of the Viterbi Algorithm to maximum likelihood sequence estimation, to include BPSK transmission over bandlimited non-linear channels. In [31] the performance of a Viterbi detector having a shorter memory than the actual channel memory of the bandlimited non-linear satellite channel is considered, and more recently [32], a simplified receiver called a "Pseudo MLSE" Processor, was derived from the MLSE Concept, and evaluated experimentally [33]. Here we extend the work of [30] to include QPSK modulation and, by inference, other modulations that can be formulated in inphase/quadrature form.

In this chapter we first describe the system model which includes uplink filtering, a BPNL and downlink thermal noise. An explicit expression for the output of the BPNL for a QPSK signal is obtained as a function of I-Q path history. The MSLE receiver structure for a channel memory of $\nu = 3$ symbols, is then derived.

2.2 The System Model

The satellite channel model is shown in Fig. 1.5. The complex signal at the output of the modulator can be written as

$$S(t) = \sum_k u_k\, p(t-kT) \exp j\omega_u t$$

where the u_k's are equally likely symbols transmitted at the symbol times kT and p(t) is a unit-energy pulse shape of width T. For QPSK, $u_k = \exp(j\phi_k)$ where $\phi_k = 2\pi i/M$, $i = 0,1,\ldots,M-1$ (M=4) are the input phase symbols to the modulator. Here we assume that the uplink noise is negligible, which is characteristic of a large satellite communication terminal.

Let $h_1(t)$ be the complex baseband response of the bandlimiting filter, with $a_1(t)$ its envelope function and $\psi_1(t)$ its phase function. Then the output of the filter may be written as

$$x(t) = \sum_k h(t-kT) \exp j[\omega_u t + \psi(t-kT) + \phi_k] \tag{2.1}$$

where $h(t) \exp j\psi(t) = p(t) * a_1(t) \exp j\psi_1(t)$, * denotes convolution and ω_u is the uplink carrier frequency.

The envelope function h(t) is assumed to be non-zero for only a finite duration which is greater than T s, the symbol time. Let this duration be LT s where L is an integer. Then defining the memory of the channel as $v = L-1$, we may write

$$h(t) \exp j\psi(t) = \sum_{i=0}^{v} h_i(t-iT) \exp [j\psi_i(t-iT)]$$

where $$h_i(t) \exp [j\psi_i(t)] = \begin{cases} h(t+iT) \exp j\psi(t+iT) & 0 \le t \le T \\ 0 \text{ otherwise} \end{cases}$$

The filter output can then be expressed in the form

$$x(t) = \sum_\ell \sum_{i=0}^{v} h_i(t-\ell T-iT) \exp [j(\omega_u t + \psi_i(t-\ell T-iT) + \phi_\ell]$$

Then letting

$$\ell = k - i \text{ and } x_k(t) = \begin{cases} x(t) & kT \le t \le (k+1)T \\ 0 & \text{otherwise} \end{cases}$$

we obtain the filter output in the k^{th} symbol period $kT \le t \le (k+1)T$ as

$$x_k(t) = \sum_{i=0}^{v} h_i(t-kT) \exp\left[j(\omega_u t + \psi_i(t-kT) + \phi_{k-i})\right] \tag{2.2}$$

This defines the input to the bandpass nonlinearity (BPNL).

2.3 The BPNL Output

From (2.2) the signal input to the BPNL during the time interval $kT \le t \le (k+1)T$ may be written as

$$x_k(t) = \text{Re}\left\{v_k(t) \exp j[\omega_u t + \theta_k(t)]\right\} \tag{2.3}$$

where
$$v_k(t) = \left[a_k^2(t) + b_k^2(t)\right]^{1/2} \tag{2.4}$$
$$\theta_k(t) = \tan^{-1}\frac{b_k(t)}{a_k(t)}$$

with

$$a_k(t) = \sum_{i=0}^{v} h_i(t-kT)\ \text{Cos}\left[\psi_i(t-kT) + \phi_{k-i}\right] \tag{2.5}$$
$$b_k(t) = \sum_{i=0}^{v} h_i(t-kT)\ \text{Sin}\left[\psi_i(t-kT) + \phi_{k-i}\right]$$

The output of the BPNL may then be written in the form

$$y_k(t) = \text{Re}\left\{G(v_k) \exp j[\omega_u(t) + \theta_k(t) + \alpha(v_k)]\right\} \tag{2.6}$$

where G(v) is the AM/AM conversion characteristic and $\alpha(v)$ is the AM/PM conversion of the bandpass non-linearity (BPNL). Assuming a Bessel function integral representation for the complex transfer characteristic $G(v) \exp[j\,\alpha(v)]$ of the BPNL [30], we obtain

$$G(v)\exp[j\,\alpha(v)] = 2\int_0^\infty F(z)\,J_1(vz)\,dz \tag{2.7}$$

for some complex-valued fucntion F(z). We can now write (2.7) as

$$G(v)\exp[j\,\alpha(v)] = \int_0^\infty Z\left[\frac{2\,F(z)}{z}\right] J_1(vz)\,dz$$

$$= H_1\left[\frac{2\,F(z)}{z}\right]$$

where $H_1[\cdot]$ denotes the Hankel transform of order 1. Now using Hankel's integral formula, we may write [42]

$$F(z) = \frac{z}{2}\int_0^\infty v\,G(v)\exp[j\,\alpha(v)]\,J_1(vz)\,dv \tag{2.8}$$

Combining (2.6) and (2.7), we can write output of the BPNL as

$$y_k(t) = \mathrm{Re}\{\exp(j\,w_u t)\,2\int_0^\infty F(z)\,J_1(v_k z)\,dz\exp(j\,\theta_k)\} \tag{2.9}$$

It is well known [40] that

$$J_1(v_k z) = \frac{-j}{2\pi}\int_{-\pi}^{\pi}\exp j[v_k z\cos\mu + \mu]\,d\mu \tag{2.10}$$

Now let $\mu = \phi - \theta_k$. Substituting into (2.10), and noting that the integrand is periodic gives

$$J_1(v_k z) = \frac{-j}{2\pi}\int_{-\pi}^{\pi}\exp j[v_k z\cos(\phi-\theta_k) + (\phi-\theta_k)]\,d\phi \tag{2.11}$$

or

$$J_1(v_k z)\,e^{j\theta_k} = \frac{-j}{2\pi}\int_{-\pi}^{\pi}\exp j[v_k z\cos(\phi-\theta_k) + \phi]\,d\phi \tag{2.11}$$

From equations (2.4) and (2.5), we have

$$\exp j[v_k z\cos(\phi-\theta_k)] = \exp j[z a_k \cos\phi + z b_k \sin\phi]$$

$$= \exp j\left\{z \sum_{i=0}^{v} h_i(t-kT)\cos[\psi_i(t-kT) + \phi_{K-i}]\cos\phi \right.$$

$$\left. + z \sum_{i=0}^{v} h_i(t-kT)\sin[\psi_i(t-kT) + \phi_{K-i}]\sin\phi\right\}$$

$$= \exp j z \sum_{i=0}^{v} h_i(t-kT)\cos[\psi_i(t-kT) + \phi_{K-i} - \phi]$$

$$= \prod_{i=0}^{v} \exp j\{z h_i(t-kT)\sin[\pi/2 - \phi + \psi_i(t-kT) + \phi_{k-i}]\} \qquad (2.12)$$

Expanding the exponential as a fourier series yields

$$e^{jz\sin\theta} = \sum_{n=-\infty}^{\infty} J_n(z)\, e^{jn\theta}$$

Using this expansion, we can write (2.12) as

$$\exp j[v_k z\cos(\phi-\theta_k)] = \sum_{n_0=-\infty}^{\infty} \cdots \sum_{n_v=-\infty}^{\infty} \prod_{i=0}^{v} J_{n_i}(z h_i(t-KT))$$

$$\exp j\left\{\sum_{i=0}^{v} n_i[\pi/2 - \phi + \psi_i(t-KT) + \phi_{K-i}]\right\} \qquad (2.13)$$

Substituting (2.11) and (2.13) into (2.9), we get

$$y_k(t) = \mathrm{Re}\left\{\exp(j\omega_u t)\,\frac{-j}{\pi} \sum_{n_0=-\infty}^{\infty} \cdots \sum_{n_v=-\infty}^{\infty} \int_0^{\infty} dz\, F(z) \prod_{i=0}^{v} J_{n_i}(z h_i(t-KT)) \right.$$

$$\left. \int_{-\pi}^{\pi} d\phi \exp j\left\{\sum_{i=0}^{v} n_i[\pi/2 - \phi + \psi_i(t-KT) + \phi_{K-i})\right\} \exp j\phi\right\}$$

$$= \mathrm{Re}\left\{\exp(j\omega_u t)\left(\frac{-j}{\pi}\right)\sum_{n_o=-\infty}^{\infty}\cdots\sum_{n_v=-\infty}^{\infty}\int_0^{\infty}F(z)\,dz\prod_{i=0}^{v}J_{n_i}(z\,h_i(t-KT))\right.$$

$$\int_{-\pi}^{\pi}d\phi\exp j\left[\phi\left(1-\sum_{i=0}^{v}n_i\right)\right]$$

$$\left.\exp j\left[\sum_{i=0}^{v}n_i[\pi/2+\psi_i(t-KT)+\phi_{K-i}]\right]\right\} \qquad (2.14)$$

Now

$$\int_{-\pi}^{\pi}d\phi\exp j\left[\phi\left(1-\sum_{i=0}^{v}n_i\right)\right]=\begin{cases}2\pi & \sum_{i=0}^{v}n_i=1\\ 0\ , & \text{otherwise}\end{cases} \qquad (2.15)$$

Making use of (2.15), (2.14) can be written as

$$y_k(t)=\mathrm{Re}\left\{\exp(j\omega_u t)\,\frac{1}{\pi}\cdot\ 2\pi\sum_{n_o=-\infty}^{n_o=\infty}\cdots\sum_{n_v=-\infty}^{\infty}\int_0^{\infty}dz\,F(z)\right.$$

$$\prod_{i=0}^{v}J_{n_i}(z\,h_i(t-KT))\cdot\ \exp j\left[\sum_{i=0}^{v}n_i\,\psi_i(t-kT)\right]$$

$$\left.\cdot\ \exp j\left[\sum_{i=0}^{v}n_i\,\phi_{K-i}\right]\right\} \qquad (2.16)$$

where

$$\sum_{i=0}^{v}n_i=1$$

or in the compact form

$$y_k(t) = \mathrm{Re}\left\{\exp(j\omega_u t) \sum_{n_0=-\infty}^{\infty} \cdots \sum_{n_v=-\infty}^{\infty} \prod_{i=0}^{v} (\exp j\phi_{k-i})^{n_i} f_n(t-kT)\right\} \tag{2.17}$$

where $$\sum_{i=0}^{v} n_i = 1 ,$$

$$f_n(t) \triangleq 2\exp j\left[\sum_{i=0}^{v} n_i \psi_i(t)\right] \int_0^{\infty} \prod_{i=0}^{v} J_{n_i}(z h_i(t))\, F(z)\, dz \tag{2.18}$$

with $$n = (n_0, \ldots n_v)$$

and where from (2.8)

$$\frac{2F(z)}{z} = \int_0^{\infty} vG(v) \exp[j\alpha(v)] J_1(vz)\, dv \tag{2.19}$$

is the first order Hankel transform of the BPNL transfer characteristic and $J_{n_i}(\cdot)$, $J_i(\cdot)$ are Bessel functions of order n_i and one respectively. In (2.17), the condition

$$\sum_{i=0}^{v} n_i = 1$$

is a consequence [30] of the bandpass representation of $y_k(t)$. We call $f_n(t)$, in (2.18), an interpulse product [30] of order m where

$$m = \sum_{i=0}^{v} |n_i| .$$

We now introduce some notation in order to obtain a more convenient form of expression for the output $y_k(t)$ of the BPNL. First let us define from eqn. (2.17) the first-order baseband waveforms

$$f_q^{(1)}\left\{(t-kT), p_k\right\} = \sum_{n_o} \cdots\cdots \sum_{n_v} \prod_{i=0}^{v} \exp(jm_i\phi_{k-i})\, f_n(t-kT) \qquad q \in (0, 1, \cdots v)$$

so that the condition $\sum_{i=0}^{v} n_i = 1,$

implies $n_i = \begin{cases} \text{odd integer} & i = q \\ 0 \text{ or even} & \text{otherwise} \end{cases}$

and let $m_i = \begin{cases} n_i - 1 & \text{if } n_i \text{ is odd} \\ n_i & \text{otherwise} \end{cases}$ (2.20)

The superscript in $f_q^{(\cdot)}$ denotes the number of indices n_i in each term of the summation that are constrained to be odd. Since m_i is always even

$$\prod_{i=0}^{v} \exp j\,\phi_{k-i} m_i = \prod_{i=0}^{v} \mathrm{Cos}(m_i\phi_{k-i})$$

This term will be 1 or –1 depending upon m_i and on whether the data phases ϕ_{k-i} correspond to transmission in the inphase (I) or quadrature (Q) channels. Note that there are two possible I-channel values and two Q-channel values for each ϕ_{k-i}. Thus, for example if $v = 3$, $f_q^{(1)}\{(t-kT), p_k\}$ will have 16 possible variations depending on the particular combination of I- and Q-channel symbols in the phase history ϕ_k, ϕ_{k-1}, ..., ϕ_{k-3}. Note that these do not correspond 1:1 with the transmitted data symbols. In general, we shall use the notation $f_q^{(1)}\{(t-kT), p_k\}$, $(p_k = 0, 1, ..., 2^{v+1}-1)$ to denote a first-order constituent waveform for the particular subsequence p_k of I or Q phase-values, where the numbers p_k do not refer to the actual phase sequence but only to whether or not the values ϕ_k, ϕ_{k-1}, ..., ϕ_{k-v} correspond to inphase or quadrature channel transmission. The I-Q phase sequence is denoted by the binary value of the number p_k, with a zero meaning I channel and a one meaning Q channel.

For example, $f_p^{(1)}\{(t-kT),1\}$ denotes a constituent waveform for a transmitted phase sequence given by I,I,I,Q. Similarly we can define third and fifth order baseband waveforms.

$$f^{(3)}_{q,r,s}\left\{(t-kT), p_k\right\} = \sum_{n_0} \cdots\cdots \sum_{n_v} \prod_{i=0}^{v} \exp(jm_i\phi_{k-i})\, f_n(t-kT)$$

$$q, r, s \in (0, 1, \ldots, v)$$

$$\text{where } n_i = \begin{cases} \text{odd} & i = q, r, s \\ 0 \text{ or even} & \text{otherwise} \end{cases}$$

$$m_i = \begin{cases} n_i - 1 & \text{if } n_i \text{ is odd} \\ n_i & \text{otherwise} \end{cases} \qquad (2.21)$$

$$f^{(5)}_{q,r,s,t,u}\left\{(t-kT), p_k\right\} = \sum_{n_0=-\infty}^{\infty} \cdots\cdots \sum_{n_v=-\infty}^{\infty} \prod_{i=0}^{v} \exp j(m_i\phi_{k-i})\, f_n(t-kT)$$

$$q, r, s, t, u \in (0, 1, \ldots, v)$$

$$\text{where } n_i = \begin{cases} \text{odd} & i = q, r, s, t, u \\ 0 \text{ or even} & \text{otherwise} \end{cases}$$

$$m_i = \begin{cases} n_i - 1 & \text{if } n_i \text{ is odd} \\ n_i & \text{otherwise} \end{cases} \qquad (2.22)$$

Higher order constituent waveforms may also be defined as required. This will depend on the length v assumed for the channel memory.

With the above notation, we can write (2.17) for a channel memory of v with p_k as a parameter in the form

$$
\begin{aligned}
y_k(t) = \mathrm{Re}\{&\exp(j\omega_u t)[\exp(j\phi_k) f_o^{(1)}\{(t-KT), p_k\} + \exp j\phi_{K-1} f_1^{(1)}\{(t-KT), p_k\} \\
&+ \ldots + \exp j\phi_{k-v} f_v^{(1)}\{(k-KT), p_k\} \\
&+ \exp j(\phi_k + \phi_{k-1} + \phi_{k-2})\, f_{0,1,2}^{(3)}\{(t-KT), p_k\} \\
&+ \text{all other possible combination of 3 data bits multiplied} \\
&\quad \text{by a corresponding weighting function of time} \\
&+ \exp j(\phi_k + \phi_{k-1} + \phi_{k-2} + \phi_{k-3} + \phi_{k-4})\, f_{0,1,2,3,4}^{(5)}\{(t-KT), p_k\} \\
&+ \text{all other possible combination of 5 data bits multiplied} \\
&\quad \text{by a corresponding weighting function of time} \\
&+ \ldots + \ldots +
\end{aligned}
\tag{2.23}
$$

Equation (2.23) is a general expression for the output of BPNL for QPSK signal.

2.4 The BPNL Output for Channel Memory v = 3

In this section we will obtain, from the general eqn. (2.23), the expression for the output of the BPNL for channel memory v = 3. Usually in satellite channels, the time-span of the ISI is moderate [32] and it has been found that in most cases a channel memory of length v=3, is a reasonable approximation to the actual duration. Therefore, in the remainder of the thesis, we will consider specifically the case v = 3. With the above notation, we can write (2.23) for v=3 with p_k as a parameter in the form

$$y_k(t) = R_e\{\exp(j\omega_u t)[\exp(j\phi_k) f_0^{(1)}\{(t-kT), p_k\} + \exp(j\phi_{k-1}) f_1^{(1)}\{(t-kT), p_k\}$$
$$+ \exp(j\phi_{k-2}) f_2^{(1)}\{(t-kT), p_k\} + \exp(j\phi_{k-3}) f_3^{(1)}\{(t-kT), p_k\}$$
$$+ \exp j(\phi_k + \phi_{k-1} + \phi_{k-2}) f_{0,1,2}^{(3)}\{(t-kT), p_k\} + \exp j(\phi_{k-1} + \phi_{k-2} + \phi_{k-3}) f_{1,2,3}^{(3)}\{(t-kT), p_k\}$$
$$+ \exp j(\phi_k + \phi_{k-2} + \phi_{k-3}) f_{0,2,3}^{(3)}\{(t-kT), p_k\} + \exp j(\phi_k + \phi_{k-1} + \phi_{k-2}) f_{0,1,3}^{(3)}\{(t-kT), p_k\}$$
$$(kT \le t \le (k+1)T) \tag{2.24}$$

We may then write the overall output of the BPNL as

$$y(t) = \sum_k y_k(t)$$

Then assuming frequency translation to the downlink frequency ω_d, and combining terms in eq. (2.24), we may write the BPNL output in the form

$$y(t) = \mathrm{Re}\Big\{\exp(j\omega_d t) \sum_k [\exp(j\phi_k) f^{(1)}\{(t-kT), p_k\} + \exp j(\phi_k + \phi_{k-1} + \phi_{k-2})$$
$$f^{(31)}\{(t-kT), p_k\} + \exp j(\phi_k + \phi_{k-2} + \phi_{k-3}) f^{(32)}\{(t-kT), p_k\}$$
$$+ \exp j(\phi_k + \phi_{k-1} + \phi_{k-3}) f^{(33)}\{(t-kT), p_k\}]\Big\} \tag{2.25}$$

where we have defined the combined baseband waveforms

$$f^{(1)}\{(t-kT), p_k\} = f_0^{(1)}\{(t-kT), p_k\} + f_1^{(1)}\{(t-(k+1)T), p_{k+1}\}$$
$$+ f_2^{(1)}\{(t-(k+2)T), p_{k+2}\} + f_3^{(1)}\{(t-(k+3)T), p_{k+3}\}$$
$$f^{(31)}\{(t-kT), p_k\} = f_{0,1,2}^{(3)}\{(t-kT), p_k\} + f_{1,2,3}^{(3)}\{(t-(k+1)T), p_{k+1}\}$$
$$f^{(32)}\{(t-kT), p_k\} = f_{0,2,3}^{(3)}\{(t-kT), p_k\} \tag{2.26}$$

and

$$f^{(33)}\{(t-kT), p_k\} = f_{0,1,3}^{(3)}\{(t-kT), p_k\}$$

We note that y(t) in any interval is a function of both the I-Q phase history denoted by p_k in the baseband waveforms and the previous data symbols. It should also be mentioned that for

$v = 3$, there will be 128 baseband waveforms corresponding to $f^{(1)}\{(t), p_k\}$, 32 waveforms to $f^{(31)}\{(t), p_k\}$ and 16 each for $f^{(32)}\{(t), p_k\}$ and $f^{(33)}\{(t), p_k\}$. It seems that the above expression is very complicated and one has to generate a large number of waveforms in order to compute the output of the BPNL $y(t)$ for $v = 3$. However, we will show in Chapter 4 that, we need to store only 8 generic waveforms for each of $f^{(1)}\{(t), p_k\}$, $f^{(31)}\{(t), p_k\}$, $f^{(32)}\{(t), p_k\}$ and $f^{(33)}\{(t), p_k\}$, to generate the above waveforms.

2.5 Determination of F(z)

The computation of the constituent waveforms in $y(t)$ requires evaluation of the integral of (2.18). This integral can be evaluated by approximating [34] the BPNL transfer characteristic $G(v)\exp[j\,\alpha(v)]$ in eqn. (2.19) by a Bessel function expansion with complex coefficients,

$$G(v)\exp[j\,\alpha(v)] = 2\sum_{k=1}^{N} b_k\, J_1\left[(2k-1)\,\frac{\pi v}{R}\right] \qquad (2.27)$$

$$0 \le v \le R$$

where R is the range of interest. We can then determine $F(z)$ by using the property of the Hankel transform that

$$J_1(va) \overset{H_1}{\longleftrightarrow} \delta(z-a)$$

and thus

$$F(z) = \sum_{k=1}^{N} b_k\, \delta\left[z-(2k-1)\,\frac{\Pi}{R}\right] \qquad (2.28)$$

$$0 \le v \le R$$

so that the integral in (2.18) can be solved, to obtain

$$\sum_{k=1}^{N} b_k \prod_{i=0}^{v} J_{n_i}\left((2k-1)\,\frac{\pi}{R}\, h_i(t)\right) \qquad (2.29)$$

2.6 The Maximum Likelihood Sequence Receiver (MLSR)

2.6.1 The Complex Envelope of Received Signal:

In this section we obtain the complex envelope of the received signal for a channel memory of v = 3. The output of the BPNL can be written from eqn. (2.25) as

$$y(t) = \mathrm{Re}\Big\{\exp(j\omega_d t)\sum_k [\exp(j\phi_k) f^{(1)}\{(t-kT), p_k\} + \exp j(\phi_k+\phi_{k-1}+\phi_{k-2})$$

$$f^{(31)}\{(t-kT), p_k\} + \exp j(\phi_k+\phi_{k-2}+\phi_{k-3}) f^{(32)}\{(t-kT), p_k\}$$

$$+ \exp j(\phi_k+\phi_{k-1}+\phi_{k-3}) f^{(33)}\{(t-kT), p_k\}]\Big\}$$

Now letting

$$f^{(1)}\{(t), p_k\} = f_p^{(1)} + j f_q^{(1)}$$

$$f^{(3\ell)}\{(t), p_k\} = f_p^{(3\ell)} + j f_q^{(3\ell)} \qquad \ell = 1, 2, 3 \tag{2.30}$$

y(t) may be written as

$$y(t) = \sum_k [f_p^{(1)}\cos(\omega_d t + \phi_k) - f_q^{(1)}\sin(\omega_d t + \phi_K))$$

$$+ f_p^{31}\cos(\omega_d t + \phi_K + \phi_{K-1} + \phi_{K-2}) - f_q^{31}\sin(\omega_d t + \phi_K + \phi_{K-1} + \phi_{K-2})$$

$$+ f_p^{32}\cos(\omega_d t + \phi_K + \phi_{K-2} + \phi_{K-3}) - f_q^{32}\sin(\omega_d t + \phi_K + \phi_{K-2} + \phi_{K-3})$$

$$+ f_p^{33}\cos(\omega_d t + \phi_K + \phi_{K-1} + \phi_{K-3}) - f_q^{33}\sin(\omega_d t + \phi_K + \phi_{K-1} + \phi_{K-3})] \tag{2.31}$$

At the receiver y(t) is available only in the presence of thermal noise. It is assumed that the received signal is coherently demodulated and filtered as shown in Fig. 2.1. For further analysis, the complex envelope of the received signal will be used. It is defined as follows:

$$y(t) = y_p(t) + j\, y_q(t)$$

$$n(t) = n_c(t) + j\, n_s(t) \tag{2.32}$$

where n(t) is the complex envelope of the downlink thermal noise and

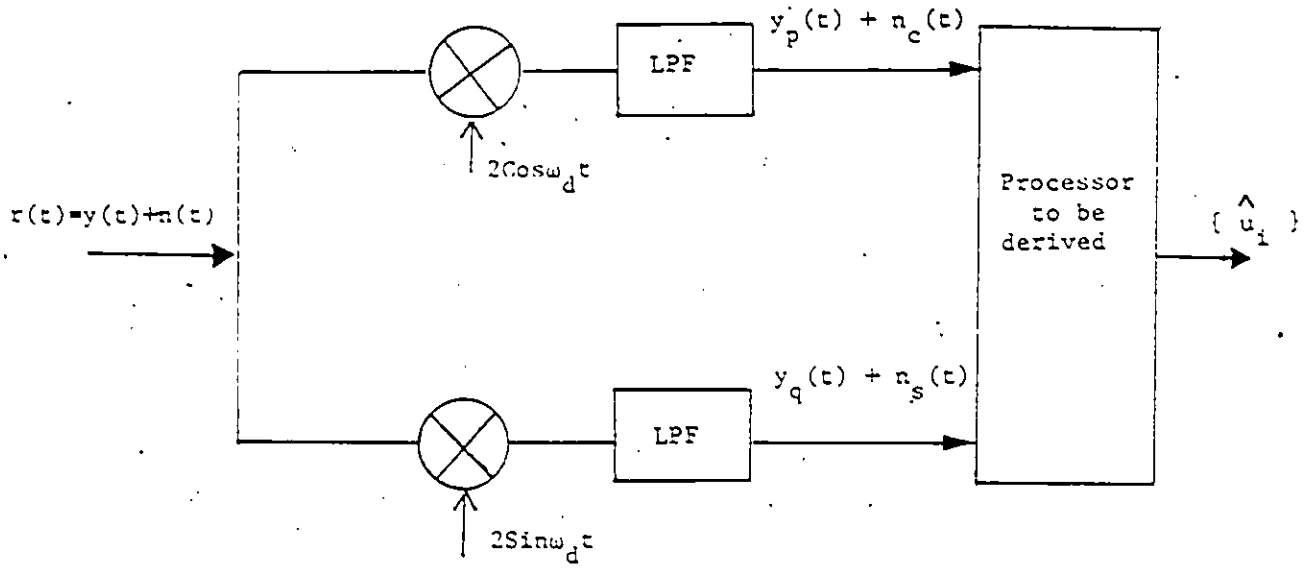

Fig. 2.1 Coherent demodulation.

$$y_p(t) = \{2 \cos \omega_d t\, y(t)\}_{LP}$$

$$y_q(t) = \{2 \sin \omega_d t\, y(t)\}_{LP}$$

$$n_c(t) = \{2 \cos \omega_d t\, n(t)\}_{LP}$$

$$n_s(t) = \{2 \sin \omega_d t\, n(t)\}_{LP} \tag{2.33}$$

where $\{\cdot\}_{LP}$ denotes lowpass filtering. In deriving the MLSE receiver we will use the complex envelope quantities defined in eqn. (2.32). With these notations y(t) can be written from (2.31) in the following form

$$\begin{aligned} y(t) = \Bigg\{ \sum_k [(\cos\phi_k + j \sin\phi_K)\, f^{(1)}\{(t-KT), p_K\} + (\cos(\phi_K + \phi_{K-1} + \phi_{K-2}) \\ + j \sin(\phi_K + \phi_{K-1} + \phi_{K-2}))\, f^{(31)}\{(t-KT), p_K\} \\ + (\cos(\phi_K + \phi_{K-2} + \phi_{K-3}) + j \sin(\phi_K + \phi_{K-2} + \phi_{K-3}))\, f^{(32)}\{(t-KT), p_K\} \\ + (\cos(\phi_K + \phi_{K-1} + \phi_{K-3}) + j \sin(\phi_K + \phi_{K-1} + \phi_{K-3}))\, f^{(33)}\{(t-KT), p_K\}] \Bigg\} \end{aligned}$$

or

$$\begin{aligned} y(t) = \sum_k \exp j\phi_k\, f^{(1)}\{(t-KT), p_K\} + \exp j(\phi_K + \phi_{K-1} + \phi_{K-2})\, f^{(31)}\{(t-KT), p_K\} \\ + \exp j(\phi_K + \phi_{K-2} + \phi_{K-3})\, f^{(32)}\{(t-KT), p_K\} \\ + \exp j(\phi_K + \phi_{K-1} + \phi_{K-3})\, f^{(33)}\{(t-KT), p_K\} \end{aligned} \tag{2.34}$$

2.6.2 Finite State Machine (FSM) Model

It has been found convenient to model the bandlimited linear channel as a finite state machine [22,35], driven by an information source. What we mean by this is, that the instantaneous output of the bandlimited linear channel is a deterministic function of the present and v previous data bits. In our satellite model, the uplink channel before the BPNL is a linear channel and it is possible to write the complex envelope of the input to the BPNL

from (2.3) as

$$x_k(t) = F(t; \{(a_k, \beta_K), ..., a_{K-v}\})$$
$$= v_k(t) \exp j\, \theta_K(t) \tag{2.35}$$

Defining the state $S_k = ((a_{k-1}, \beta_{k-1}), \ldots (a_{k-v}, \beta_{k-v}))$ and the state transition

$$\xi_k = (S_{K+1}, S_K)$$
$$= ((a_k, \beta_k), ..., (a_{k-v}, \beta_{k-v})),$$

in terms of these notations, we can write (2.35) as

$$x_k(t) = F(t; (a_K, \beta_K), S_k) = F(t; \xi_k)$$

The output of the uplink bandlimited linear channel is further acted upon by an instantaneous BPNL. It is possible to express the complex output of the BPNL for $v = 3$, from (2.23) as

$$y(t) = F'(t; (a_k, \beta_k), S_K) = F'(t; \xi_k)$$
$$= \exp j\phi_k f_0^{(1)}\{(t-kT), p_k\} + \exp j\phi_{K-1} f_1^{(1)}\{(t-KT, p_k\}$$
$$+ \exp j\phi_{K-2} f_2^{(1)}\{(t-kT), p_k\} + \exp j\phi_{k-3} f_3^{(1)}\{(t-KT, p_k\}$$
$$+ \exp j(\phi_K + \phi_{K-1} + \phi_{K-2}) f_{0,1,2}^{(2)}\{(t-KT), p_k\}$$
$$+ \exp j(\phi_{K-1} + \phi_{K-2} + \phi_{K-3}) f_{0,1,2}^{(3)}\{(t-KT), p_k\}$$
$$+ \exp j(\phi_K + \phi_{K-2} + \phi_{K-3}) f_{0,2,3}^{(3)}\{(t-KT), p_k\}$$
$$+ \exp j(\phi_K + \phi_{K-1} + \phi_{K-2}) f_{0,1,3}^{(3)}\{(t-KT), p_k\} \tag{2.36}$$

It is clear from (2.36) that the output of the BPNL for $v = 3$, is a function of present and past data bits. Thus we can think of the $y_k(t)$ as the output of a FSM, since the past histories of a FSM can affect its future behaviour in only a finite number of ways. The present output can be affected by v previous inputs in $N_s = 4^v$ ways, where N_s is the number of possible states of the FSM.

2.6.3 The MLSR Structure

The objective of the receiver is to estimate the transmitted sequences $\{u_i\}$ from the received signal

$$r(t) = y(t; \{u_i\}) + n(t) \quad t \in I \tag{2.37}$$

where the observation interval I is assumed to be long enough that the precise conditions at its boundaries are insignificant to the total observation. y(t) is the complex envelope of the output of the BPNL, and n(t) is the complex envelope of the White Gaussian noise added at the front-end of the receiver. The FSM starts from a specified initial state, say S_0, and then traces a path history $\{S_0, S_1, ...\}$ depending upon the particular transmitted sequence. The succession of states of the FSM constitute a v^{th} order Markov Process. Forney [22,35] has introduced a description of such a process known as a trellis. Here each node corresponds to a distinct state at a given time, and each branch represents a transition to some new state at the next instant of time. The trellis begins and ends at the known states S_0 and S_K. Its most important property is that for every possible state sequence or realization of a FSM, $\{S_i\}$, there corresponds a unique path in it and vice versa. That is

$$\{(\alpha_i, \beta_i), ...\} \overset{1-1}{\longleftrightarrow} \{S_i, ...\} \overset{1-1}{\longleftrightarrow} \{\text{Paths in trellis}\}$$

The maximum likelihood sequence receiver (MLSR) determines the best estimate of the complex symbol sequence $\{u_i\} = a_i\} = \{\cos \phi_i, \sin \phi_i\}$ as follows:

Declare $\{u_i\} = \{u_i^*\}$ if

$$\Lambda [r(t); \{u_i^*\}] = \text{Max}_{\{\alpha_i, \beta_i\}} \Lambda[r(t): \{\alpha_i, \beta_i\}]$$

where $\Lambda[r(t); \{\alpha_i, \beta_i\}]$ is the likelihood ratio. For the special case of WGN, it is given by [36]

$$\Lambda [r(t); \{\alpha_i, \beta_i\}] = \exp \left\{ \text{Re} \left[\frac{1}{N_o} \int_I r(t)\, y^*(t: \{\alpha_i, \beta_i\})\, dt \right] - \frac{1}{2N_o} \int_I |y(t; \{\alpha_i, \beta_i\}|^2\, dt \right\} \tag{2.38}$$

Substituting $y(t; \{\alpha_i, \beta_i\})$ from (2.34) into (2.38) we get

$$\Lambda[r(t);\{\alpha_i,\beta_i\}] = \exp\left\{\mathrm{Re}\left[\frac{1}{N_o}\int_I r(t)\cdot \sum_i [\exp j\phi_i f^{(1)}\{(t-iT),p_i\}\right.\right.$$

$$+ (I)_{\phi_i} f^{(31)}\{(t-iT),p_i\} + (II)_{\phi_i} f^{(32)}\{(t-iT),p_i\} + (III)_{\phi_i} f^{(33)}\{(t-iT),p_i\}]^* dt$$

$$- \frac{1}{2N_o}\int_I \Big| \sum_i [\exp j\phi_i f^{(1)}\{(t-iT),p_i\} + (I)_{\phi_i} f^{(31)}\{(t-iT),p_i\}$$

$$\left.\left. + (II)_{\phi_i} f^{(32)}\{(t-iT),p_i\} + (III)_{\phi_i} f^{(33)}\{(t-iT),p_i\}\Big|^2 dt\right\}\right.$$

$$= \exp\left\{\frac{1}{2N_o}\left[2\,\mathrm{Re}\Big(\sum_i \exp(-j\phi_i) Z_i^1(p_i) + (I)^*_{\phi_i} Z_i^{31}(p_i)\right.\right.$$

$$+ (II)^*_{\phi_i} Z_i^{32}(p_i) + (III)^*_{\phi_i} Z_i^{33}(p_i)\Big)$$

$$- \sum_i \sum_k \mathrm{Re}\Big(\exp j\phi_i \exp(-j\phi_k) S_{i-k}^{1,1} + (I)_{\phi_i}(I)^*_{\phi_k} S_{i-k}^{31,31}$$

$$+ (II)_{\phi_i}(II)^*_{\phi_i}\delta_{i,k} S_o^{32,32} + (III)_{\phi_i}(III)^*_{\phi_i} S_o^{33,33}\delta_{i,k}$$

$$+ 2\exp(j\phi_i)(I)^*_{\phi_k} S_{i-k}^{1,31} + 2\exp(j\phi_i)(II)^*_{\phi_i} S_{i-k}^{1,32}$$

$$+ 2\exp(j\phi_i)(III)^*_{\phi_k} S_{i-k}^{1,33} + 2(I)_{\phi_i}(II)^*_{\phi_i} S_{i-k}^{31,32}$$

$$\left.\left. + 2(I)_{\phi_i}(III)^*_{\phi_i} S_{i-k}^{31,33} + 2(II)_{\phi_i}(III)^*_{\phi_i} S_{i-k}^{32,33}\delta_{i,k}\Big)\right]\right\} \qquad (2.39)$$

where

$$(I)_{\phi_i} = \exp j(\phi_i + \phi_{i-1} + \phi_{i-2})$$

$$(II)_{\phi_i} = \exp j(\phi_i + \phi_{i-2} + \phi_{i-3})$$

$$(III)_{\phi_i} = \exp j(\phi_i + \phi_{i-1} + \phi_{i-3})$$

and $(\cdot)^*$denotes the complex conjugate. Also using the notation $<a(t), b(t)>$ to denote the inner product $\int a(t)\, b^*(t)dt$, we may write

$$S_i^{\ell}(p_i) \triangleq < r(t), f^{(\ell)}\{(t-iT), p_i\} >, \quad \ell = 1, 31, 32, 33$$

$$S_{i-j}^{\ell_1,\ell_2} \triangleq < f^{(\ell_1)}\{(t-iT), p_i\}, f^{(\ell_2)}\{(t-jT), p_j\} >, \; i-j = -3, -2, -1, 0$$

$$S_{i-j}^{31,31} \triangleq < f^{(31)}\{(t-iT), p_i\}, f^{(31)}\{(t-jT), p_j\} >, \; i-j = -1, 0$$

$$S_o^{\ell^1,\ell^1} \triangleq < f^{(\ell^1)}\{(t), p\}, f^{(\ell^1)}\{(t), p\} >, \; \ell^1 = 31, 32, 33$$

$$S_o^{32,33} \triangleq < f^{(32)}\{(t), p\}, f^{(33)}\{(t), p\} >$$

$$S_{i-j}^{1,31} \triangleq < f^{(1)}\{(t-iT), p_i\}, f^{(31)}\{(t-jT), p_j\} >, \; i-j = -3, -2, \ldots 0, 1$$

$$S_{i-j}^{1,\ell} \triangleq < f^{(1)}\{(t-iT), p_i\}, f^{(\ell_2)}\{(t-jT), p_j\} >, \quad \begin{matrix} \ell_2 = 32, 33, \\ i-j = -3, -2, -1, 0 \end{matrix}$$

$$S_{i-j}^{31,\ell_3} \triangleq < f^{(31)}\{(t-iT), p_i\}, f^{(\ell_3)}\{(t-jT), p_j\} >, \quad \begin{matrix} \ell_3 = 32, 33, \\ i-j = -1, 0 \end{matrix}$$

In equation (2.39), the quantities $Z_i^1(p_i)$, $Z_i^{31}(p_i)$, $Z_i^{32}(p_i)$ and $Z_i^{33}(p_i)$ can be interpreted as sample values taken at the symbol rate from the outputs of "matched filters" with impulse response functions in the kth symbol interval given by

$$\begin{aligned} g_{MF}^{(1)}\{(t), p_k\} &= f^{(1)^*}\{(kT-t), p_k\} \\ g_{MF}^{(31)}\{(t), p_k\} &= f^{(31)^*}\{(kT-t), p_k\} \\ g_{MF}^{(32)}\{(t), p_k\} &= f^{(32)^*}\{(kT-t), p_k\} \\ g_{MF}^{(33)}\{(t), p_k\} &= f^{(33)^*}\{(kT-t), p_k\} \end{aligned} \tag{2.40}$$

The sequences $\{Z_i^1(p_i)\}$, $\{Z_i^{31}(p_i)\}$, $\{Z_i^{32}(p_i)\}$ and $\{Z_i^{33}(p_i)\}$ contain all information about the received signal and hence form a set of sufficient statistics for computing the likelihood ratio. It can be seen from equations (2.26) and (2.40) that the impulse responses are dependent on the value of the I-Q phase history p_k. For the special case of a channel memory of $v=3$, this means that there are 128 filter responses corresponding to $g_{MF}^{(1)}\{(t), p_k\}$, 32

filters to $g_{MF}^{(31)}\{(t), p_k\}$ and 16 filters each to $g_{MF}^{(32)}\{(t), p_k\}$ and $g_{MF}^{(33)}\{(t), p_k\}$. For a longer memory ($v>3$), even more filter responses arise. The computation of the quantities $\{S_{i-k}^{1,1}\}$ etc. may be very tedious, since they are also dependent on the p_k's and thus there are a large number of them. However, we will see in Chapter 4 that, in the situations of interest, neglecting these quantities has negligible effect on the receiver's performance, and therefore will not consider them further here.

The structure of the maximum likelihood receiver can now be specified. It consists of a bank of matched filters $g_{MF}^{(1)}\{(t), p_k\}$, $g_{MF}^{(31)}\{(t), p_k\}$, $g_{MF}^{(32)}\{(t), p_k\}$ and $g_{MF}^{(33)}\{(t), p_k\}$ with output symbol rate samplers, followed by a processor called the maximum likelihood sequence estimator (MLSE). The MLSE determines the most probable sequence $\{a_i, \beta_i\}$ as the one that maximizes (2.39) or equivalently that assigns a minimum value to the path metric [37] given by

$$J_I(\{a_i, \beta_i\}) = -\ell n\, \Lambda[r(t); \{a_i, j\beta_i\}] \tag{2.41}$$

Defining [22,35] the state at time kT as $S_k = \{(a_{k-1}, \beta_{k-1}), \ldots, (a_{k-v}, \beta_{k-v})\}$ and the corresponding state transitions as $\xi_k = (S_{k+1}, S_k)$, it is then possible [35] to write the path metric of equation (2.41) as the sum of branch metrics,

$$J_I(\{a_i, \beta_i\}) = \sum_i \lambda(\xi_i) \tag{2.42}$$

where the branch metrics $\lambda(\xi_i)$ are given by

$$\lambda(\xi_i) = -2\mathrm{Re}\Big\{\Big[(a_i - j\beta_i)Z_i^1(p_i) + (\mathrm{I})^*_{\phi_i} Z_i^{31}(p_i) + (\mathrm{II})^*_{\phi_i} Z_i^{32}(p_i)$$

$$+ (\mathrm{III})^*_{\phi_i} Z_i^{33}(p_i)\Big] + S_o^{1,1} + S_o^{31,31} + S_o^{32,32} + S_o^{33,33}$$

$$+ 2\Big[(a_i + j\beta_i)\sum_{\ell=-3}^{-1}(a_{i+\ell} - j\beta_{i+\ell})S_\ell^{1,1} + (a_i + j\beta_i)$$

$$(a_{i-3} - j\beta_{i-3})S_1^{31,31} + (\mathrm{I})_{\phi_i}\Big(\sum_{\ell=-3}^{0}(a_{i+\ell} - j\beta_{i+\ell})S_\ell^{1,31}\Big)$$

$$+ \Big((a_i + j\beta_i)(\mathrm{I})^*_{\phi_{i-1}} S_1^{1,31}\Big) + (\mathrm{II})_{\phi_i}\Big(\sum_{\ell=-3}^{0}(a_{i+\ell} - j\beta_{i+\ell})S_\ell^{1,32}\Big)$$

$$+ (\mathrm{III})_{\phi_k}\sum_{\ell=-3}^{0}(a_{i+\ell} - j\beta_{i+\ell})S_\ell^{1,33} + (\mathrm{II})_{\phi_i}(\mathrm{III})^*_{\phi_k} S^{32,33}\delta_{i,k}$$

$$+ (\mathrm{II})_{\phi_i}\sum_{\ell=-1}^{0}(\mathrm{I})^*_{\phi_{i+\ell}} S_\ell^{31,32}$$

$$+ (\mathrm{III})_{\phi_i}\sum_{\ell=-1}^{0}(\mathrm{I})^*_{\phi_{i+\ell}} S_\ell^{31,33}\Big]\Big\} \qquad (2.43)$$

Equations (2.42) and (2.43) can be interpreted as follows: Given a set of sufficient statistics $\{(Z_i^1(p_i), Z_i^{31}(p_i), Z_i^{32}(p_i), Z_i^{33}(p_i)\}$, every branch in the trellis may be assigned a length given by (2.43). It can now be inferred from (2.26), (2.40) and (2.43) that for each allowable state transition $\xi_i = (S_{i+1}, S_i)$ there are 128 possible parallel branches thus producing 128 possible parallel paths between states, unlike the binary case of [30] where there are no parallel branches. Since all 128 parallel branches have a common path history to time i, we need to retain only that branch among the parallel branches with minimum branch metric value. This minimum branch metric value corresponds to the maximum matched filter outputs. This observation allows us to eliminate all but four of the branches, so that only the metrics of these four branches into each time $(i+1)$ state need to be compared in

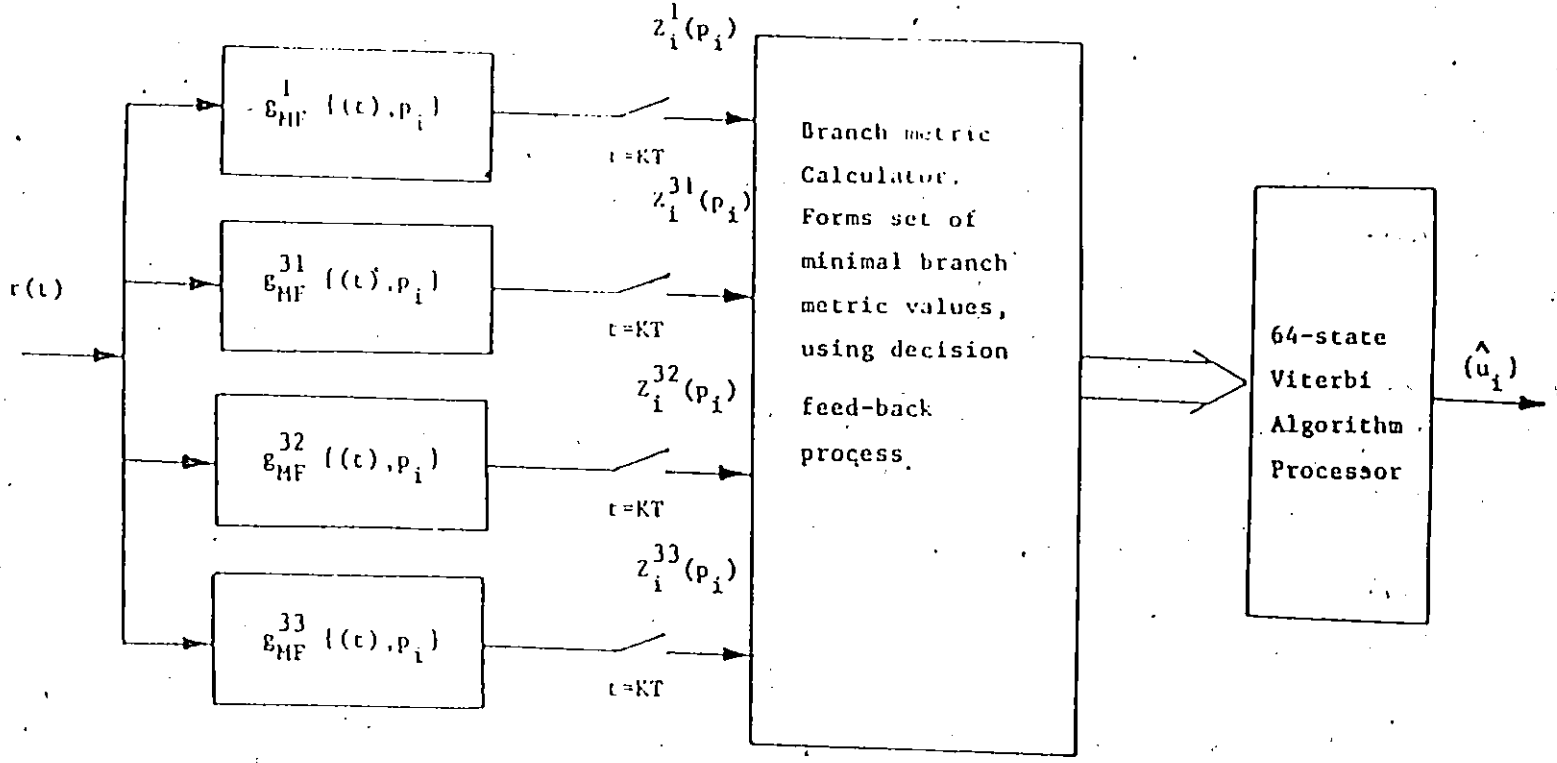

Fig. 2.2 Structure of the MLSE for a channel memory of v = 3.

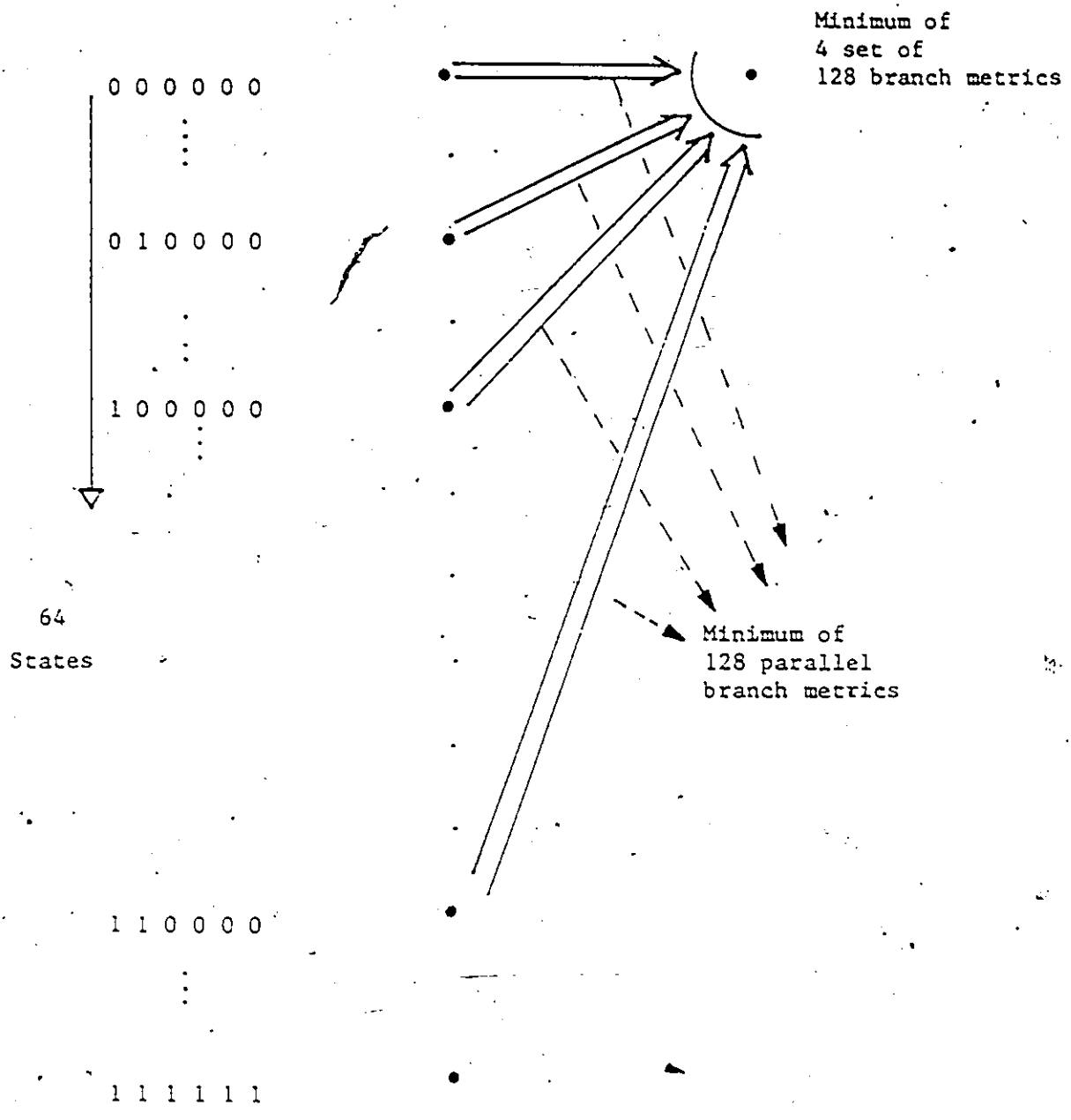

Fig. 2.3 Computation of minimum branch metric for optimum MLSE receiver v = 3.

order to determine the survivor path metrics at time (i+1). The length assigned to each of these four branches is the minimum branch metric within each of the 4 sets of 128 branch metric values given by (2.43). A block diagram of the receiver structure for the case v=3 is shown in Figure 2.2, where we note that by processing the matched filter outputs, to retain only those corresponding to the minimum branch metrics, prior to the MLSE processor, we are actually performing the add-compare-select process of the Viterbi Algorithm (VA) in two stages, the first being to choose the best path terminating in each state from each group of parallel paths and the second being to choose from the resulting subset the overall best path or survivor. Figure 2.3 shows how the survivor path can be calculated.

2.7 Conclusions

In this chapter we have derived an explicit expression for the output of a BPNL for QPSK signalling as a function of the I-Q path history p_k. We think that our representation is quite useful for satellite channels where ISI is usually not severe ($v \leq 3$). An optimum MLSE receiver structure for receiving QPSK signals over satellite channel is then developed. This optimum receiver is very complex and requires extremely large memory. However, we will see in Chapter 4 that it is sufficient, for a moderate value of v, say $v = 3$, to store only eight waveforms for each of the four filters, and that to generate the minimum branch metric value only two metric values need to be compared. It can also be shown that as v increases beyond 3 the number of filters increases rapidly, but that in any practical situation similar dramatic reductions can be made.

CHAPTER 3

MLSR ERROR PERFORMANCE

3.1 Introduction

In this Chapter, an upperbound on the probability of symbol error of the MLSR, at moderate to high SNR is developed. We are interested in finding $Pe = Pr[\hat{u}_j = u_j]$, which is the probability of symbol error. Since consecutive symbol errors are generally not independent of each other, the concept of sequence error events will be used [22,35,37] in the analysis. Error events are sequences of symbol errors that intuitively are short compared with the mean time between them and that occur independently of each other.

We also obtain, a simplified expression of an upperbound on the probability of symbol error of MLSR, for the case when single error events are dominant. Our analysis is an extension of the corresponding analysis for the BPSK signalling over nonlinear channels [30].

3.2 Error Events

To evaluate the performance of the MLSR receiver realized by a Viterbi Algorithm, we note that an error will occur if for a given correct path due to the transmitted sequence $\{u_k; k = 0, 1, 2, \ldots\}$, the Viterbi Algorithm chooses another path through the trellis, corresponding to a maximum likelihood sequence $\{\hat{u}_k; k = 0, 1, 2 \ldots\}$. We define state $\hat{S}_k = (\hat{u}_{k-v}, \ldots \hat{u}_{k-1})$ as a maximum likelihood estimate of actual state $S_k = (u_{k-v}, \ldots u_{k-1})$ at time k. The maximum likelihood sequence $\{\hat{u}_k; k = 0, 1, \ldots\}$ results in a sequence of states $\{\hat{S}_k; k = 0, 1, \ldots\}$, where we let $\{S_k; k = 1, 2, \ldots\}$ be the actual states generated by the transmitted data sequence $\{u_k; k = 0, 1, \ldots\}$.

Let us now suppose that the Viterbi Algorithm chooses some path, namely that with the largest metric, through the trellis diagram. This path will coincide with the correct transmitted path at any state as shown in Fig. 3.1. Those segments where two paths diverge at some point k, and remerge for the first time at k_2, correspond to error events. Following [22,25,38], an error occurs whenever $\{S_k\}$ and $\hat{S}_k\}$ are not the same over a finite interval. In particular, an error event occurs whenever there exists a k_1 and k_2 such that

$$\begin{aligned} \hat{S}_{k_1} &= S_{k_1} \\ \hat{S}_k &\neq S_k \quad k = k_1 + 1, \ldots k_2 - 1 \\ \hat{S}_{k_2} &= S_{k_2} \end{aligned} \tag{3.1}$$

This error event is represented by a state flow graph as shown in Fig. 3.2. The number of times the actual state S_k and the estimated state $\hat{S}_k$ are not the same is defined as the length of an error event and we denote it by n_e. For the above error event that starts at k_1 and ends at k_2, the length is $n_e = k_2 - k_1 - 1$. Clearly the smallest length of an error event is $n_e \geq v$. Since $\hat{S}_{k_1} = S_{k_1}$, and $\hat{S}_{k_2} = S_{k_2}$,

we have

$$\begin{aligned} \hat{u}_k = u_k \ , \quad & k_1 - v \leq k \leq k_1 - 1 \\ & k_2 - v \leq ; k \leq ; k_2 - 1 \end{aligned}$$

from the definition of S_k. However, $\hat{u}_{k_1} = u_{k_1}$ and $\hat{u}_{k_2-v-1} \neq u_{k_2-v-1}$. Hence, we may alternatively define an error event ε as

$$\varepsilon = [K_1; \{\hat{u}_k - u_k\}_{K_1}^{K_2-v-1}] = [K_1; \{\hat{u}_k - u_k\}_{K_1}^{K_1+n_e-v}] \tag{3.2}$$

Let $$\{e_k\} = \{\hat{u}_k\} - \{u_k\}$$

Then

$$\varepsilon = [K_1; \{e_K\}_{K_1}^{K_1+n_e-v}] \tag{3.3}$$

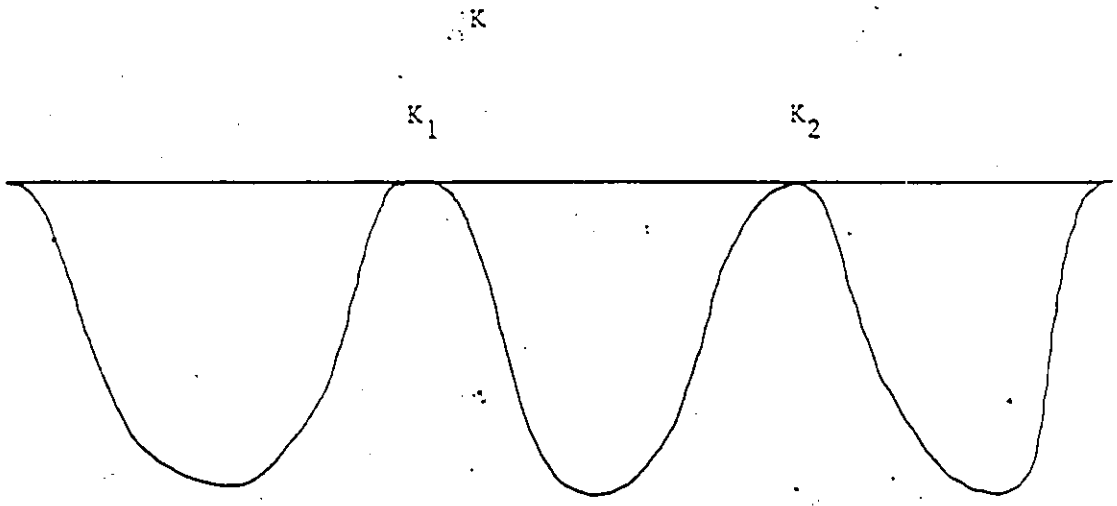

Fig. 3.1 Correct path and incorrect path chosen by VA.

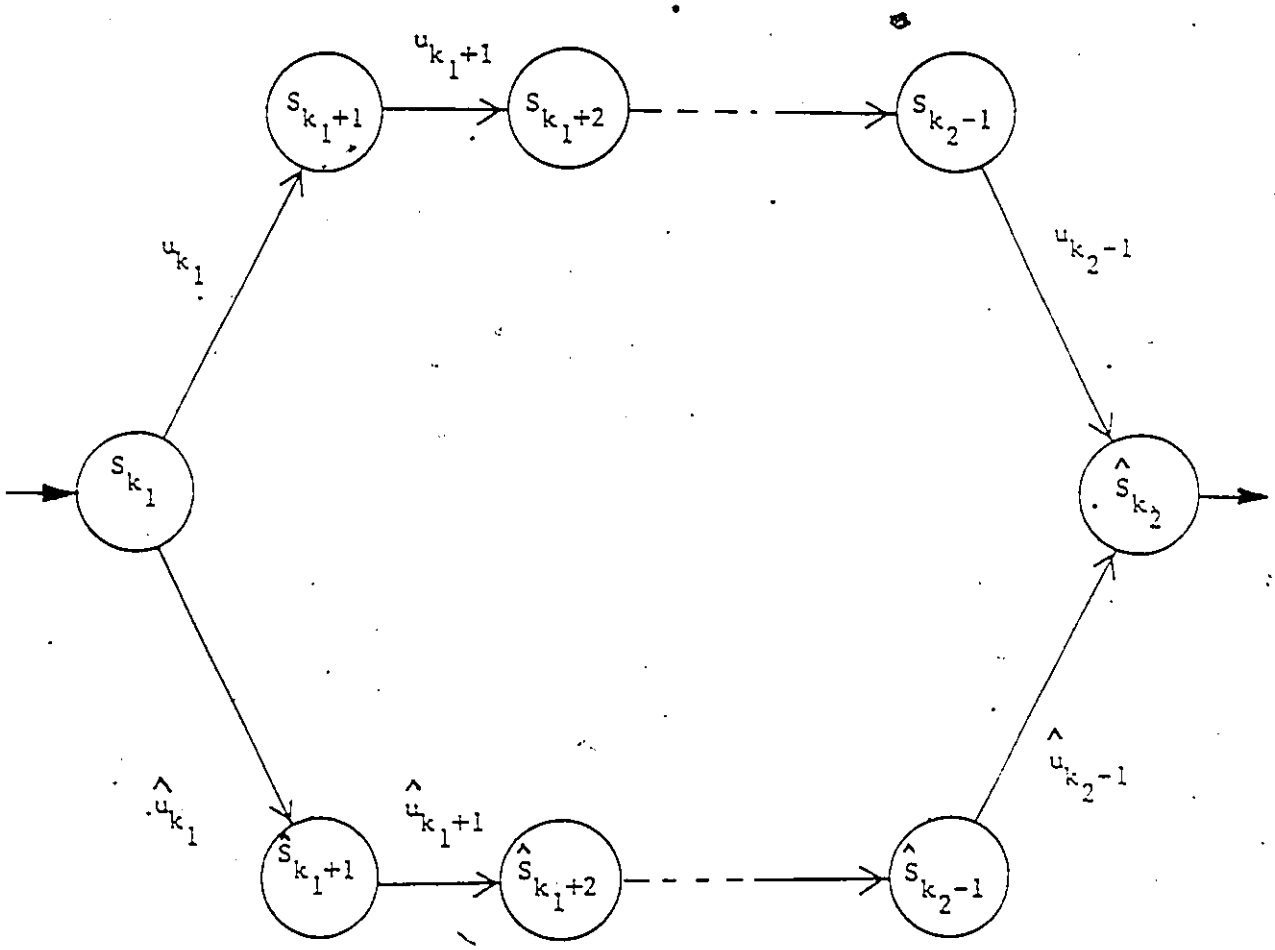

Fig. 3.2 An error event at time k_1.

where $k_1 + n_c - v$ is the last place of disagreement after k_1 prior to the next segment of at least v consective symbol agreements. Let us denote the alphabet set by A. For the special case of QPSK transmission,

$$A = \{\pm 1, \pm j\}$$

3.3 Probability of an Error Event

In this section we will develop an upperbound on the Probability P(ε) of a particular error event ε with an error sequence

$$\{e_i\}_{K_1}^{K_1+n_c-v}$$

which starts at K_1. Let us first define the set of allowable state sequence segments

$$\{S_i\}_{K_1}^{K_1+n_c+1}$$

as

$$S_c = \left\{ \{S_i\}_{K_1}^{K_1+n_c+1} \;\middle|\; \{S_i\}_{K_1}^{K_1+n_c+1} \overset{1-1}{\longleftrightarrow} \{u_i\}_{K_1-v}^{K_1+n_c} \right.$$

$$\left. \text{such that } (u_i + e_i) \in A,\ K_1 \le i \le K_1 + n_c - v \right\} \tag{3.4}$$

For Error event ε to happen, two subevents must occur:

$$\varepsilon 1:\ \{u_i\}_{K_1-v}^{K_1+n_c+1} \overset{1-1}{\longleftrightarrow} \{S_i\}_{K_1}^{K_1+n_c+1} \in S_c$$

and

ε2: the noise terms are such that $\{u_i\}_{K_1-v}^{K_1+n_c} + \{e_i\}_{K_1}^{K_1+n_c-v}$ has maximum likelihood

Then we can write

$$P(\varepsilon) = \sum_{\{S_i\} \in S_c} P\left(\{S_i\}_{K_1}^{K_1+n_c+1}\right) P\left(\varepsilon_2 \,|\, \{S_i\}_{K_1}^{K_1+n_c+1}\right) \tag{3.5}$$

There is no easy way to find

$$P\left(\varepsilon_2 \middle| \{S_i\}_{K_1}^{K_1+n_c+1}\right)$$

and so we introduce the subevent

ε_2^1: the noise terms are such that $\{u_i\}_{K_1-v}^{K_1+n_c} + \{e_i\}_{K_1}^{K_1+n_c-v}$ has greater likelihood than

$\{u_i\}_{K_1-v}^{K_1+n_c}$ but not necessarly maximum likelihood. Clearly

$$\varepsilon_2^1 \supset \varepsilon_2.$$

Hence $P(\varepsilon)$ can be written as

$$P(\varepsilon) \leq \sum_{\{S_i\}} P\left(\{S_i\}_{K_1}^{K_1+n_c+1}\right) P\left(\varepsilon_2^1 \middle| \{S_i\}_{K_1}^{K_1+n_c+1}\right) \tag{3.6}$$

For $u_i \in A$, i.e QPSK signalling, we can say that

$$\begin{aligned} \text{card}(S_c) &= M^{n_c+v+1-W_H(\varepsilon)} \\ P(\{S_i\}) &= M^{-(n_c+v+1)} \end{aligned} \tag{3.7}$$

where $M = 4$

and Card (S_c) = cardinality of the set S_c

$W_H(\varepsilon)$ = Hamming weight of the error event ε

The event ε_2^1 occurs if

$$J_1\left(\{u_i\}_{K_1-v}^{K_1+n_c} + \{e_i\}_{K_1}^{K_1+n_c-v}\right) \leq J_1\left(\{u_i\}_{K_1-v}^{K_1+n_c}\right) \tag{3.8}$$

In appendix A, we show that for the case $v = 3$, equation (3.8) is equivalent to the inequality

$$2\mathrm{Re}\left\{\sum_i \left[Y_i^1 n_i^1 + Y_i^2 n_i^{31} + Y_i^3 n_i^{32} + Y_i^4 n_i^{33}\right]\right\} \gtrless$$

$$\mathrm{Re}\left\{\sum_i \sum_k \left[Y_i^1 Y_k^{1*} S_{i-k}^{1,1} + Y_i^2 Y_k^{2*} S_{i-k}^{31,31}\right.\right.$$

$$+ Y_i^{3*} Y_k^3 S_o^{32,32}\delta_{i,k} + Y_i^{4*} Y_i^4 S_o^{33,33}\delta_{i,k}$$

$$+ 2\left(Y_i^{1*} Y_k^2 S_{i-k}^{1,31} + Y_i^{1*} Y_i^3 S_{i-k}^{21,32} + Y_i^{1*} Y_l^4 S_{i-k}^{1,33}\right.$$

$$\left.\left.\left. + Y_i^{2*} Y_k^3 S_{i-k}^{31,32} + Y_i^{2*} Y_i^4 S_{i-k}^{31,33} + Y_i^{3*} Y_i^4 S_{i-k}^{32,33}\delta_{i,k}\right)\right]\right\} \tag{3.9}$$

where

$$Y_i^1 = e^{j(\phi_i + e_i)} - e^{j\phi_i}$$

$$Y_i^2 = (\mathrm{I})_{\phi_i + e_i} - (\mathrm{I})_{\phi_i}$$

$$Y_i^3 = (\mathrm{II})_{\phi_i + e_i} - (\mathrm{II})_{\phi_i}$$

$$Y_i^4 = (\mathrm{III})_{\phi_i + e_i} - (\mathrm{III})_{\phi_i}$$

and $n_i^\ell = \langle n(t), f^{(\ell)}\{(t - iT), A\}\rangle$, $\ell = 1, 31, 32, 33$

Similar results may be obtained for other values of v. From this it is clear that the left hand side of (3.9) is a gaussian random variable with mean zero and variance

$$\sigma^2\left(\varepsilon : \{S_i\}_{K_1 - v}^{K_1 + n_c + 1}\right) = 2 N_o d^2\left(\varepsilon : \{S_i\}_{K_1 - v}^{K_1 + n_c + 1}\right) \tag{3.10}$$

where

$$d^2\left(\varepsilon: \{S_i\}_{K_1-\nu}^{K_1+n_c+1}\right) = 2R_e\left\{\sum_i \sum_k \left[Y_i^1 Y_k^{1*} S_{i-k}^{1,1} + Y_i^2 Y_k^{2*} S_{i-k}^{31,31}\right.\right.$$

$$+ Y_i^{3*} Y_k^3 S^{32,32}\delta_{i,k} + Y_i^{4*} Y_i^4 S^{33,33}\delta_{i,k} + 2\left(Y_i^{1*} Y_k^2 S_{i-k}^{1,31}\right.$$

$$+ Y_i^{1*} Y_i^3 S_{i-k}^{1,32} + Y_i^{4*} Y_1^3 S_{i-k}^{1,33} + Y_i^{2*} Y_k^3 S_{i-k}^{31,32}$$

$$\left.\left.\left.+ Y_i^{2*} Y_k^4 S_{i-k}^{31,33} + Y_i^{3*} Y_i^4 S_{i-k}^{32,33}\delta_{i-k}\right)\right]\right\} \tag{3.11}$$

From (3.8) to (3.11) it is clear that

$$P\left(\varepsilon_2^1 | \{S_i\}_{K_1}^{K_1+n_c+1}\right)$$

is the probability that a gaussian variable with mean zero and variance,

$$\sigma^2\left(\varepsilon: \{S_i\}_{K_1}^{K_1+n_c+1}\right), \text{ exceeds } d^2\left(\varepsilon: \{S_i\}_{K_1}^{K_1+n_c+1}\right)$$

That is we may write

$$P\left(\varepsilon_2^1 | \{S_i\}_{K_1}^{K_1+n_c+1}\right) = Q\left[(2N_o)^{-1/2} d\left(\varepsilon: \{S_i\}_{K_1}^{K_1+n_c+1}\right)\right] \tag{3.12}$$

where

$$Q(x) = \frac{1}{\sqrt{2\pi}} \int_x^\infty \exp(-t^2/2)\,dt$$

Substituting (3.12) into (3.6), we get

$$P(\varepsilon) \le P\left(\{S_i\}_{K_1}^{K_1+n_c+1}\right) \sum_{\{S_i\} \in S_c} Q\left[(2N_o)^{-1/2} d\left(\varepsilon: \{S_i\}_{K_1}^{K_1+n_c+1}\right)\right] \tag{3.13}$$

Defining $\overline{d(\varepsilon)}$ by the equality, we may write

$$Q\left[(2N_o)^{-1/2}\ \overline{d(\varepsilon)}\right] = \frac{1}{\text{Card}\,(S_c)} \sum_{\{S_i\} \in S_c} Q\left[(2N_o)^{-1/2} d\left(\varepsilon: \{S_i\}_{K_1}^{K_1+n_c+1}\right)\right] \tag{3.14}$$

Then, since $Q(\cdot)$ is a monotonic function of its argument, we can find $\overline{d(\varepsilon)}$ as a unique solution of the transcendental equation (3.14). Therefore, after substituting from (3.7) we can write (3.13) as

$$P(\varepsilon) = \frac{1}{M^{W_H(\varepsilon)}} Q\left[(2N_o)^{-1/2}\ \overline{d(\varepsilon)}\right] \tag{3.15}$$

3.4 Probability of Symbol Error

In order to bound the probability of an error, let E be the set of all error events ε starting at time K_1. Since the events ε are mutually exclusive,

$$P(E) = \sum_{\varepsilon \in E} P(\varepsilon) \le \sum_{\varepsilon \in E} \frac{1}{M^{W_H(\varepsilon)}} Q\left[(2 N_o)^{-1/2} \overline{d(\varepsilon)} \right]. \tag{3.16}$$

Now let D be the set of all possible $d(\varepsilon)$. For each $d \in D$, let E_d be the subset of all error events for which $d(\varepsilon) = d$. Then, from (3.16) we have

$$P(E) \le \sum_{d \in D} Q\left(\frac{d}{\sqrt{2 N_o}} \right) \left| \sum_{\varepsilon \in E_d} \frac{1}{M^{W_H(\varepsilon)}} \right| \tag{3.17}$$

To compute the probability of symbol error, we use the following reasoning as given in [22,38]. An error in the K_1 position occurs if the error event begins in the K_1 position or in some previous position such that the error sequence element corresponding to the K_1 position is nonzero. Thus there are $W_H(\varepsilon)$ positions in which an error event can start and involve an error in position K_1. Now the bound that has been developed for the probability of an error event is independent of the starting index. So the upperbound on the probability of a particular error event starting at K_1 is converted to an upperbound on the probability that a particular error sequence corresponds to error in position K_1 by multiplying the former by $W_H(\varepsilon)$.

The Probability of Symbol error may then be upperbounded by

$$P_e \le \sum_{\varepsilon \in E} W_H(\varepsilon) P(\varepsilon) \le \sum_{d \in D} Q\left(\frac{d}{\sqrt{2 N_o}} \right) \sum_{\varepsilon \in E_d} \left| \frac{1}{M^{W_H(\varepsilon)}} \right| W_H(\varepsilon) \tag{3.18}$$

Because of the exponential decrease of the $Q(\cdot)$ function, this expression will be dominated at moderate to high signal-to-noise ratio by the term involving the minimum value d_{min} of d, so that we may approximate the bound on probability of symbol error as

$$P_e \le K Q\left[\frac{d_{min}}{\sqrt{2 N_o}} \right] \tag{3.19}$$

where

$$K = \sum_{\varepsilon \in E_{d_{min}}} \left[\frac{1}{M^{W_H(\varepsilon)}} \right] W_H(\varepsilon) \tag{3.20}$$

and

$$E_{d_{min}} = \left\{ \varepsilon \in E \;\middle|\; \bar{d}(\varepsilon) = d_{min} \right\}$$

3.5 Single Error Events

In this section we first derive the sufficient conditions for single-error events to be the dominating source of error and then obtain a simplified expression for the probability of symbol error.

Let

$$d_o \triangleq \overline{d(\varepsilon_o)}, \text{ where } \varepsilon_o = \{K_1; e_{K_1} = 0, e_i = 0 \text{ if } i = K_1\}$$

Then ε_o will be the dominating source of error at moderate to high signal to noise ratio, if multiple-error events with distance $\overline{d(\varepsilon)}$ smaller than d_o do not exist. In the first case, e_i's in the definition of ε are constrained to take non-zero values. We now write the following decomposition of $d^2(\varepsilon; \{S_i\})$ for $v = 3$ from (3.11):

$$d^2(\varepsilon;\{S_i\}) = d^2(\varepsilon_o;\{S_i\}) + \mathrm{Re}\left\{ \sum_{i=K_1+1}^{K_1+n_\varepsilon-\nu} \sum_{\ell} [Y_i^1 Y_{i-\ell}^{1*} S_\ell^{1,1}] \right.$$

$$+ 2 \sum_{i=K_1+\nu}^{K_1+n_\varepsilon-\nu} \sum_{\ell} [Y_i^{1*} Y_{i-\ell}^{2} S_\ell^{1,31} + Y_i^{1*} Y_{i-\ell}^{3} S_\ell^{1,32} + Y_i^{1*} Y_{i-\ell}^{4} S_\ell^{31,33}]$$

$$+ 2 \sum_{i=K_1+\nu}^{K_1+n_\varepsilon-1} \sum_{\ell} [Y_i^{2*} Y_{i-\ell}^{3} S_\ell^{31,32} + Y_i^{2*} Y_{i-\ell}^{4} S_\ell^{31,33}]$$

$$+ \sum_{i=K_1+\nu}^{K_1+n_\varepsilon-1} \sum_{\ell} [Y_i^{2} Y_{i-\ell}^{2*} S_\ell^{31,32}] + \sum_{i=K_1+\nu+1}^{K_1+n_\varepsilon} Y_i^{3*} Y_{i-\ell}^{3} S_\ell^{32,32}]$$

$$\left. + Y_i^{4*} Y_{i-\ell}^{4} S_\ell^{33,33} + 2 Y_i^{3*} Y_i^{4} S^{32,33}] \right\} \tag{3.21}$$

where

$$d^2(\varepsilon_o;\{S_i\}) = Y_{K_1}^{1} Y_{K_1}^{1*} S_o^{1,1} + \mathrm{Re}\left\{ 2\, Y_{K_1}^{1*} \sum_{\ell} [Y_{K_1-\ell}^{2} S_\ell^{1,31} Y_{K_1-\ell}^{3} S_\ell^{1,32} \right.$$

$$+ Y_{K_1-\ell}^{4} S_\ell^{1,33}] + 2 \sum_{i=K_1}^{K_1+\nu-1} \sum_{\ell} [Y_i^{2*} Y_{i-\ell}^{3} S_\ell^{31,32} + Y_i^{2*} Y_{i-\ell}^{4} S_\ell^{31,33}]$$

$$\left. + \sum_{i=K_1}^{K_1+\nu} [(Y_i^{3})^* Y_i^{3} S^{32,32} + (Y_i^{4})^* (Y_i^{4}) S^{33,33} + 2 Y_i^{3*} (Y_i^{4}) S^{32,33}] \right\} \tag{3.22}$$

Now

$$d^2(\varepsilon;\{S_i\}) = d^2(\varepsilon_o;\{S_i\}) + \sum_{i=K_1+1}^{K_1+n_c-v} [Y_i^1 Y_i^{1*} S_o^{1,1} + \mathrm{Re}\{\sum_{\ell}$$

$$+ Y_i^1 Y_{i-\ell}^{1*} S_\ell^{1,1}\}] + \mathrm{Re}\left\{2 \sum_{i=K_1+1}^{K_1+n_c-v} \sum_{\ell} [Y_i^{1*} Y_{i-\ell}^2 S_\ell^{1,31}\right.$$

$$\left. + Y_i^{1*} Y_{i-\ell}^3 S_\ell^{1,32} + Y_i^{1*} Y_{i-\ell}^4 S_\ell^{1,33}]\right\} + \sum_{i=K_1+v}^{K_1+n_c-1} [Y_i^2 Y_i^{2*} S_o^{31,31}$$

$$+ \mathrm{Re}\left\{\sum_{\ell} Y_i^2 Y_{i-\ell}^{2*} S_\ell^{31,31}\}\right] + \mathrm{Re}\left\{2 \sum_{i=K_1+v}^{K_1+n_c-1} \sum [Y_i^{2*} Y_{i-\ell}^3 S_\ell^{31,32} + Y_i^{2*} Y_{i-\ell}^4 S_\ell^{31,33}]\right\}$$

$$+ \left\{\sum_{i=K_1+v+1}^{K_1+n_c} [(Y_i^3)^* (Y_i^3) S^{32,32} + Y_i^{4*} Y_i^4 S^{33,33} + 2(Y_i^3)^* (Y_i^3) S^{32,33}\right\} \tag{3.23}$$

or

$$d^2(\varepsilon;\{S_i\}) \geq d^2(\varepsilon_o;\{S_i\}) + \sum_{i=K_1+1}^{K_1+n_c-v} \left[Y_i^1 Y_i^{1*} S_o^{1,1} - |\mathrm{Re}\{\sum_{\ell} Y_i^1 Y_{i-\ell}^{1*} S_\ell^{1,1}\}|\right]$$

$$- 2 \sum_{i=K_1+1}^{K_1+n_c-v} \sum_{\ell} \left[|\mathrm{Re}\{Y_i^{1*} Y_{i-\ell}^2 S_\ell^{1,31}\}| + |\mathrm{Re}\{Y_i^{1*} Y_{i-\ell}^3 S_\ell^{1,32}\}|\right.$$

$$\left. + |\mathrm{Re}\{Y_i^{1*} Y_{i-\ell}^4 S_\ell^{1,33}\}|\right] + \sum_{i=K_1+v}^{K_1+n_c-1} [Y_i^2 Y_i^{2*} S_o^{31,31}$$

$$- \mathrm{Re}\left\{\sum_{\ell} Y_i^2 Y_{i-\ell}^{2*} S_\ell^{31,31}\}\right] - 2 \sum_{i=K_1+v}^{K_1+n_c-1} \sum_{\ell} \left[|\mathrm{Re}\{Y_i^{2*} Y_{i-\ell}^3 S_\ell^{31,32}\}|\right.$$

$$\left. + |\mathrm{Re}\{Y_i^{2*} Y_{i-\ell}^4 S_\ell^{31,33}\}|\right] + \sum_{i=K_1+v+1}^{K_1+n_c} \left[(Y_i^3)^* (Y_i^3) S^{32,32}\right. \tag{3.24}$$

$$\left. + Y_i^{4*} Y_i^4 S^{33,33} - 2|\mathrm{Re}\{(Y_i^3)^* (Y_i^3) S^{32,33}\}|\right].$$

Observing that

$$|Y_i^1 Y_{i-\ell}^{1*}| \le Y_i Y_i^* \le 4$$

and

$$|\mathrm{Re}\left\{ \sum_{\ell}{}' Y_i^1 Y_{i-\ell}^{1*} S_\ell^{1,1} \right\}| \le 4 \sum_{\ell}{}' |S_\ell^{1,1}|$$

we can write (3.24) as

$$d^2(\varepsilon; \{S_i\}) \ge d^2(\varepsilon_o; \{S_i\}) + 4 \Bigg\{ \sum_{i=K_1+1}^{K_1+n_c-\nu} \Bigg[S_o^{1,1} - \sum_{\ell}{}' |S_\ell^{1,1}|$$

$$- 2 \sum_{\ell} [|S_\ell^{1,31}| + |S_\ell^{1,32}| + |S_\ell^{1,33}|]$$

$$+ \sum_{i=K_1+\nu}^{K_1+n_c-1} [S_o^{31,31} - \sum_{\ell}{}' |S_\ell^{31,31}| - 2 \sum_{\ell} (|S_\ell^{31,32}| + |S_\ell^{31,33}|)]$$

$$+ \sum_{i=K_1+\nu+1}^{K_1+n_c} [S^{32,32} + S^{33,33} - 2|S^{31,32}|] \Bigg\} \qquad (3.25)$$

Since the quantities inside the square brackets in (3.25) are independent of the summation indices, it is possible to write

$$d^2(\varepsilon; \{S_i\}) \ge d^2(\varepsilon_o; \{S_i\}) + 4 \sum_{i=1}^{n_c-\nu} \Bigg\{ S_o^{1,1} - S_o^{31,31} + S^{32,32} + S^{33,33}$$

$$- \sum_{\ell}{}' |S_\ell^{1,1}| - 2 \sum_{\ell} [|S_\ell^{1,31}| + |S_\ell^{1,32}| + |S_\ell^{1,33}|$$

$$- \sum_{\ell}{}' |S_\ell^{31,31}| - 2 \sum_{\ell} [|S_\ell^{31,32}| + |S_\ell^{31,33}|] - 2 S_\ell^{32,33}| \Bigg\} \qquad (3.26)$$

Now $$d^2(\epsilon; \{S_i\}) \ge d^2(\epsilon_o; \{S_i\}) \qquad (3.27)$$

if $$\{\cdot\} \ge 0$$

or

$$S_o^{1,1} + S_o^{31,31} + S^{32,32} + S^{33,33} > \sum_{\ell}' |S_\ell^{1,1}| + 2 \sum_{\ell} [|S_\ell^{1,31}| + |S_\ell^{1,32}| + |S_\ell^{1,33}|$$

$$+ \sum_{\ell}' |S_e^{31,31}| - 2 \sum_{\ell} [|S_\ell^{31,32}| + |S_\ell^{31,33}|] + 2|S_\ell^{32,33}| \tag{3.28}$$

which gives the first condition. If we now let $e_i (i = K_1$ or $K_1 + n_e - v$ by definition) assume zero values, then we can show from (3.23) by following a similar procedure, that

$$d^2(\varepsilon; \{S_i\}) \geq d^2\{\varepsilon_o; \{S_i\}\}$$

if

$$S_o^{31,31} + S^{32,32} + S^{33,33} \geq \sum_{\ell}' |S_\ell^{31,31}| + \sum [|S_\ell^{31,32}| + |S_\ell^{31,33}|] + 2|S_\ell^{32,33}| \tag{3.29}$$

which gives the second condition. When conditions in (3.28) and (3.29) are satisfied, we can state that

$$\overline{d^2(\varepsilon)} \geq \overline{d^2(\varepsilon_o)}$$

From (3.19), we can now write the expression for the probability of symbol error as

$$Pe = Q\left[\frac{do}{\sqrt{2N_o}}\right] \tag{3.30}$$

3.6 Conclusion

In this Chapter, we have derived an upperbound on the Probability of error in terms of average distance. Two sufficient conditions for single errors to be dominant, are also derived. Finally, we obtain a simplified expression for the upperbound on the probability of error of MLSE Receiver, when single-errors are dominant.

CHAPTER 4

SIMULATION OF MLSR AND DEVELOPMENT OF SUB-OPTIMUM RECEIVER

4.1 Introduction

In this Chapter, we evaluate the performance of the MSLR developed in Chapter 2, for a digital satellite communication link. The performance of the MLSR at low to moderate SNR is estimated through computer simulation. While at moderate to high SNR, where computer simulation takes too much time, the MLSR performance is estimated using the upperbound developed in Chapter 3. The problem of reducing the memory and complexity requirements of the MLSR, is also addressed in this Chapter.

Furthermore, a sub-optimum receiver structure, which approximates MLSR is developed. The performance of the sub-optimum receiver is evaluated using computer simulation. In each case the probability of error performance is compared with that of the matched filter bound attained in a linear non- bandlimited additive white gaussian noise channel.

4.2 Receiver Performance

4.2.1 The Satellite Channel Model Assumed for Simulation

In the satellite channel model, we first assume that the bandlimiting in the uplink is introduced by a fourth-order Chebyshev filter as suggested in [39]. The uplink filtering is assumed to include all filtering done at the transmitter and at the input of the satellite for $2BT = 1$, where B is the one-sided bandwidth. Its impulse response is shown in Fig. 4.1. The TWTA characteristics are typical of those used in an INTELSAT IV satellite. The coefficients

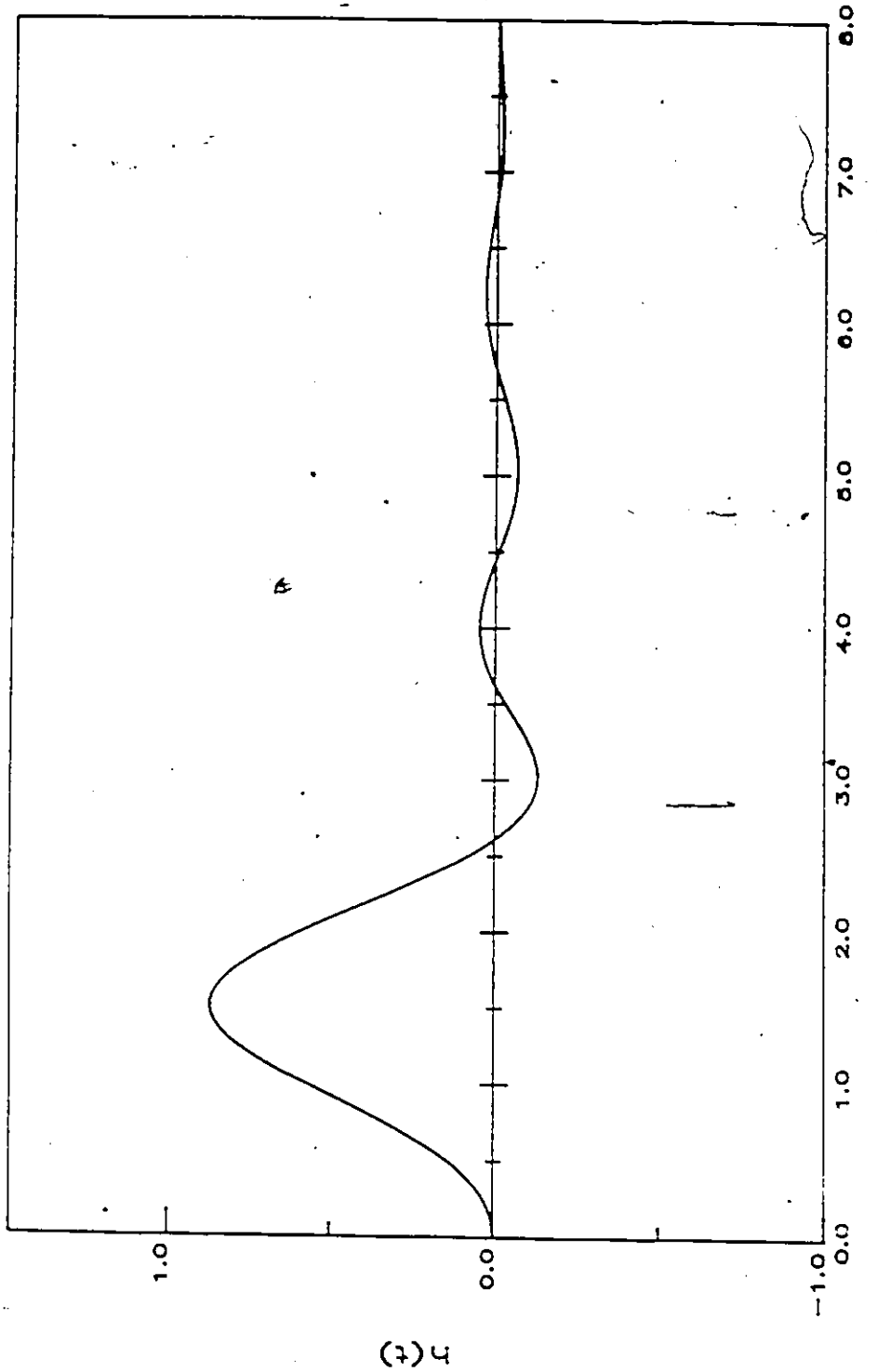

Fig. 4.1 The pulse response of a fourth-order Chebyshev filter [39], for 2BT = 1.

of the Bessel function expansion for the complex transfer characteristic G(v) exp[j α (v)] of the BPNL were obtained from [34].

4.2.2 Memory Requirements

As explained in Chapter 2, for a channel memory of v = 3, there are 128 filter responses corresponding to $g_{MF}^{(1)}\{(t-kT),p_k\}$. In order, in the simulation, to generate these responses with smaller storage, we generated and stored the generic waveforms defined as the vectors of waveform segments

$$F1(p_k) = f^{(1)}\{(t-kT), p_k\},$$

$$\text{where } p_k = p_{k+1} = p_{k+2} = p_{k+3}$$

$$F31(p_k) = f^{(31)}\{(t-kT),p_k\}, \qquad (4.1)$$

$$\text{where } p_k = p_{k+1}$$

$$F32(p_k) = f^{(32)}\{(t-kT),p_k\}$$

$$F33(p_k) = f^{(33)}\{(t-kT),p_k\}$$

Clearly, for a channel memory v = 3, there will be sixteen of each of these waveforms. The sampled waveforms $F1(p_k)$ and $F31(p_k)$ for a TWTA input back-off of 0 dB are shown in Figures 4.2(a)–(p) and 4.3(a)–(p) respectively. The other two waveforms $F32(p_k)$ and $F33(p_k)$ were found to be insignificant for the channels being considered, and were neglected in the simulation. This made it possible to generate the matched filter responses $g_{MF}^{(1)}\{(t-kT),p_k\}$ and $g_{MF}^{(31)}\{(t-kt),p_k\}$ given by (12) and (18), as a suitable combination of segments of the generic waveforms defined in (4.1). For example, to generate $f^{(1)}\{(t-kT),p_k\}$, with $p_k = 2$, $p_{k+1} = 4$, $p_k + 2 = 9$ and $p_{k+3} = 2$, we choose F1(2) in the 0 to T period, F1(4) in the T to 2T period, F1(9) in the 2T to the 3T period and F1(2) in the 3T to 4T period, where T is the symbol duration. Hence, it is sufficient to store only 16 complex waveforms each for $F1(p_k)$ and $F31(p_k)$. Furthermore, the storage requirement can be reduced by one half by

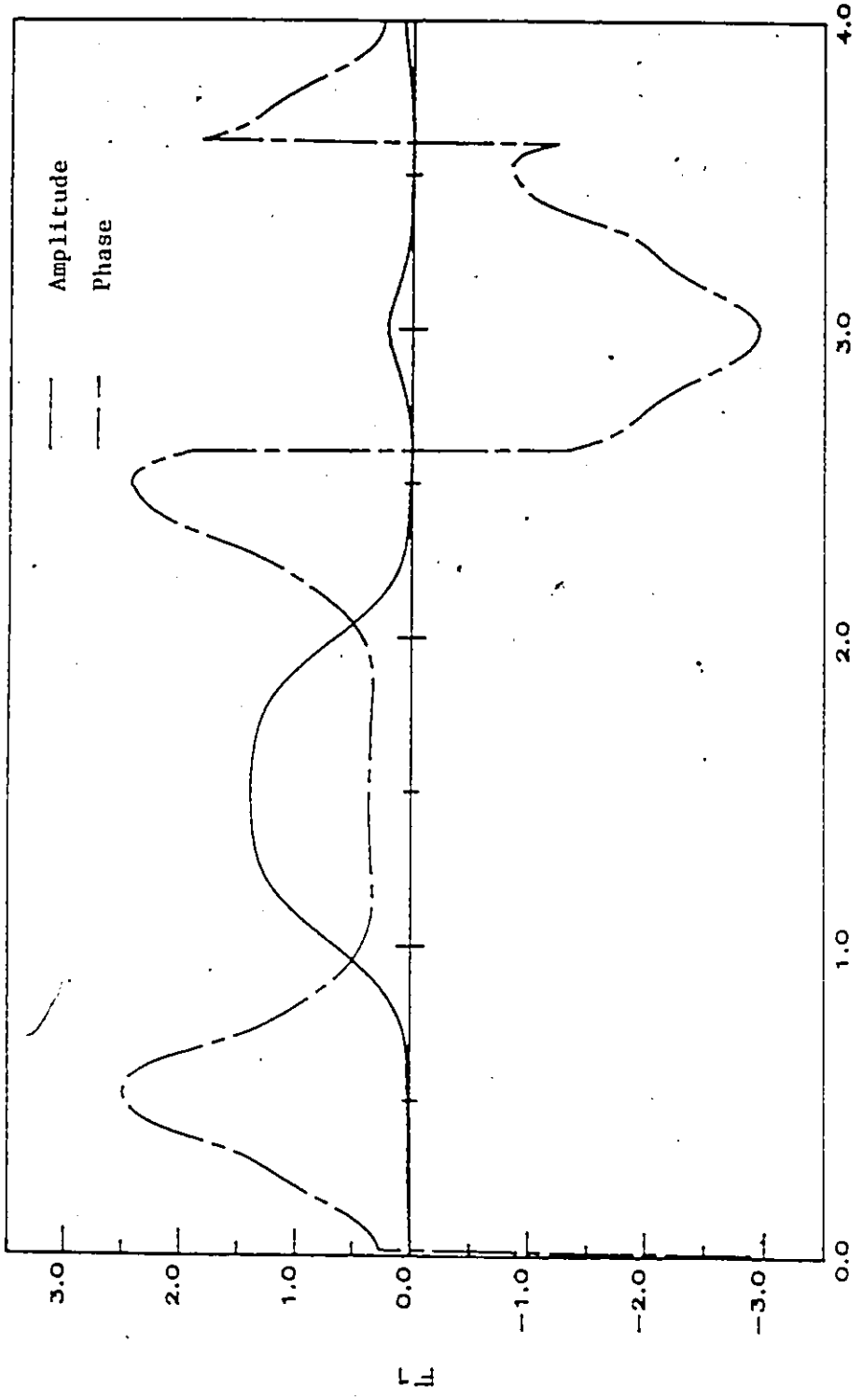

Fig. 4.2(a) The generic waveform F1(0) for TWTA input back-off of 0 dB.

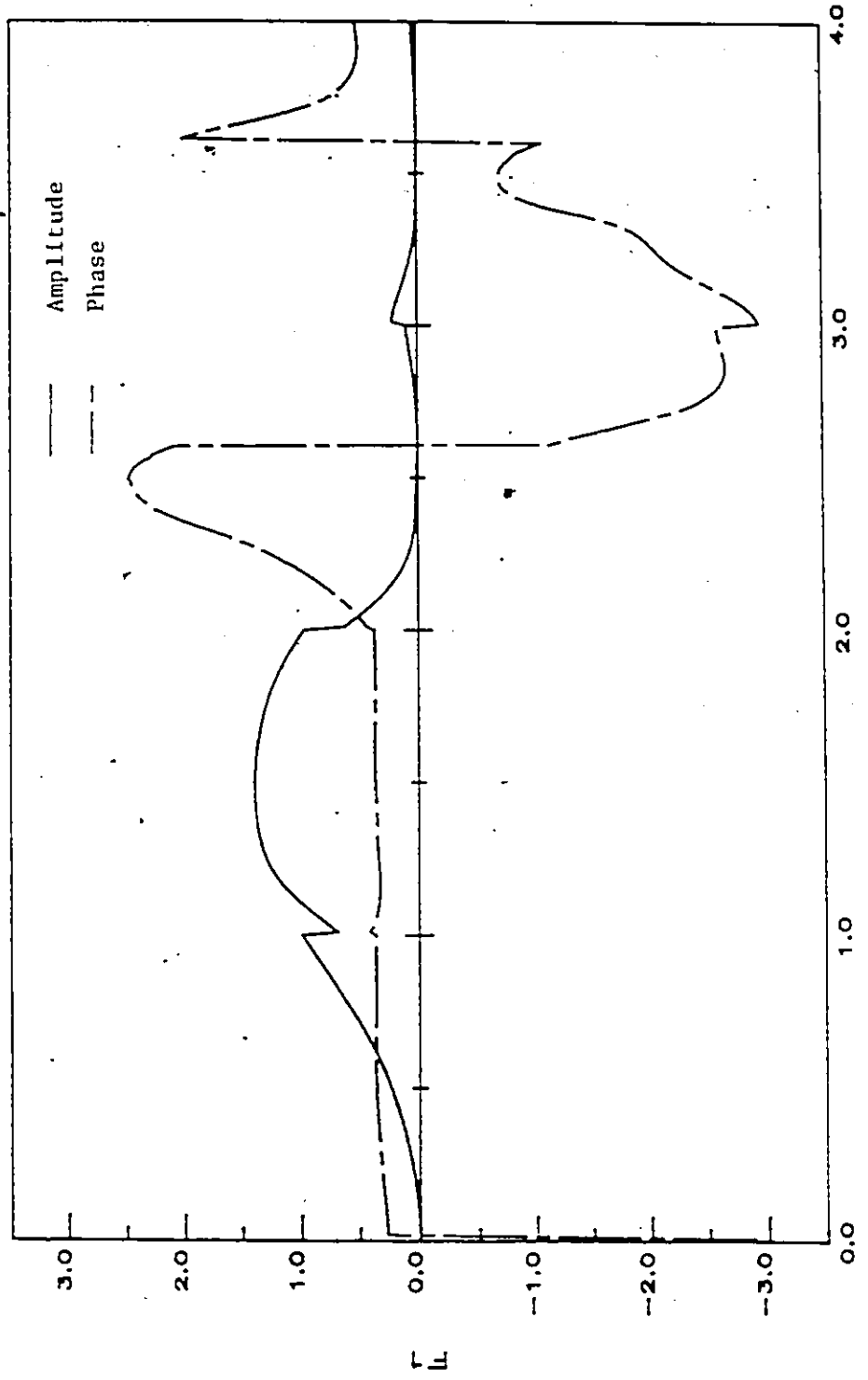

Fig. 4.2(b) The generic waveform F1(1) for TWTA input back-off of 0 dB.

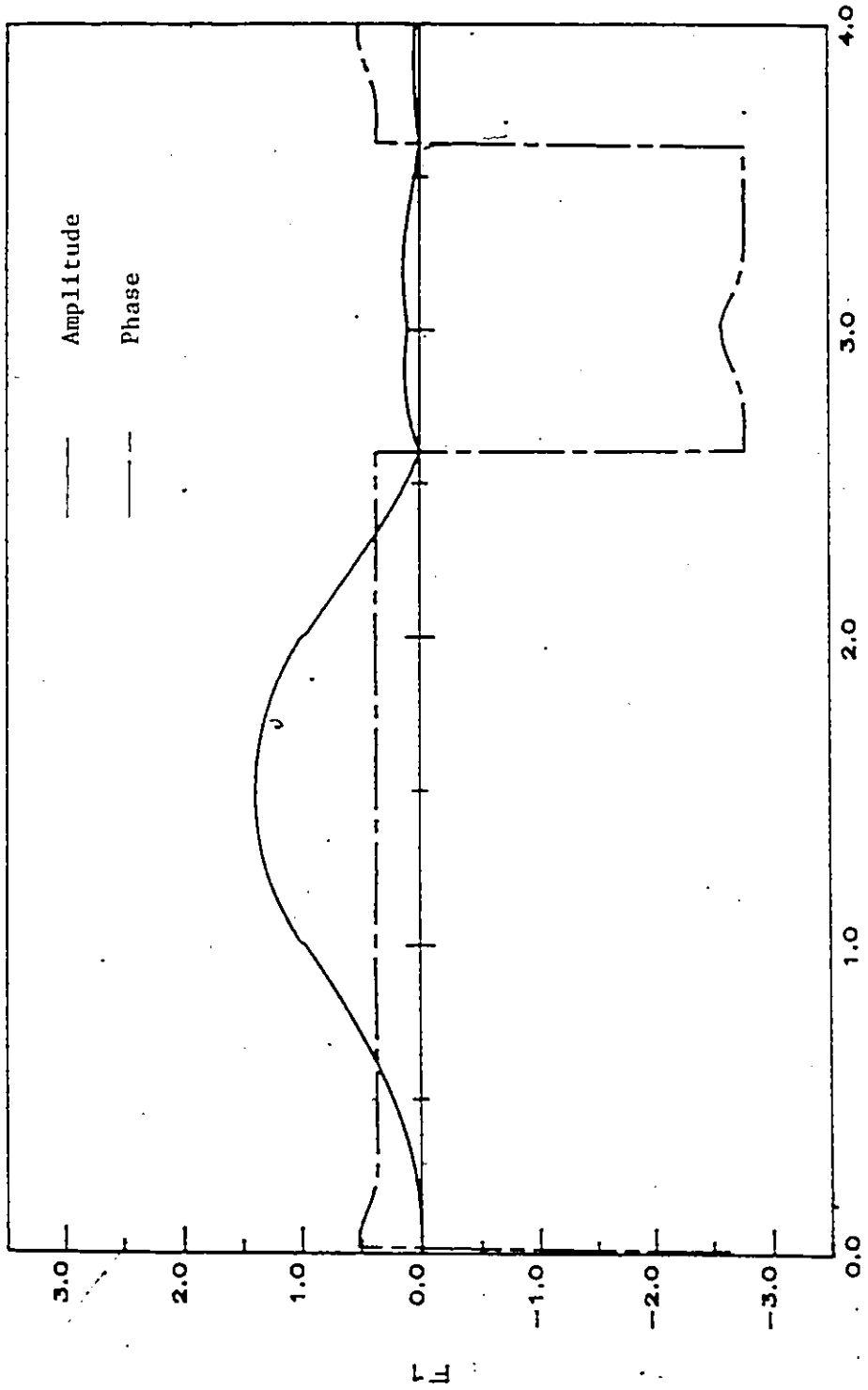

Fig. 4.2(c) The generic waveform F1(2) for TWTA input back-off of 0 dB.

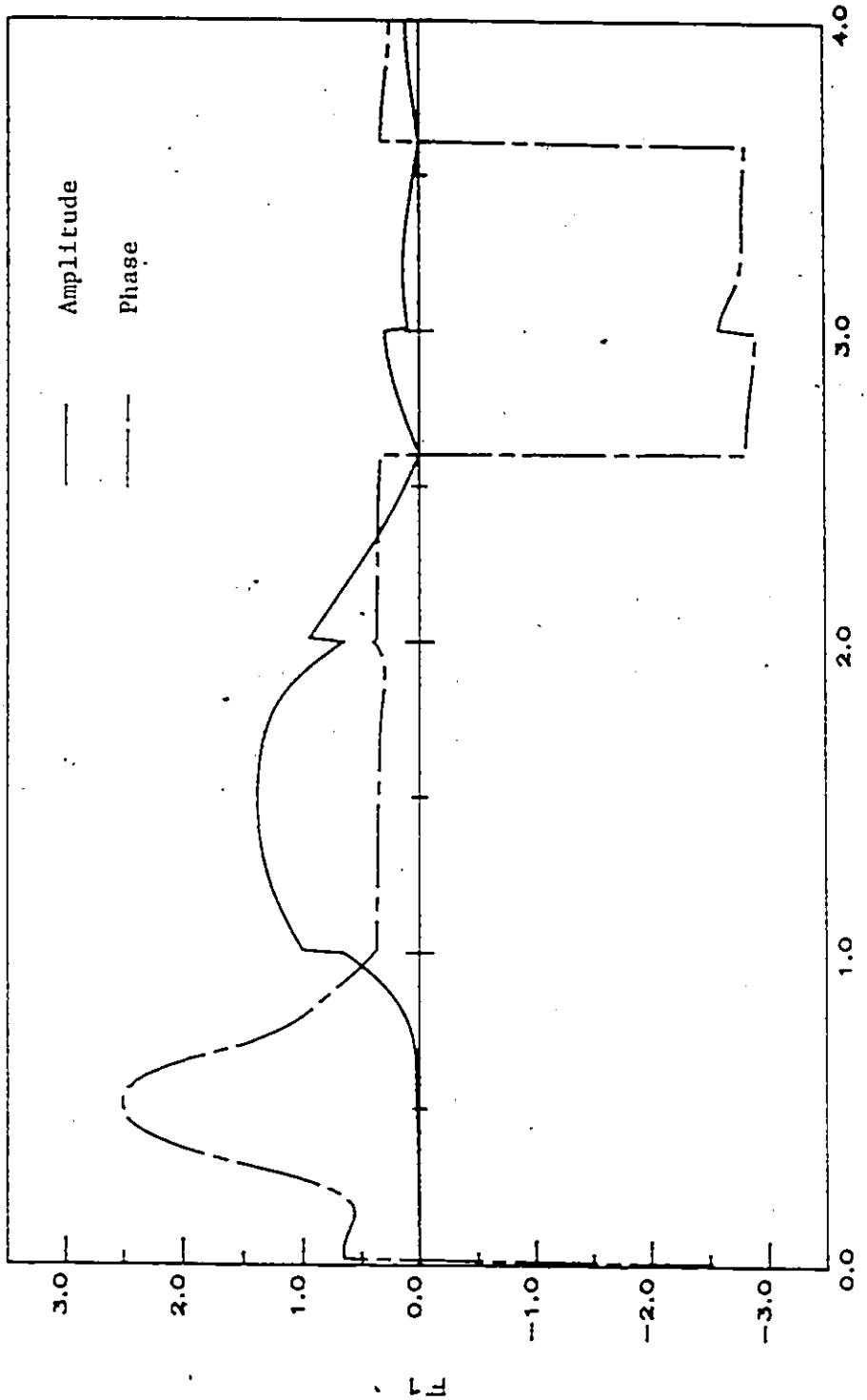

Fig. 4.2(d) The generic waveform F1(3) for TWTA input back-off of 0 dB.

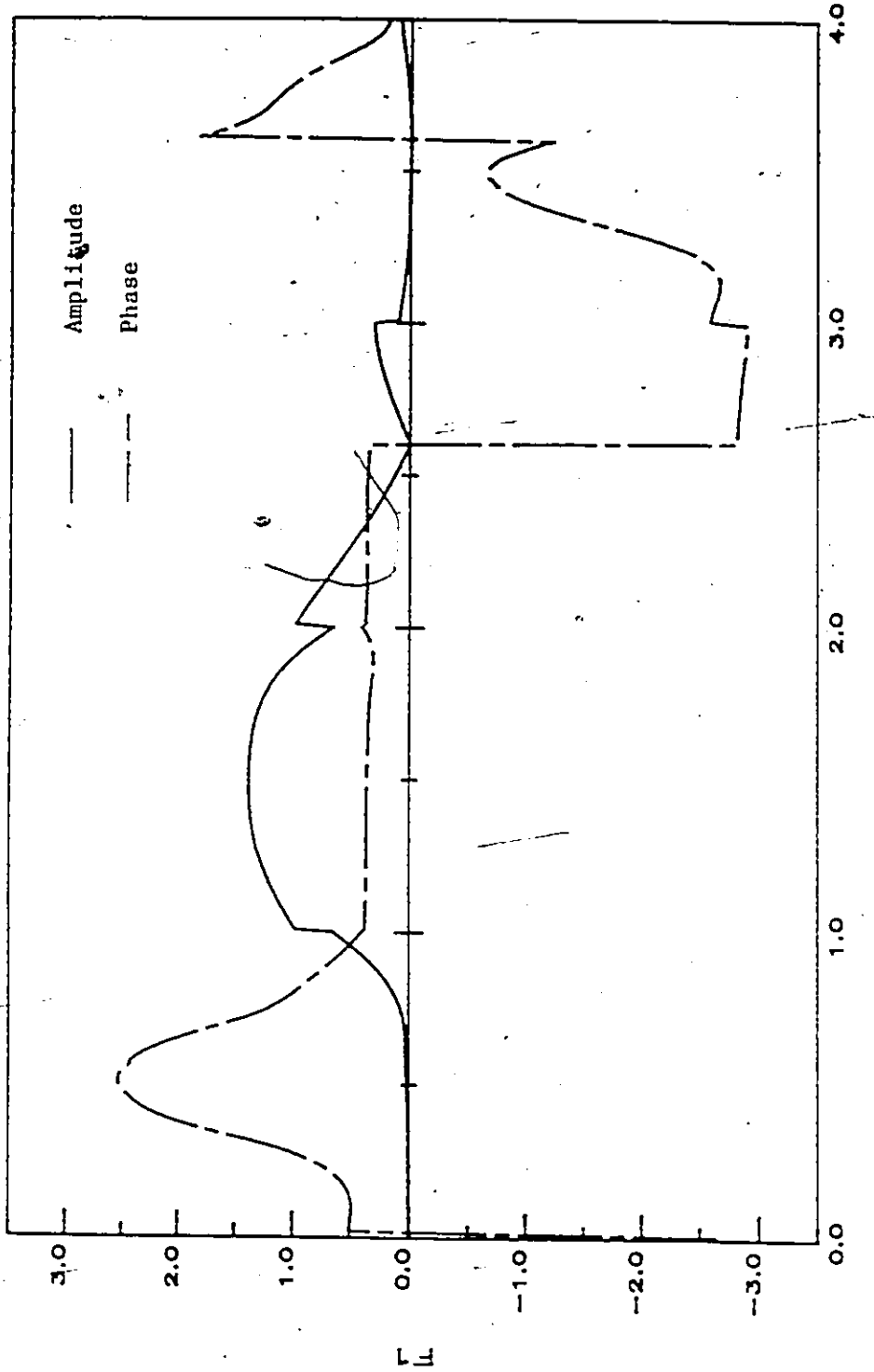

Fig. 4.2(c) The generic waveform F1(4) for TWTA input back-off of 0 dB.

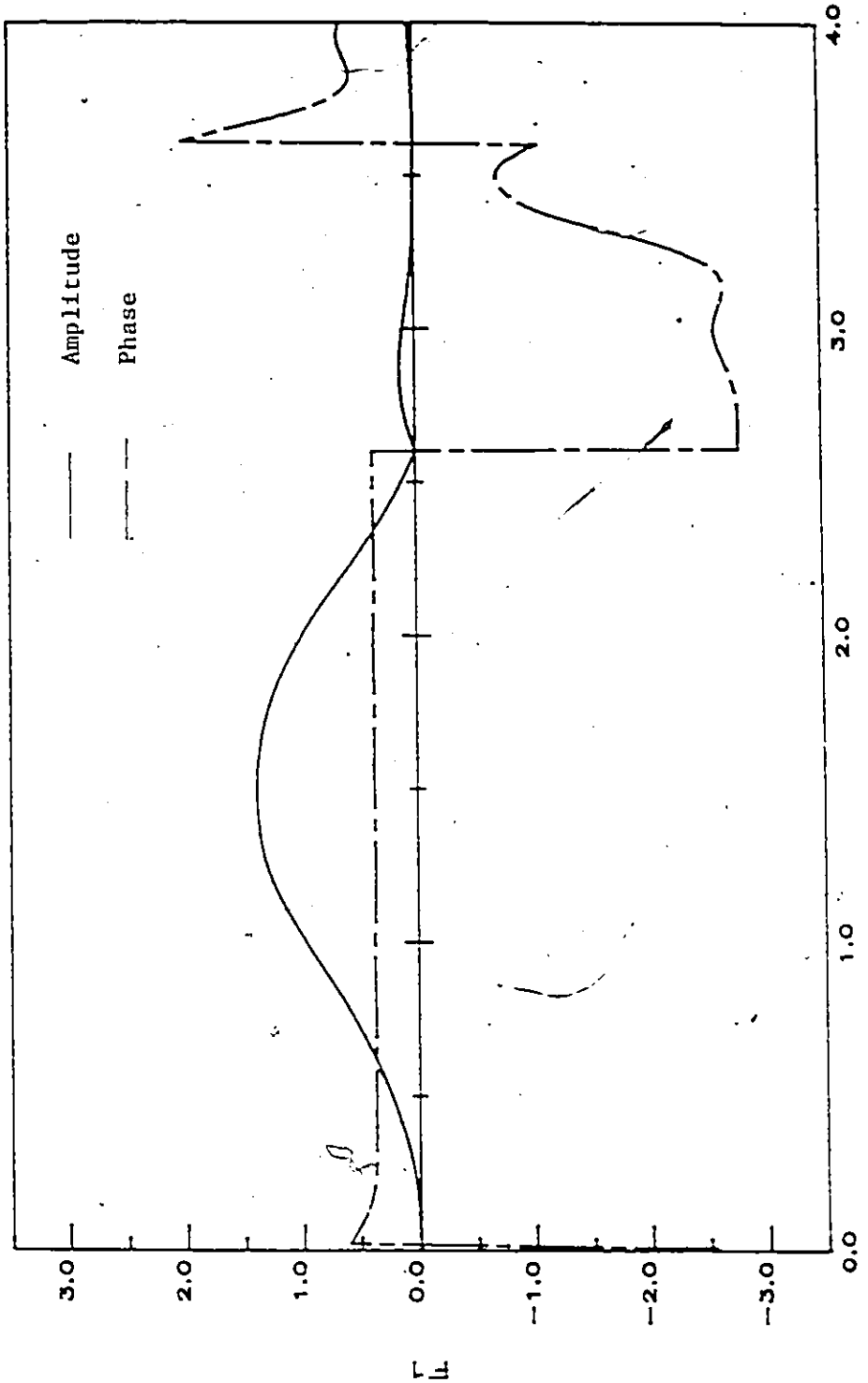

Fig. 4.2(f) The generic waveform F(5) for TWTA input back-off of 0 dB.

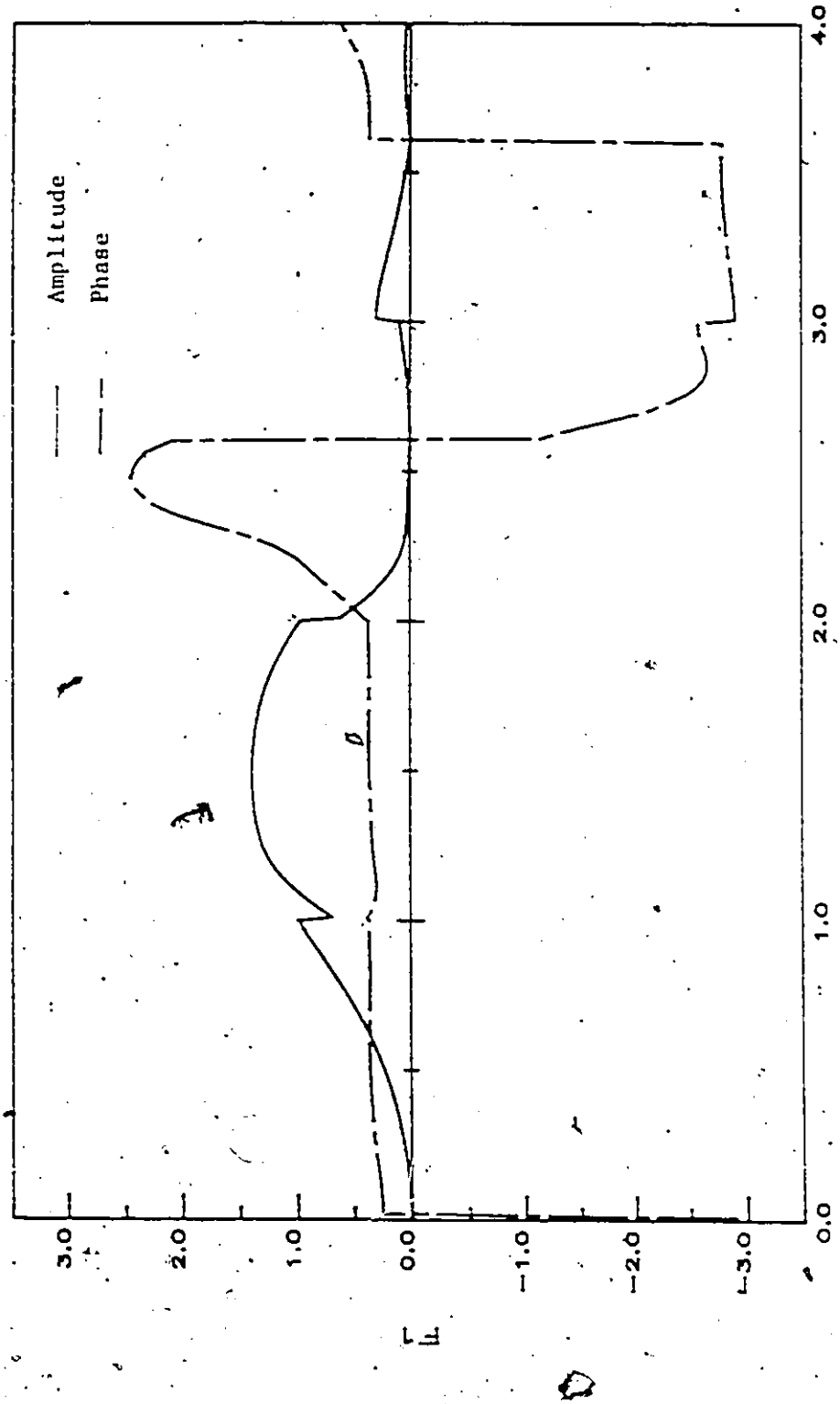

Fig. 4.2(g) The generic waveform F1(6) for TWTA input back-off of 0 dB.

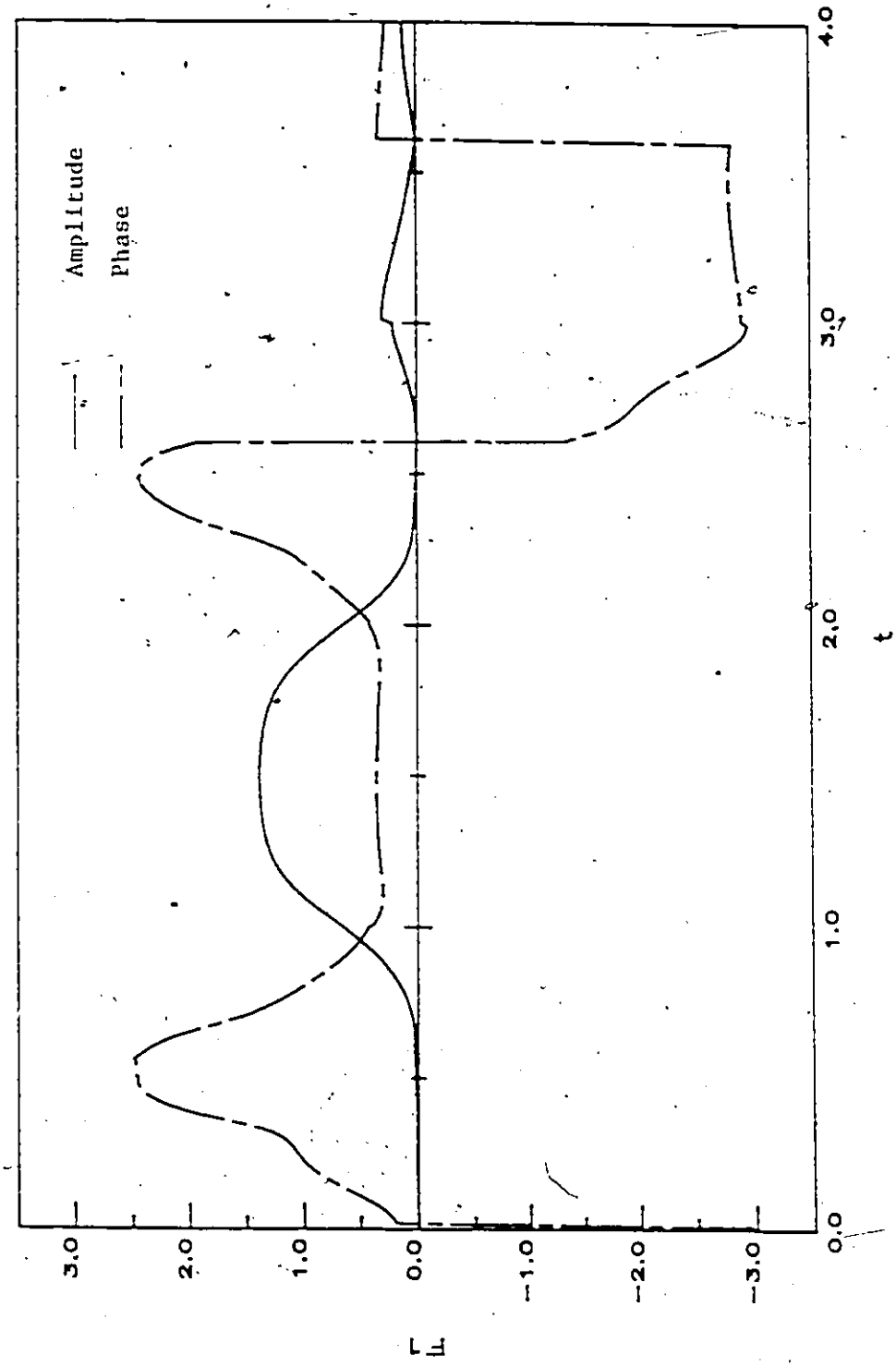

Fig. 4.2(b) The generic waveform F1(7) for TWTA input back-off of 0 dB.

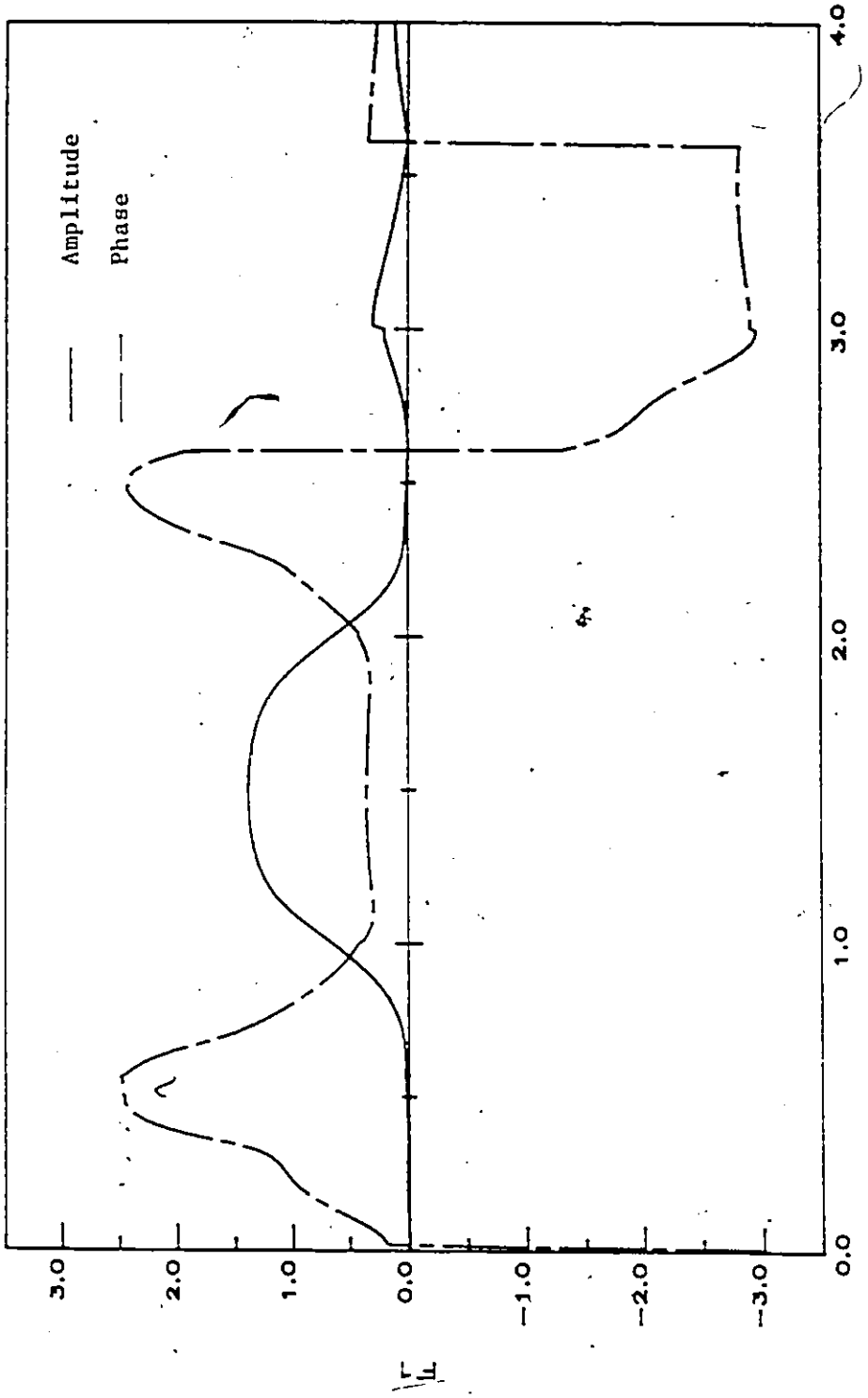

Fig. 4.2(i) The generic waveform F1(8) for TWTA input back-off of 0 dB.

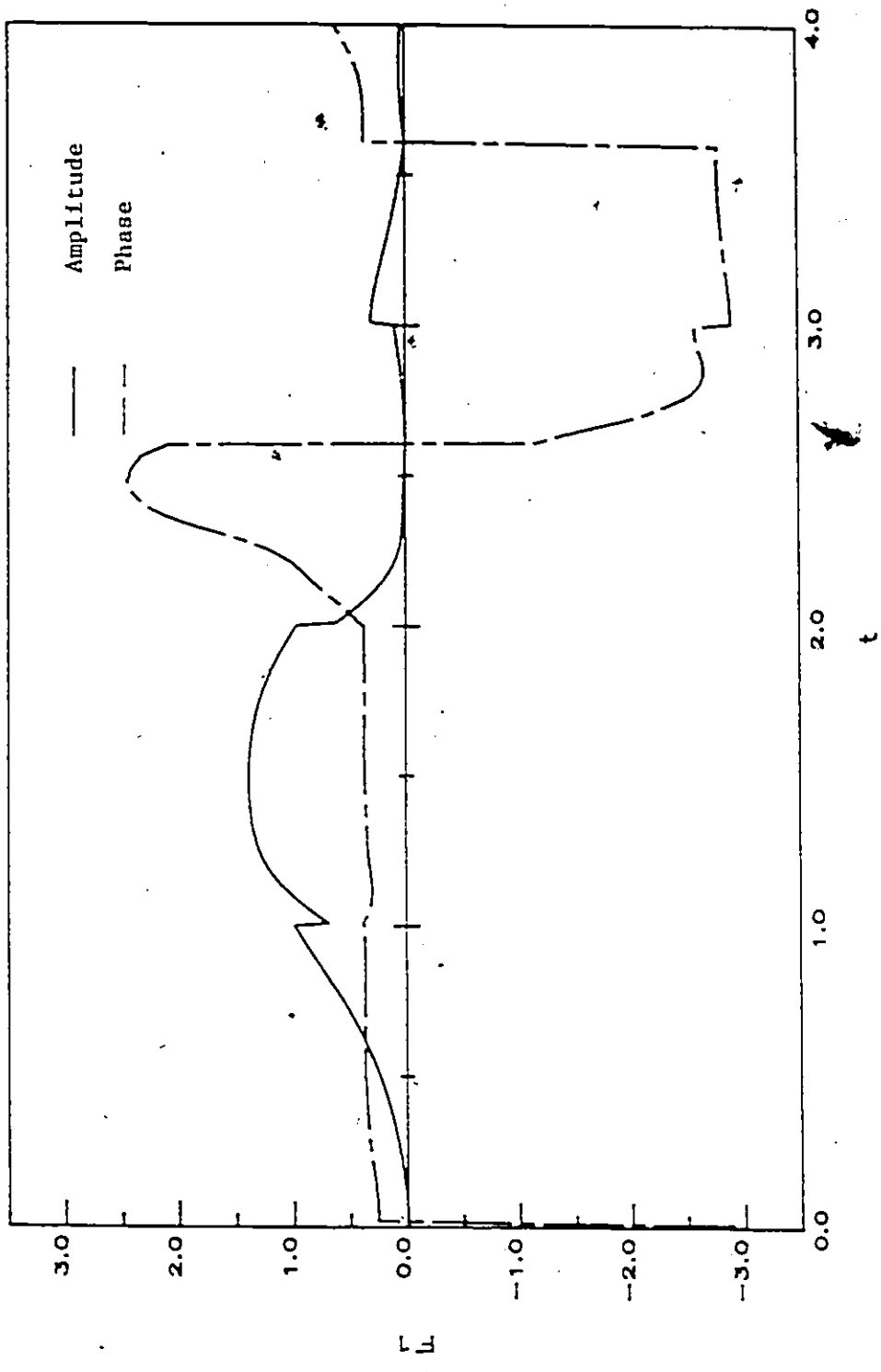

Fig. 4.2(j) The generic waveform F1(9) for TWTA input back-off of 0 dB.

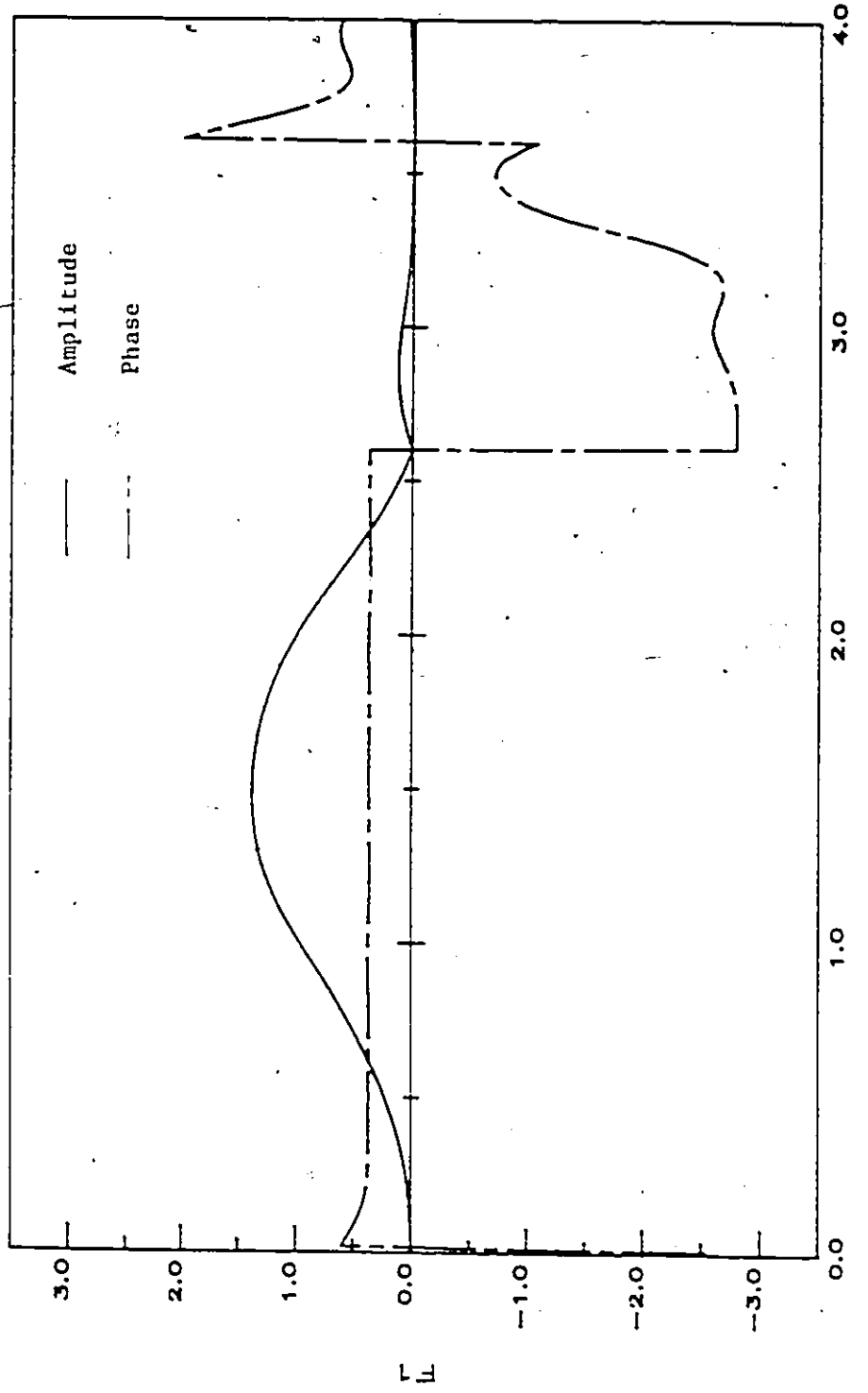

Fig. 4.2(k) The generic waveform F1(10) for TWTA input back-off of 0 dB.

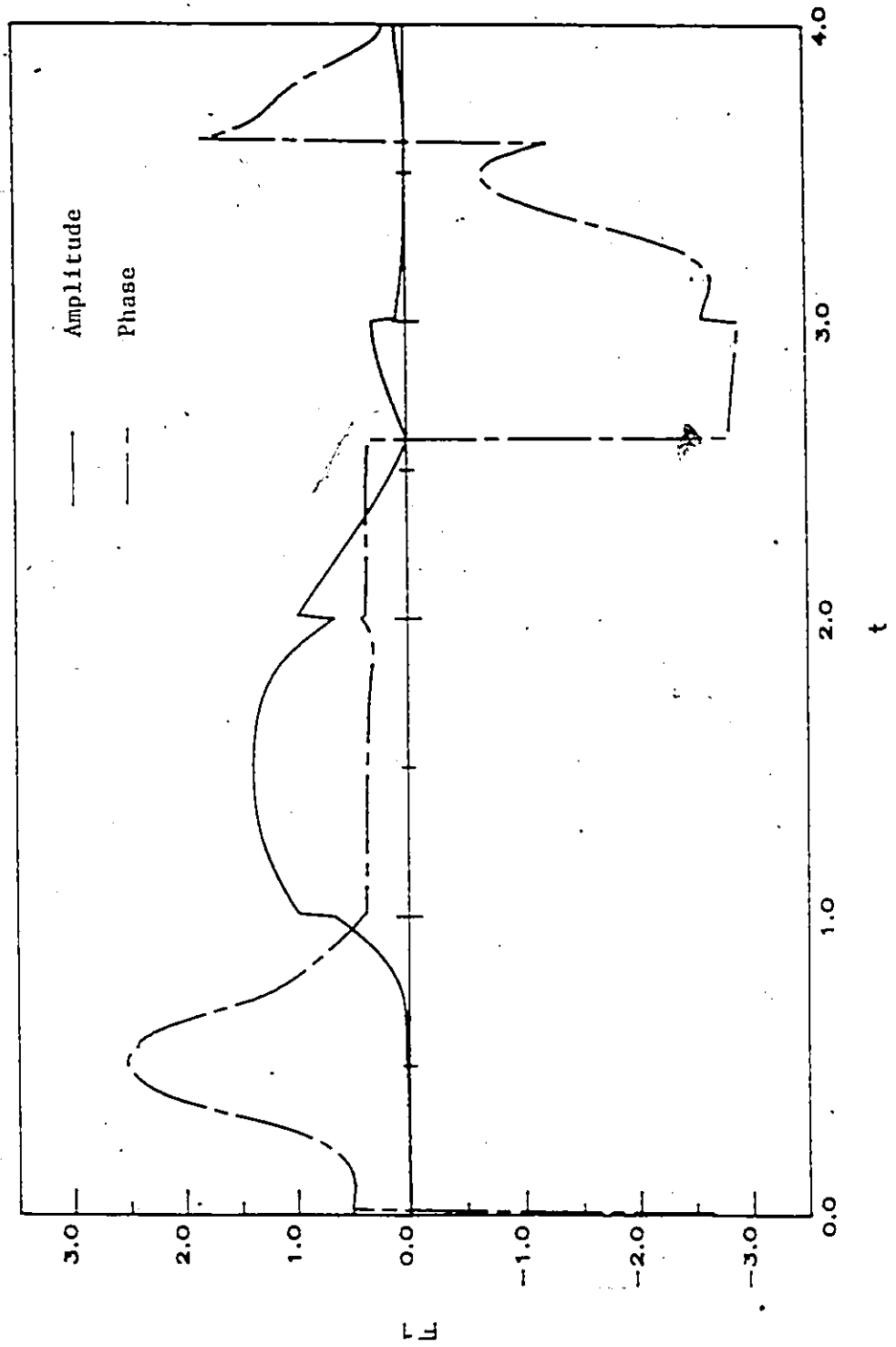

Fig. 4.2(1) The generic waveform F1(11) for TWTA input back-off of 0 dB.

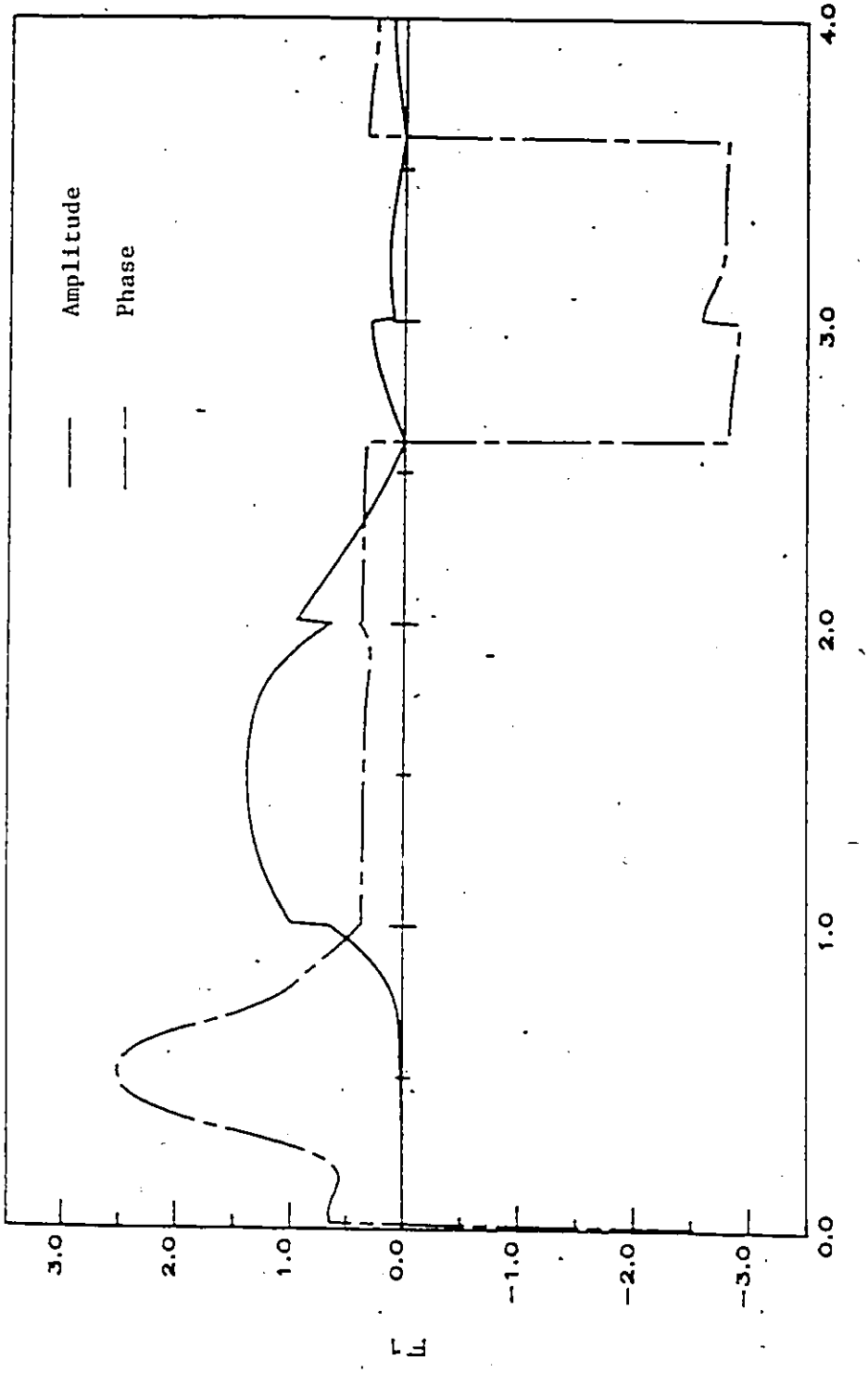

Fig. 4.2(m) The generic waveform F1(12) for TWTA input back-off of 0 dB.

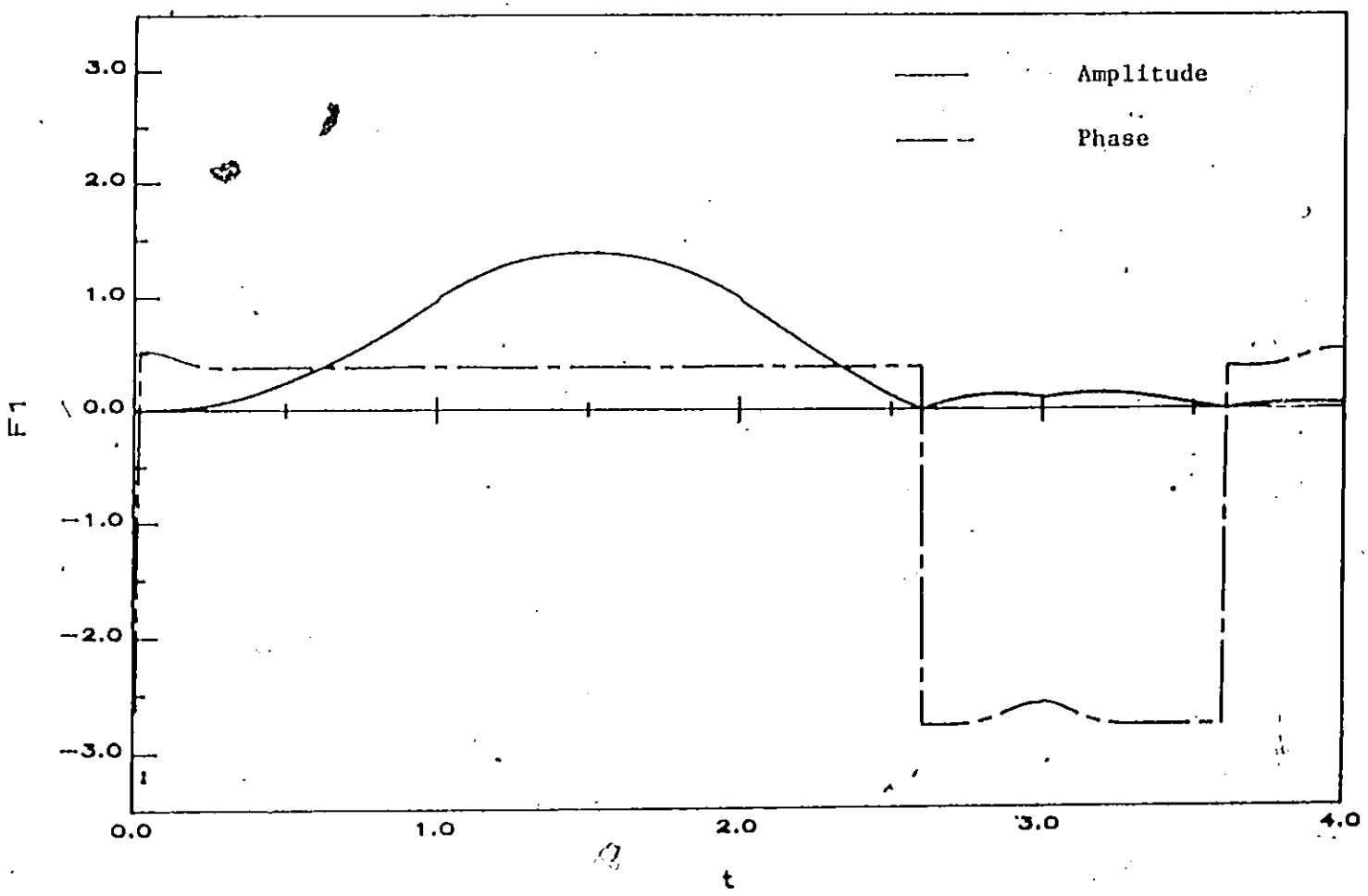

Fig. 4.2(n) The generic waveform F1(13) for TWTA input back-off of 0 dB.

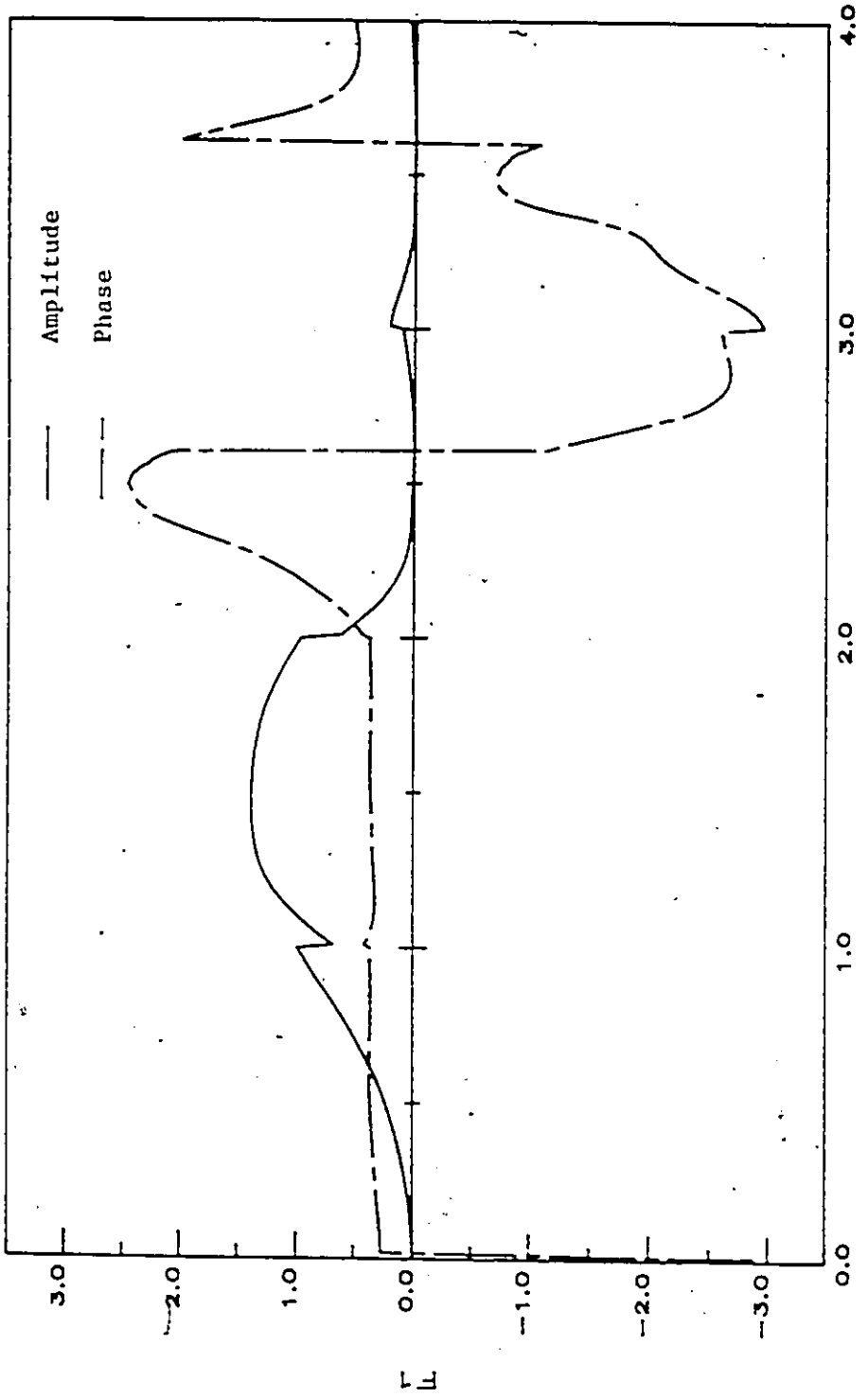

Fig. 4.2(o) The generic waveform F1(14) for TWTA input back-off of 0 dB.

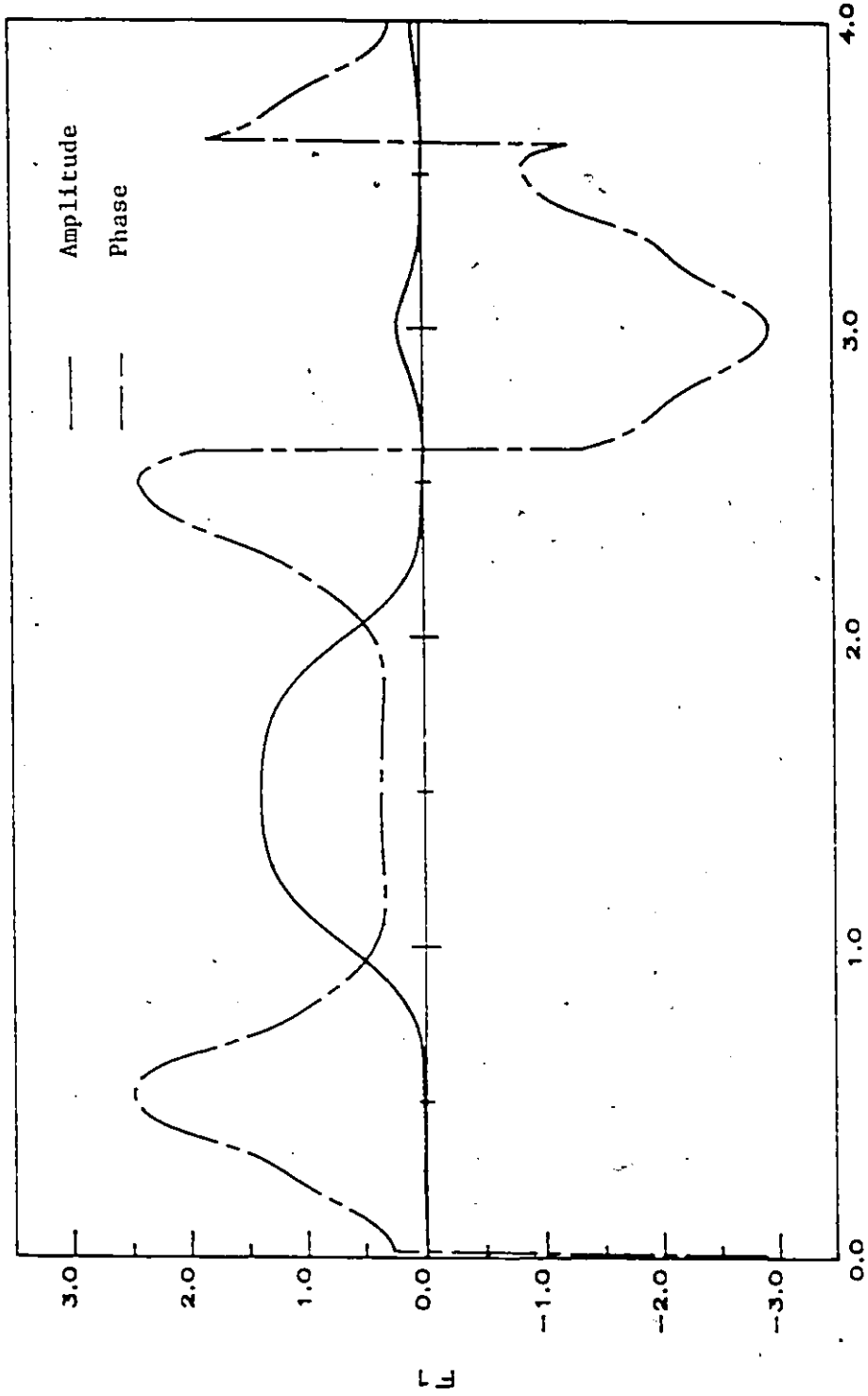

Fig. 4.2(p) The generic waveform F1(15) for TWTA input back-off of 0 dB.

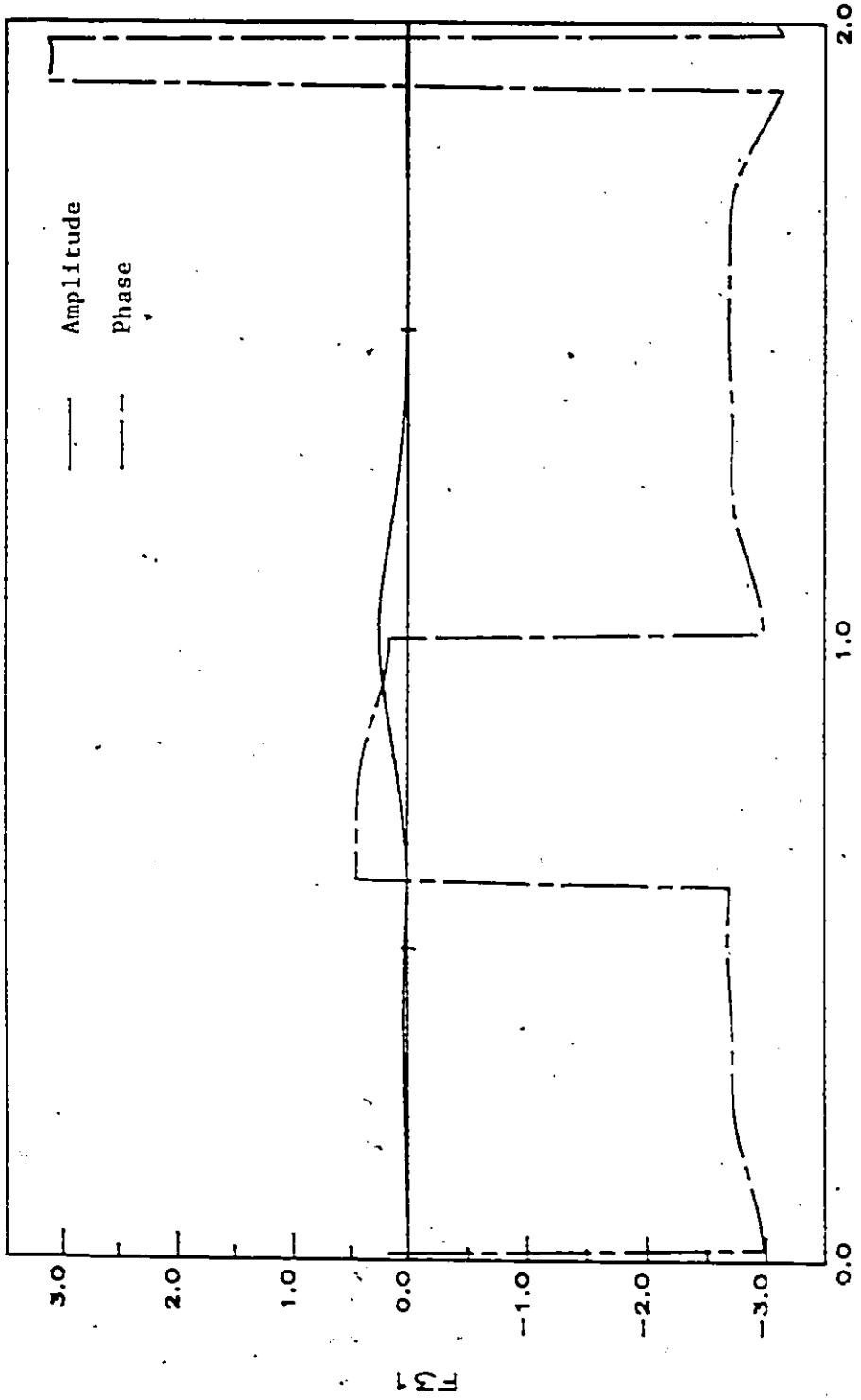

Fig. 4.3(a) The generic waveform F31(0) for TWTA input back-off of 0 dB.

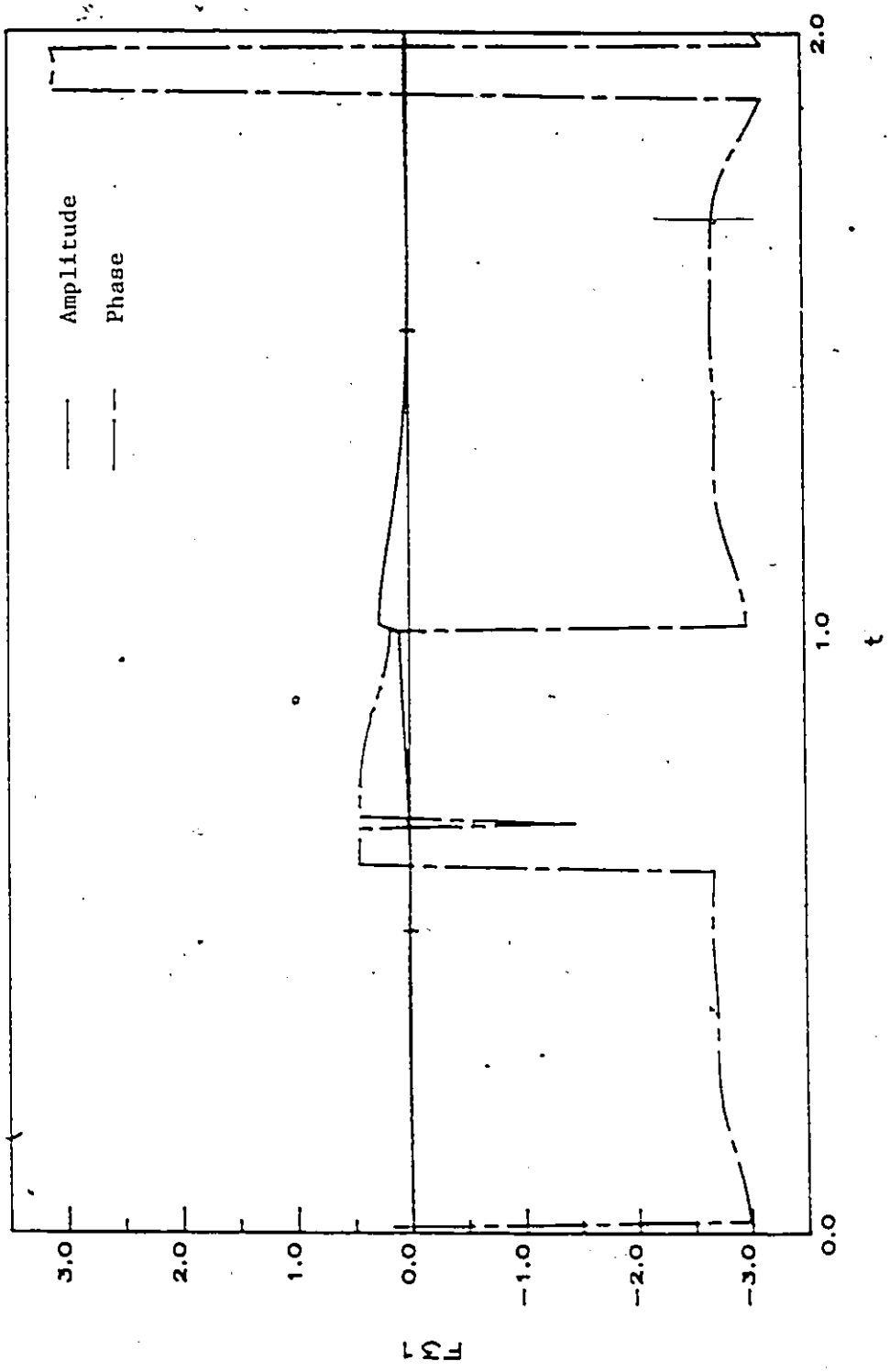

Fig. 4.3(b) The generic waveform F31(1) for TWTA input back-off of 0 dB.

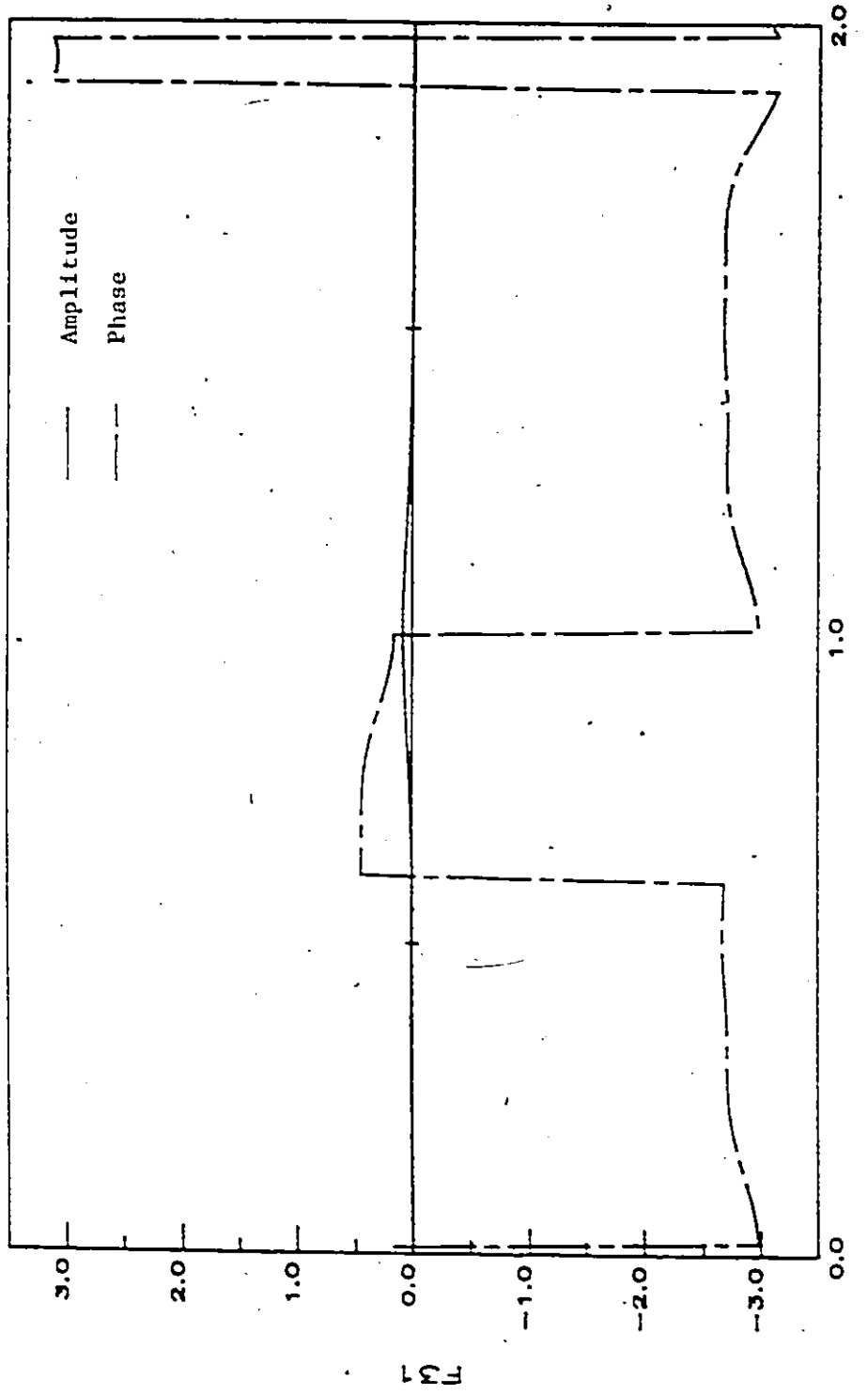

Fig. 4.3(c) The generic waveform F31(2) for TWTA input back-off of 0 dB.

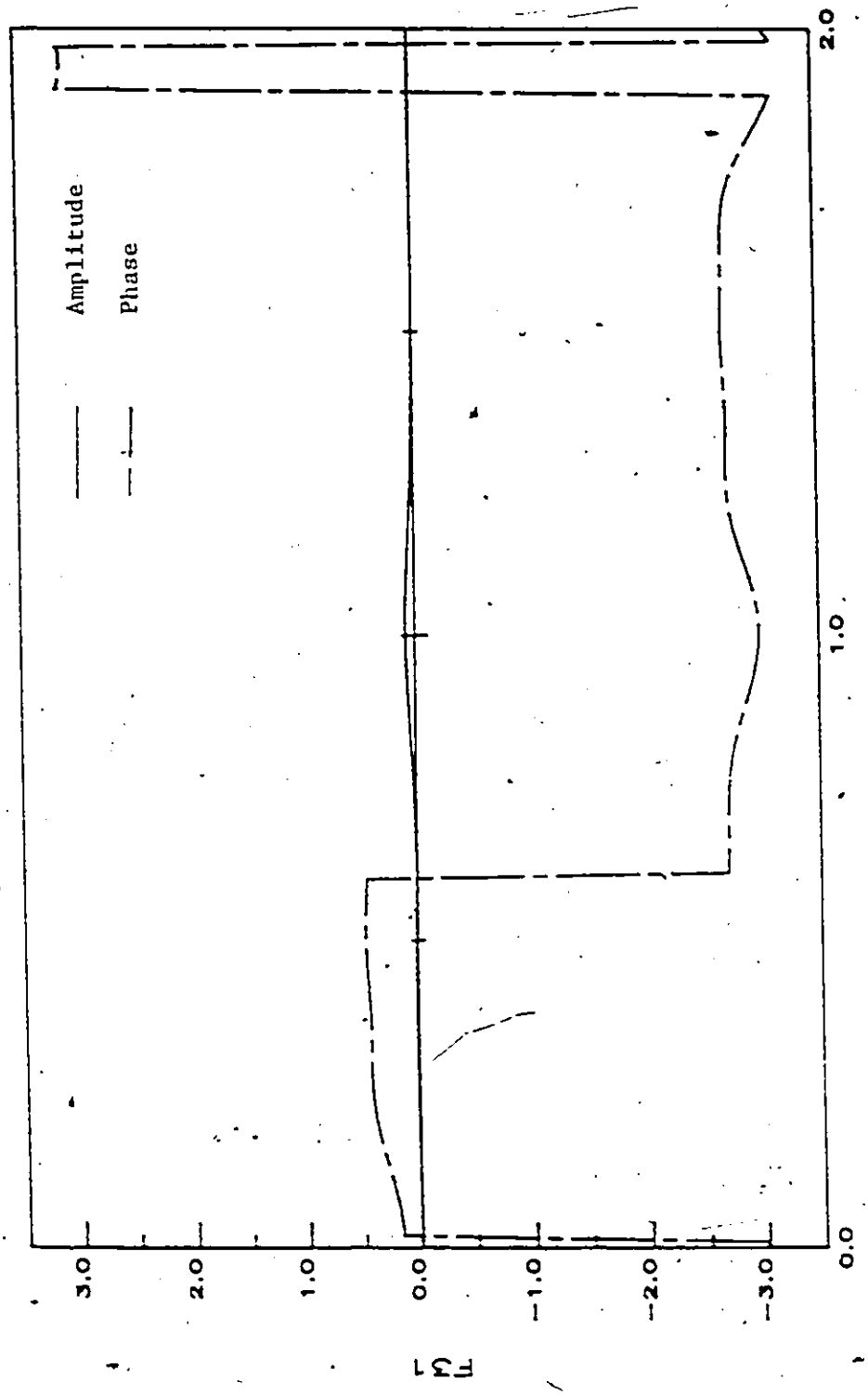

Fig 4.3(d) The generic waveform F31(3) for TWTA input back-off of 0 dB.

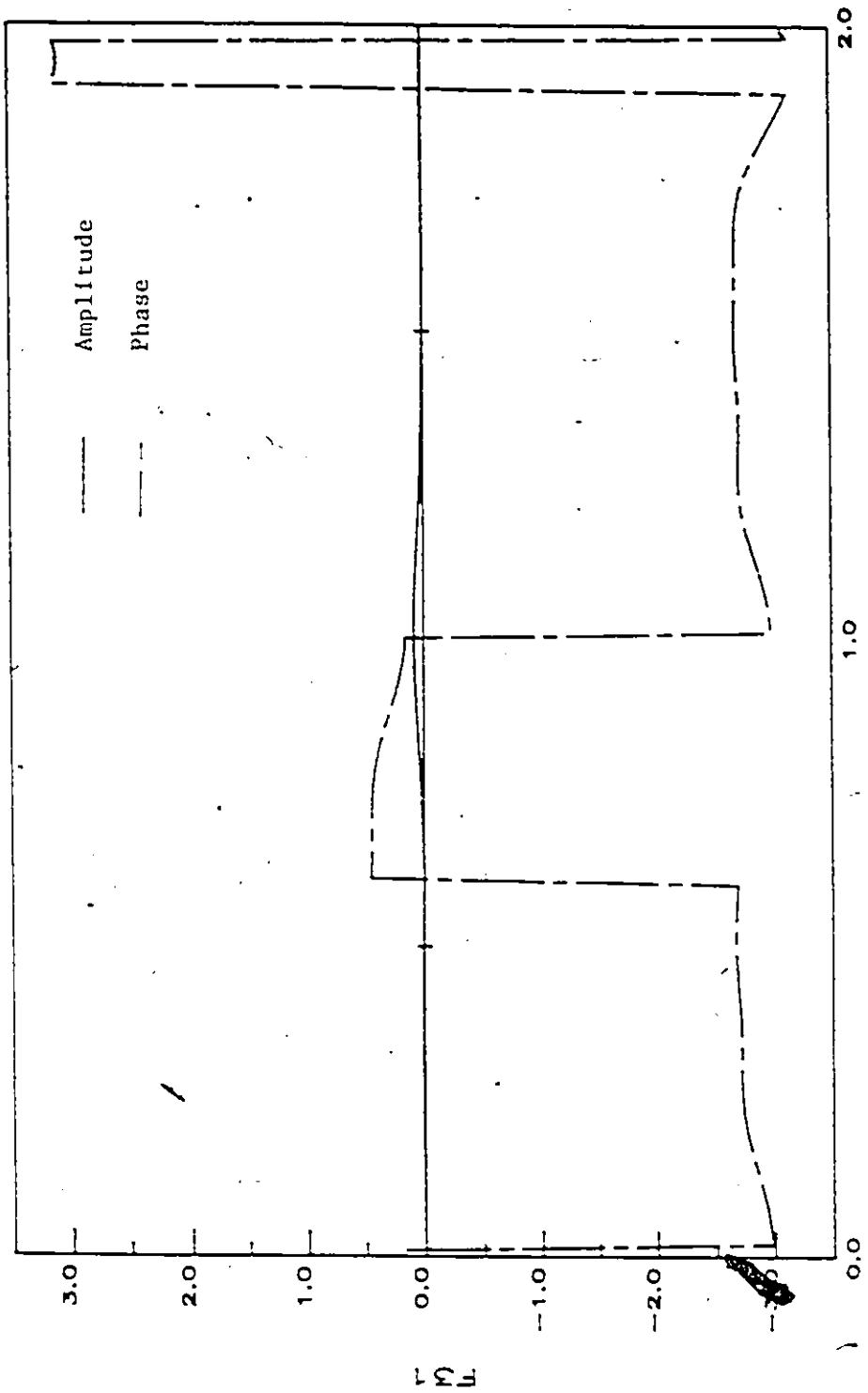

Fig. 4.3(e) The generic waveform F31(4) for TWTA input back-off of 0 dB.

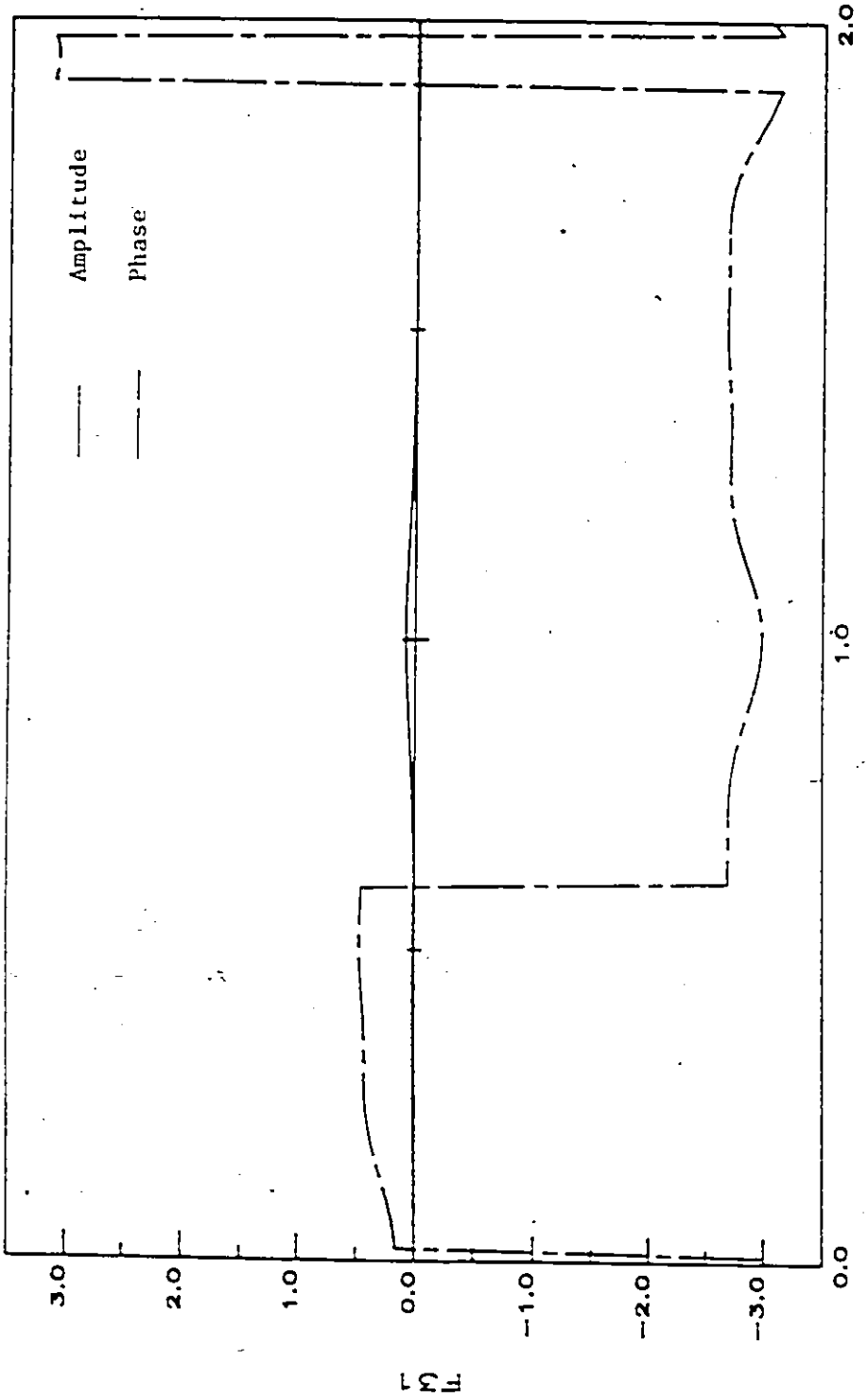

Fig. 4.3(f) The generic waveform F31(5) for TWTA input back-off of 0 dB.

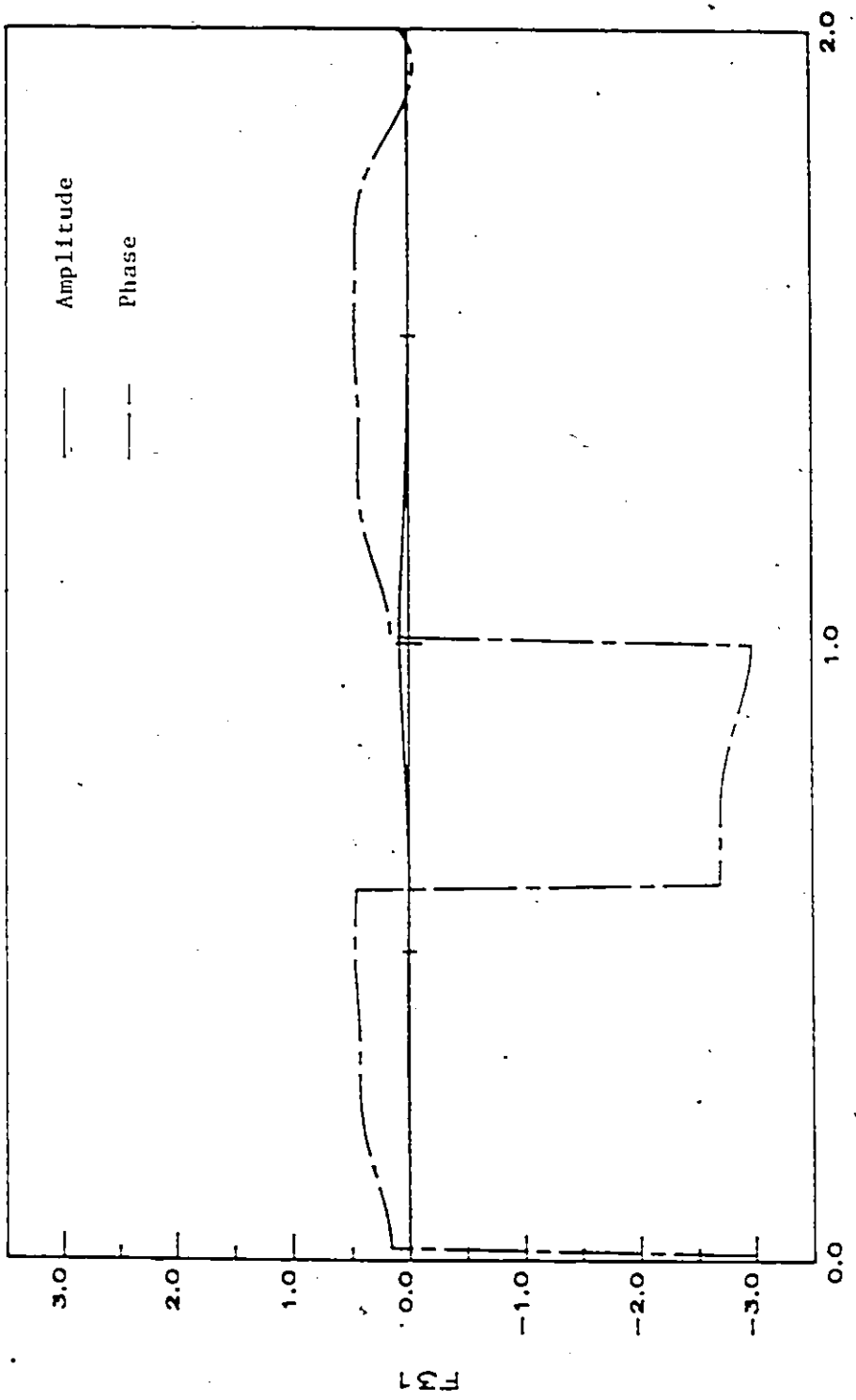

Fig. 4.3(g) The generic waveform F31(6) for TWTA input back-off of 0 dB.

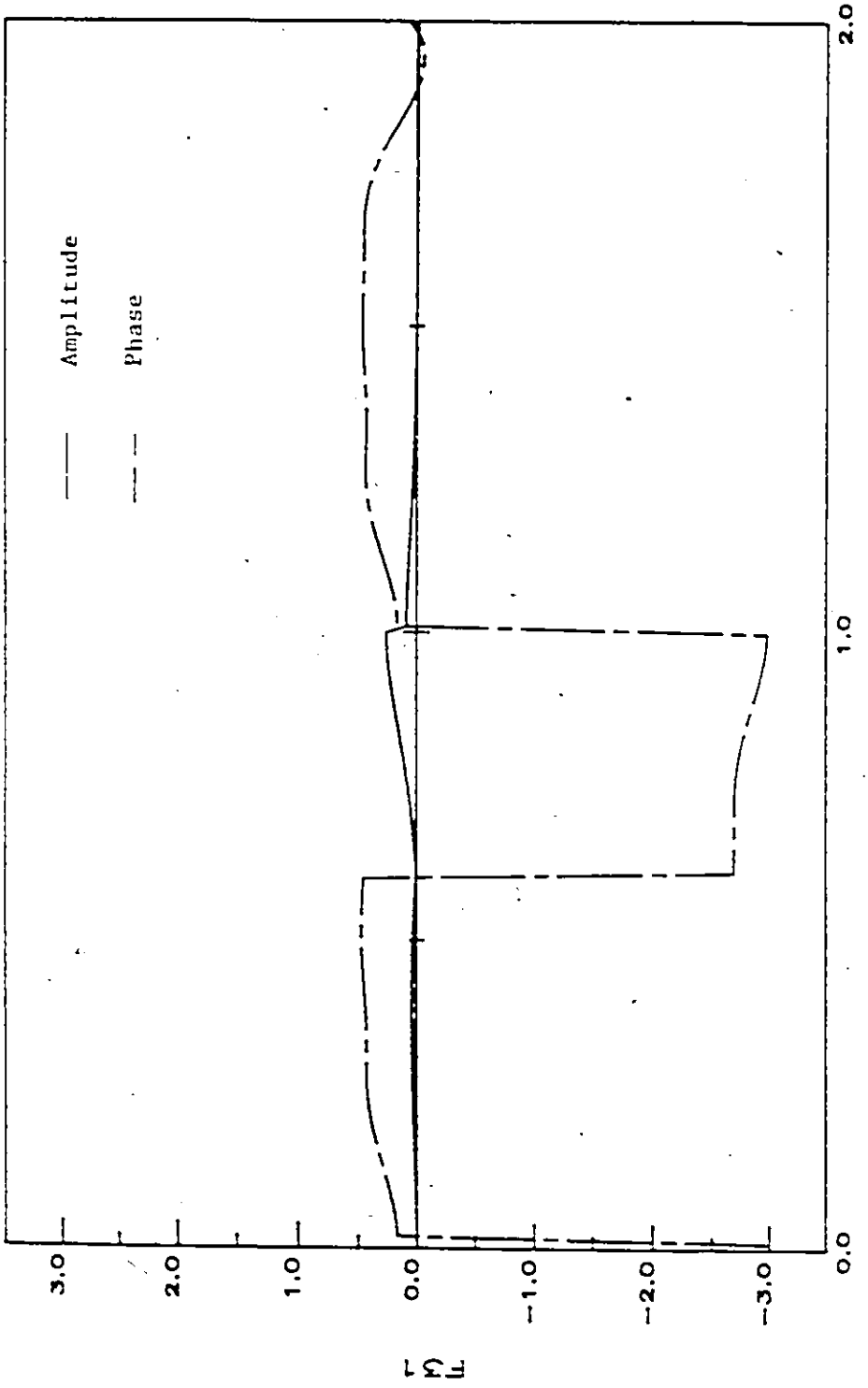

Fig. 4.3(h) The generic waveform F31(7) for TWTA input back-off of 0 dB.

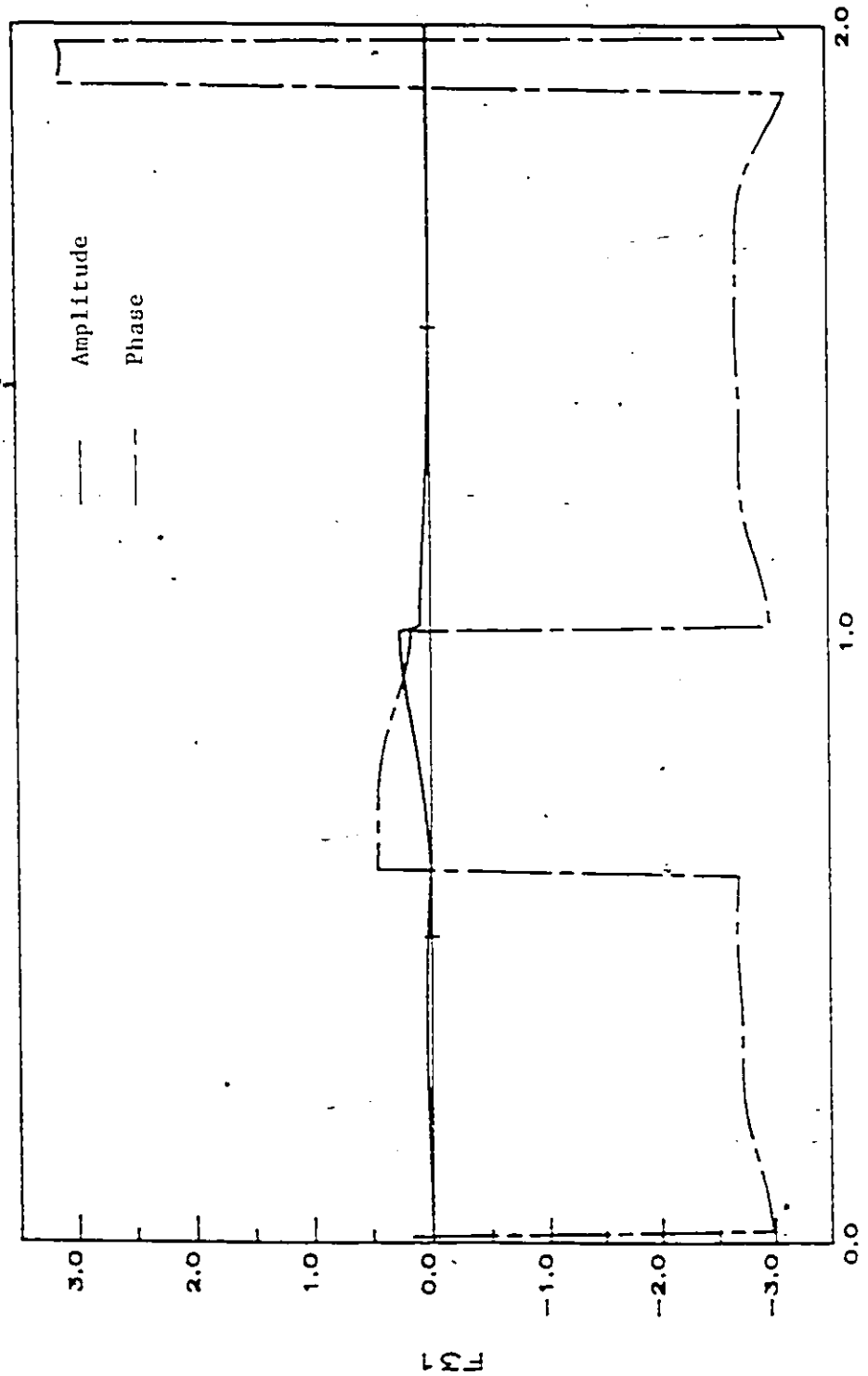

Fig. 4.3(i) The generic waveform F31(8) for TWTA input back-off of 0 dB.

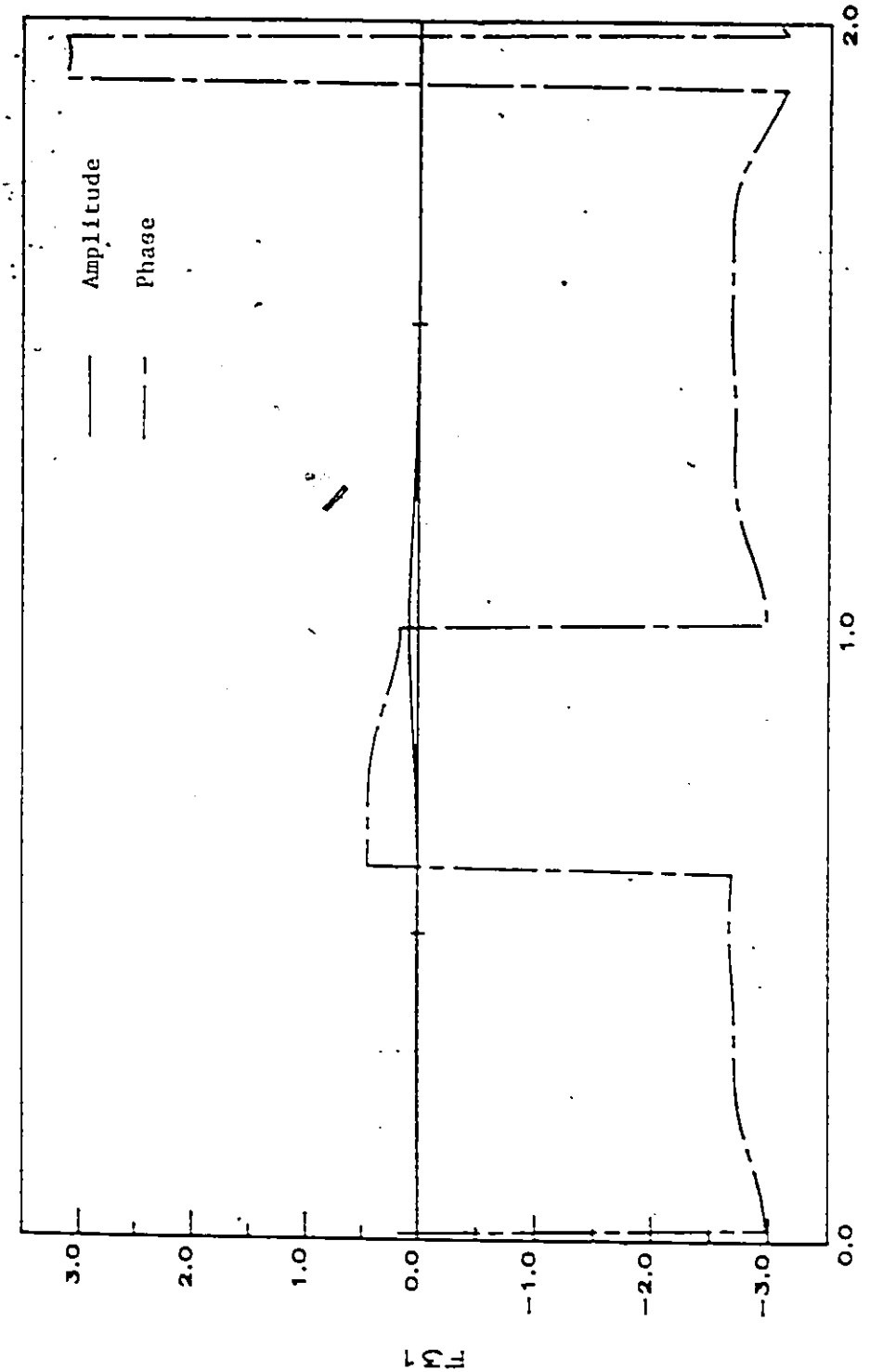

Fig. 4.3(j) The generic waveform F31(9) for TWTA input back-off of 0 dB.

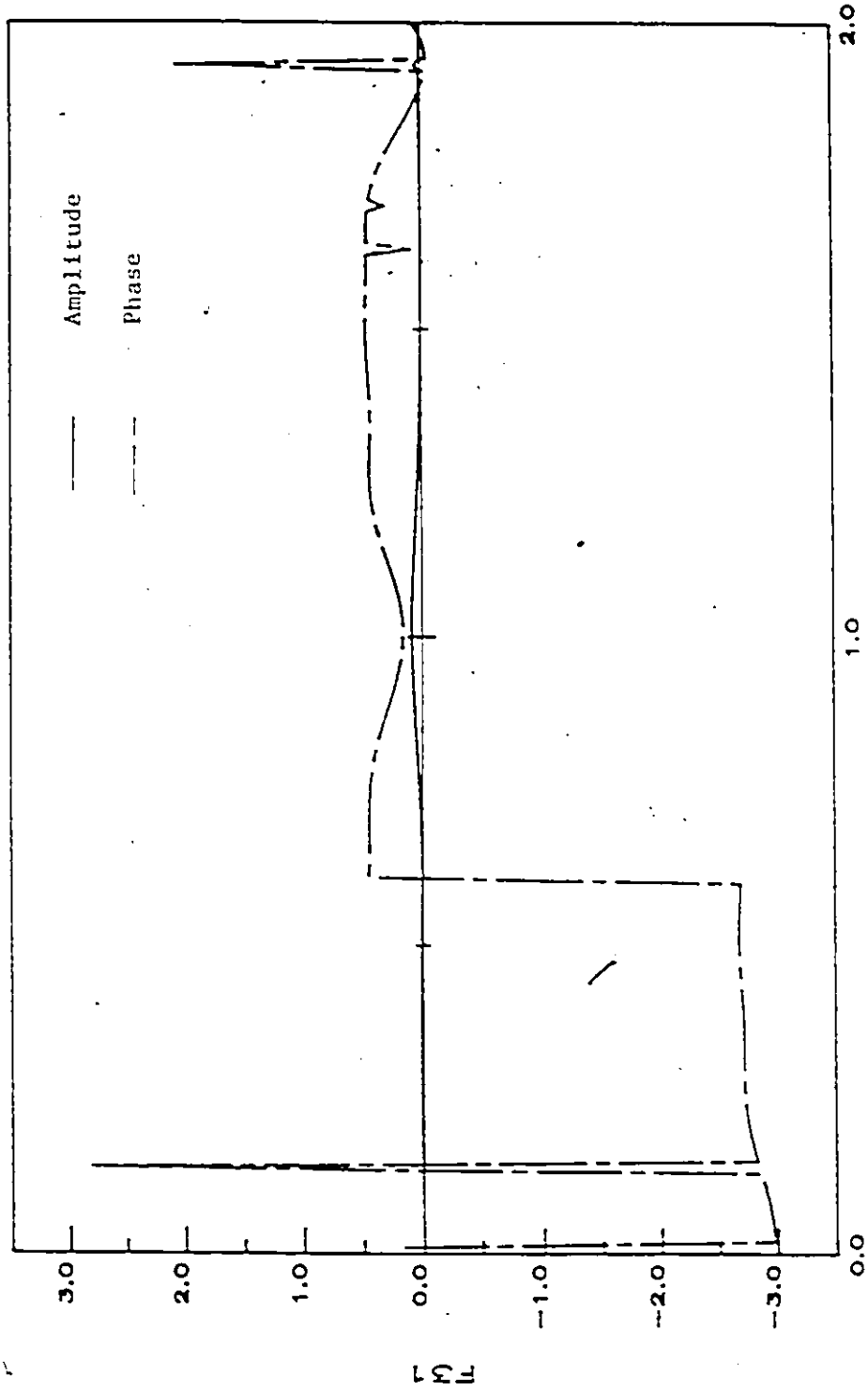

Fig. 4.3(k) The generic waveform F31(10) for TWTA input back-off of 0 dB.

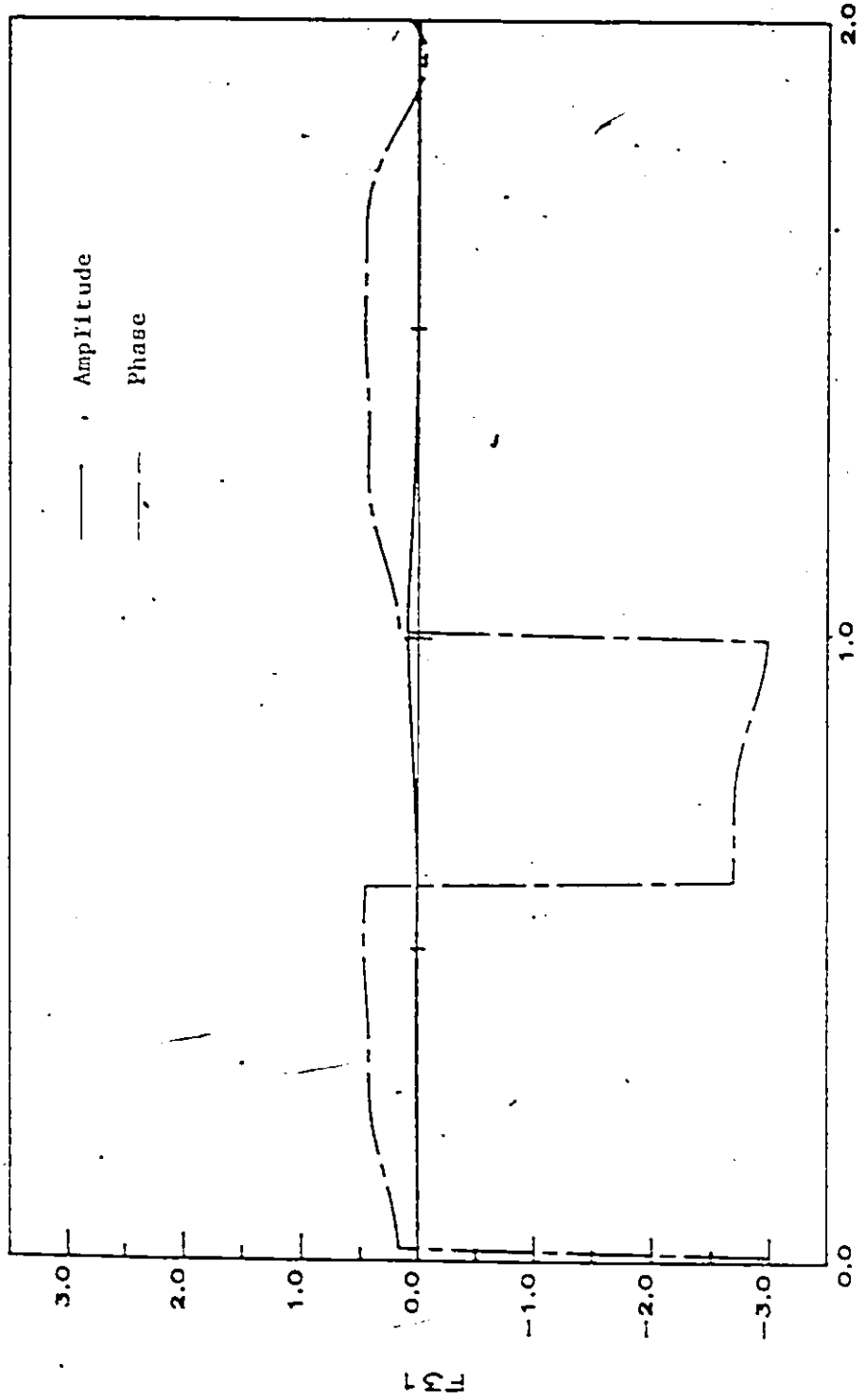

Fig. 4.3(1) The generic waveform F31(11) for TWTA input back-off of 0 dB.

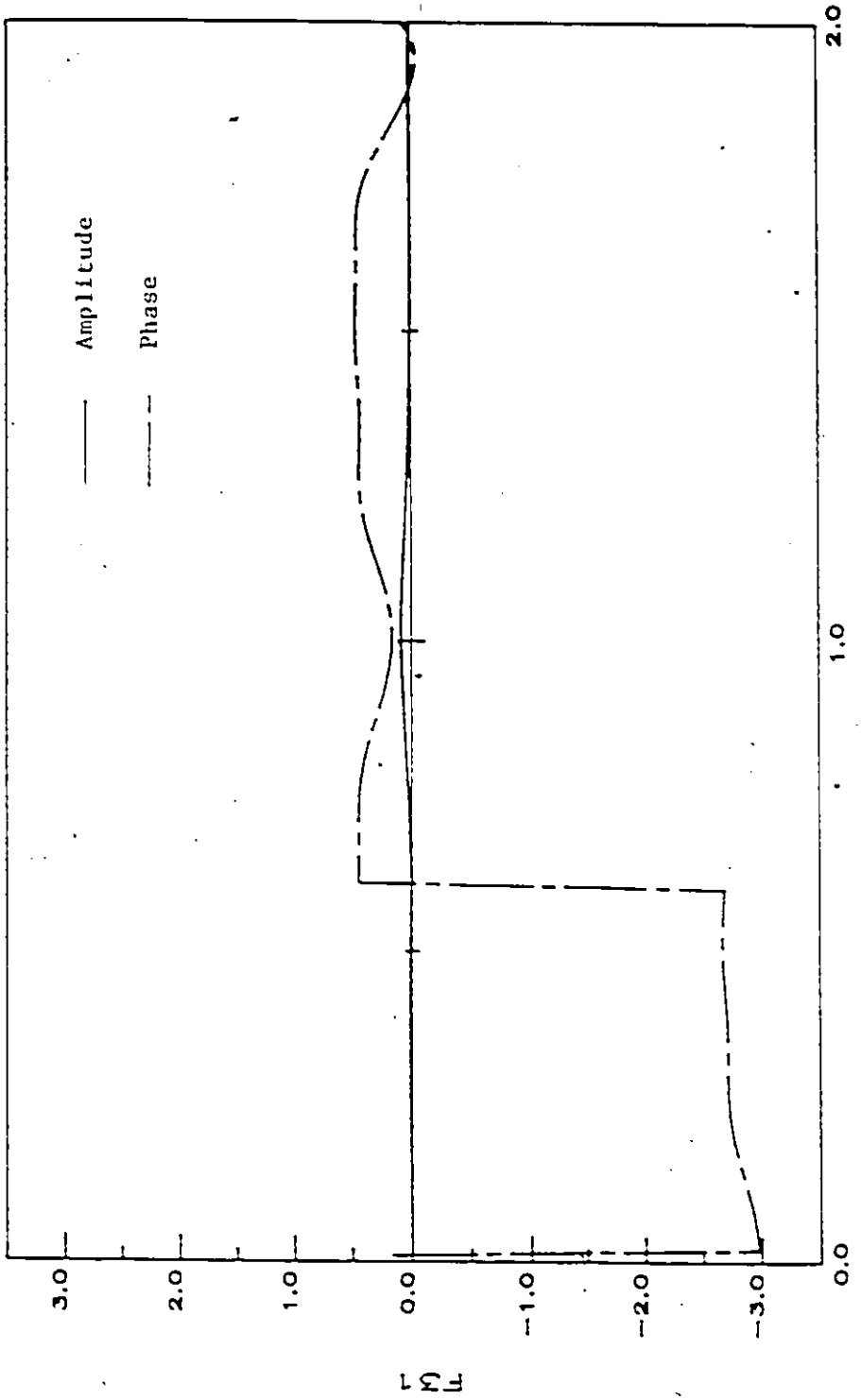

Fig 4.3(m) The generic waveform F31(12) for TWTA input back-off of 0 dB.

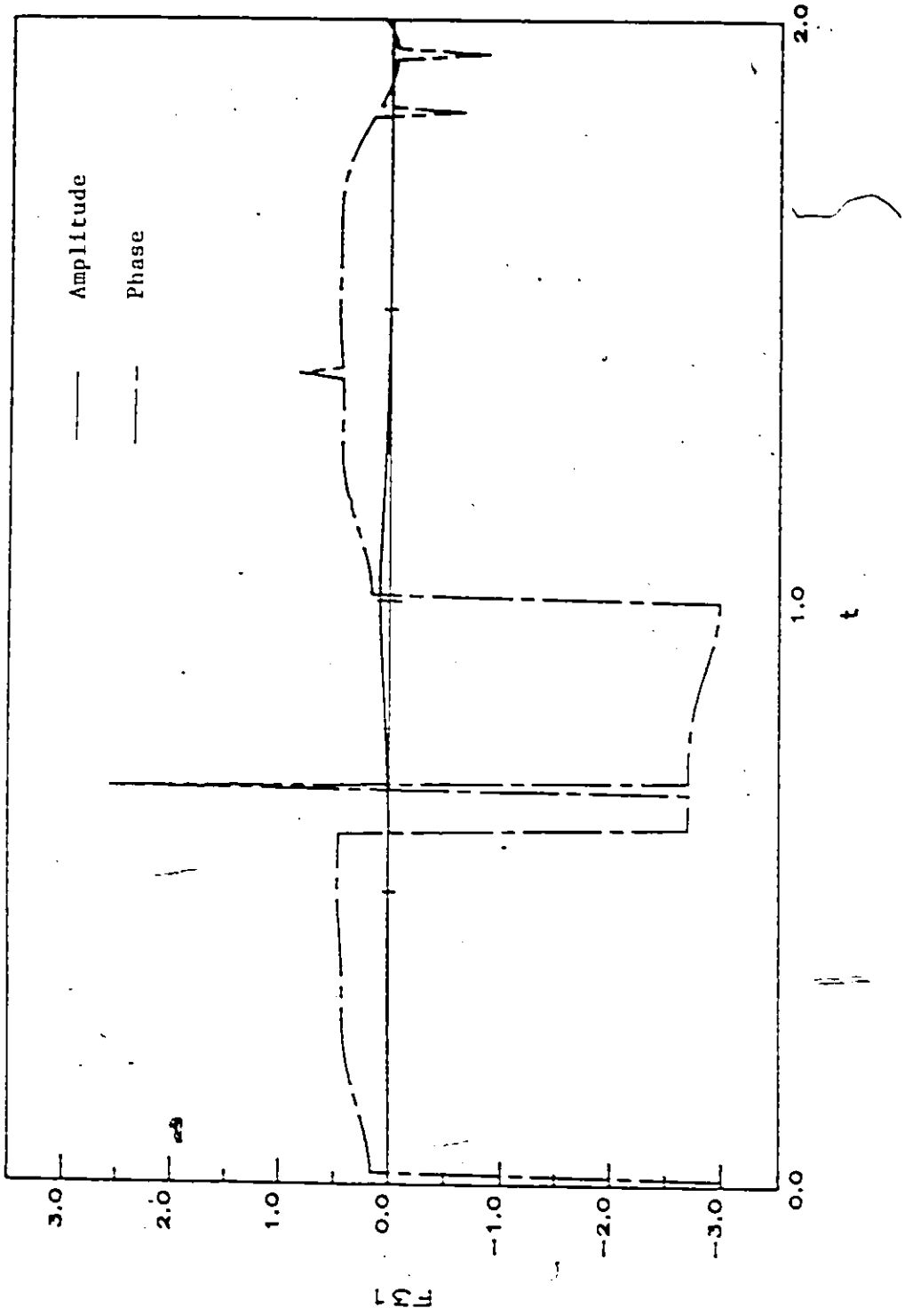

Fig. 4.3(n) The generic waveform F31(13) for TWTA input back-off of 0 dB.

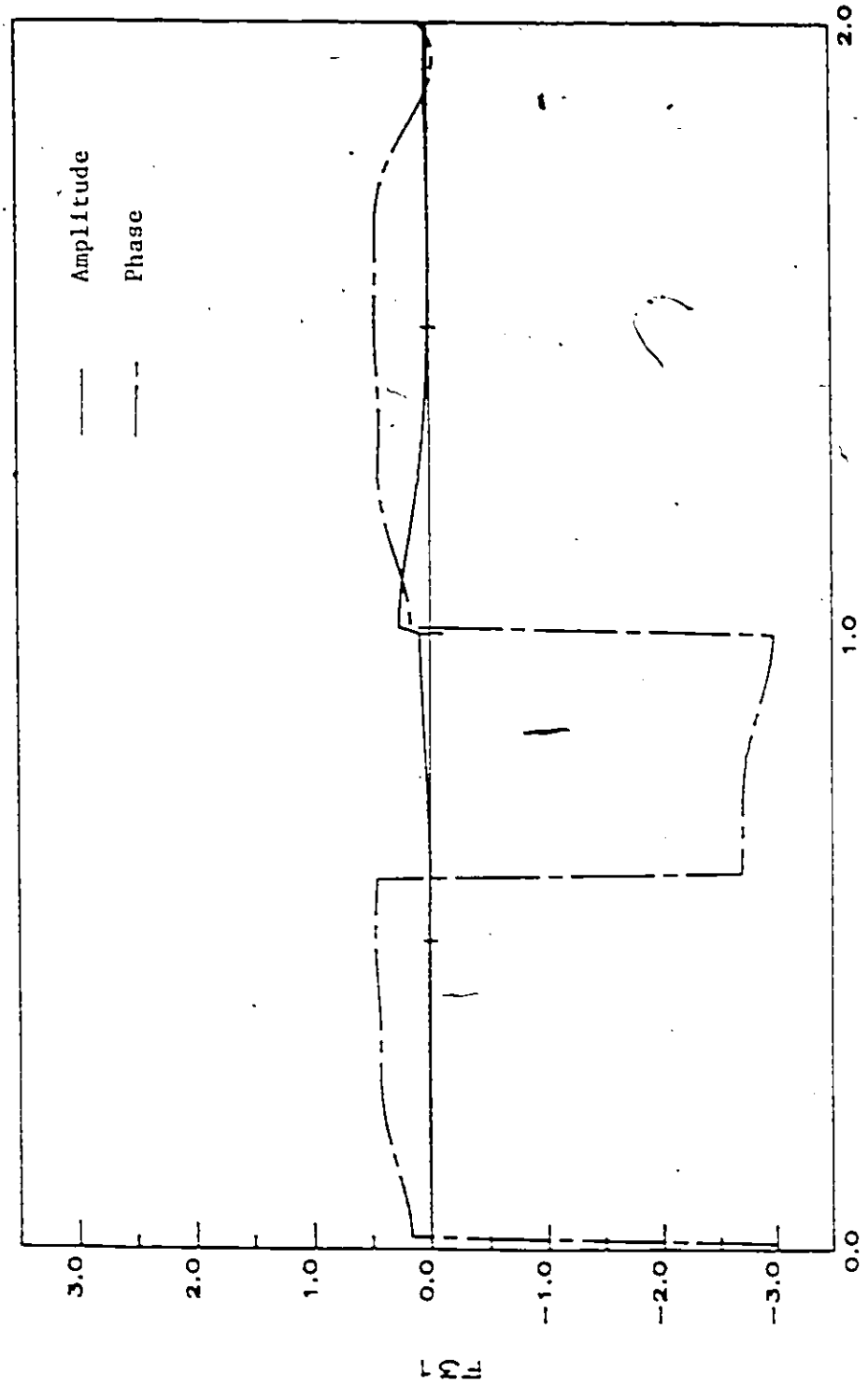

Fig. 4.3(o) The generic waveform F31(14) for TWTA input back-off of 0 dB.

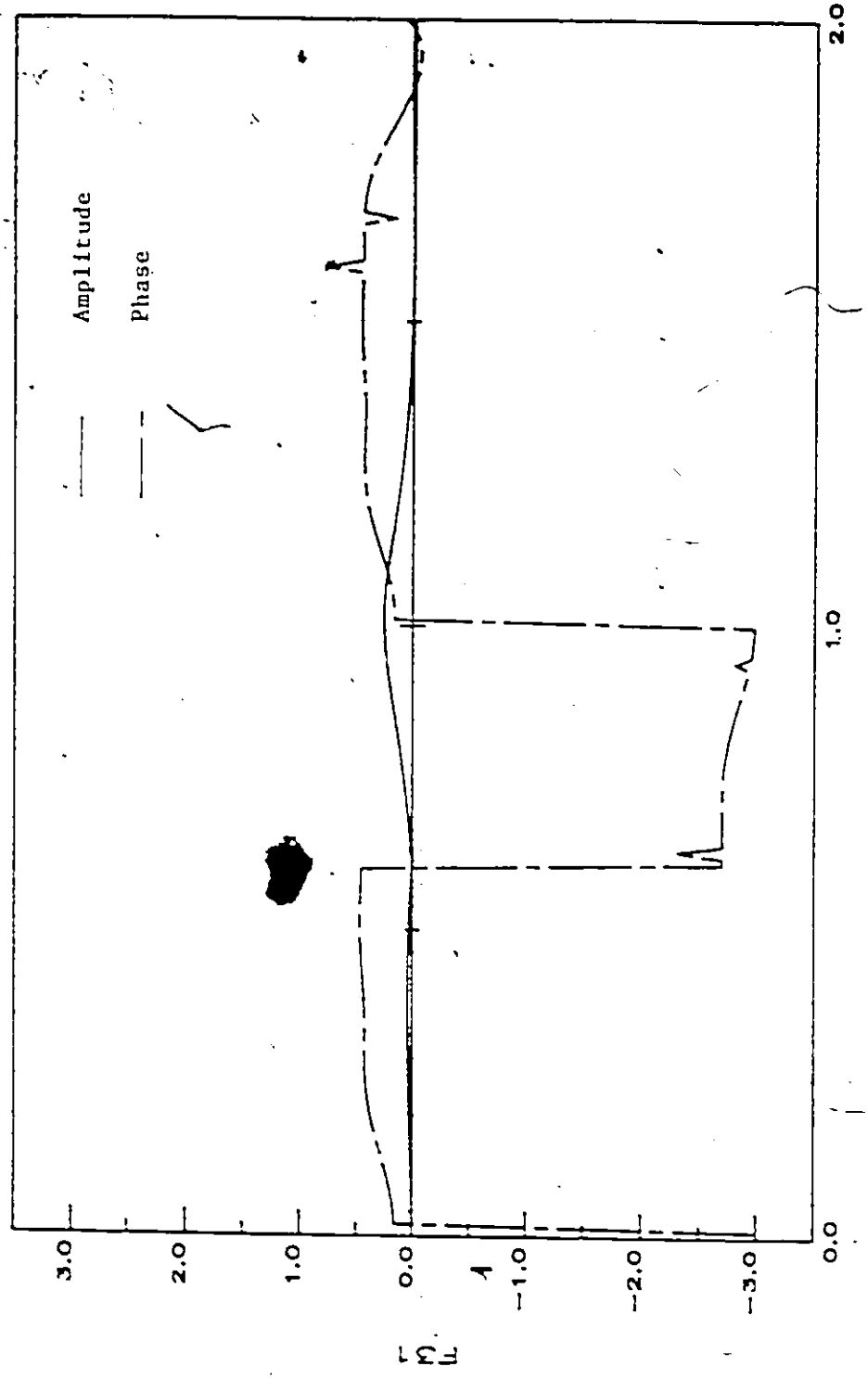

Fig. 4.3(p) The generic waveform F31(15) for TWTA input back-off of 0 dB.

observing that $F1(p_k) = F1(15-p_k)$ and $F31(p_k) = -F31(15-p_k)$. Therefore, we need to store only 8 of each of the complex waveforms ($F1(p_k)$ and $F31(p_k)$ instead of 16.

4.2.3 The Computation of the Branch Metric

To compute the minimum branch metric value for each transition thereby eliminating parallel branches in an optimum way, we must compare the 128 branch metric values given by (2.43). It is clear that the required minimum metric value corresponds to the maximum matched filter outputs, so if we find the maximum matched filter outputs $Z_i(p_k)$ and $Z_i^{31}(p_k)$, the corresponding minimum metric value can be calculated using (2.43). This, however, results in a very complex receiver. To avoid this, we use here a suboptimum procedure which enables us to compute the minimum branch metric in a simple manner. The procedure is analogous to decision feedback processing, and is explained as follows. Let, for example, the time $(k+1)T$ combination of p_k's corresponding to the maximum matched filter output $Z_k^1(p_k)$ be $p_k = 2$, $p_{k+1} = 4$, $p_{k+2} = 9$, and $p_{k+3} = 2$. then at the next instant of time, the values of p_k's will be $p_{k+1} = 4$, $p_{k+2} = 9$, $p_{k+3} = 2$, and $p_{k+4} = 4$ or 5. The required minimum metric value is thus estimated as the minimum of only two metric values. The initial sequence of p_k's, which is required for receiver startup, may be estimated by any one of the following methods: (a) we can determine the initial sequence of p_k's corresponding to the maximum matched filter outputs by exhaustive search; (b) we can estimate the initial sequence of p_k's by a single sample decision (c) since the filter responses in our case are not very different for various combinations of p_k's, we can arbitrarily set the initial sequence of p_k's and after a short transient period the receiver process will settle to the correct sequence. Note that we must provide storage for the short sequence of p_k values.

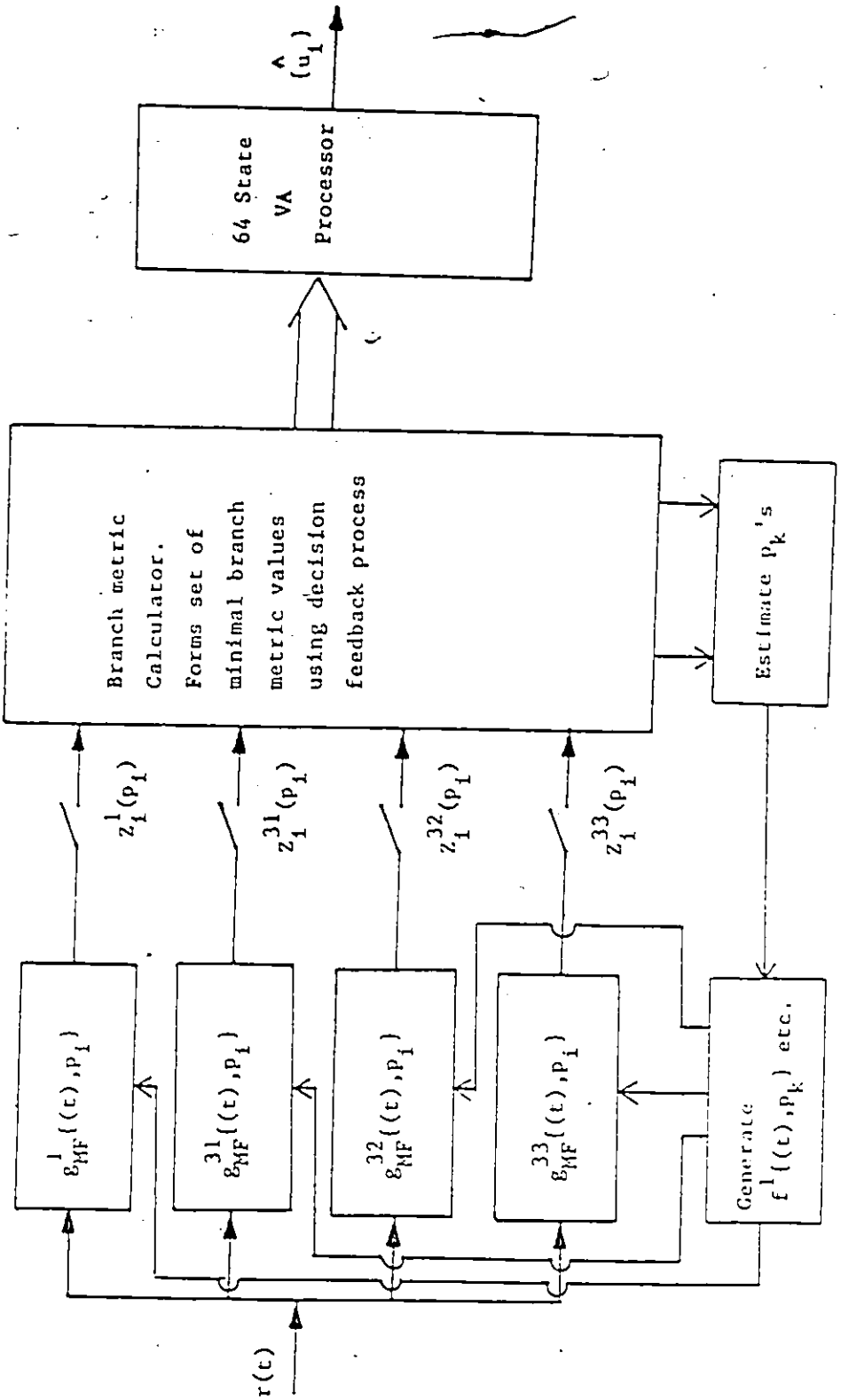

Fig. 4.4 The maximum likelihood sequence receiver as simulated for channel memory of v = 3.

4.2.4 Simulation Results

Figure 4.4 shows the structure of the MLSR as simulated for a channel memory $v = 3$. The error performance of the MLSR at low to moderate signal-to-noise ratio was estimated by computer simulation. For the simulation, we used matched filter waveforms generated as above, and a 64 state Viterbi detector with a decision depth of 20. The branch metrics are computed as explained in the preceding paragraph with the initial sequence of p_k's being arbitrarily set. Only the first four terms of the branch metric given by (2.43) were actually used. The other terms were found to be very small and therefore were not used in the simulation. The resulting simulated probability of bit error is shown in Figure 4.5. For comparison purposes, the matched filter bound attained in an additive white gaussian noise channel is also plotted in Figure 4.5. In addition, it was found by simulation that single-error error events are dominant. Hence the probability of error was estimated using the approximate bound of equation (3.30). We note that this upper bound looks as if it is the lower bound in Figure 4.5. The reason for this is that in the simulation we used only the first four terms of the branch metric given by (2.43) rather than the complete branch metric. This, as can be seen, leads to a rather minor degradation in performance, and, in fact, equation (3.30) provides a good estimate of the error rate.

As mentioned earlier, the complex waveforms used in simulation were generated for a TWTA input back-off of 0 dB. The input back-off B_i is defined as follows

$$B_i = 10 \log_{10} \frac{P_{in}}{(P_{in})_{max}}$$

where P_{in} = actual average input power

$(P_{in})_{max}$ = minimum input power required to drive the BPNL into saturation.

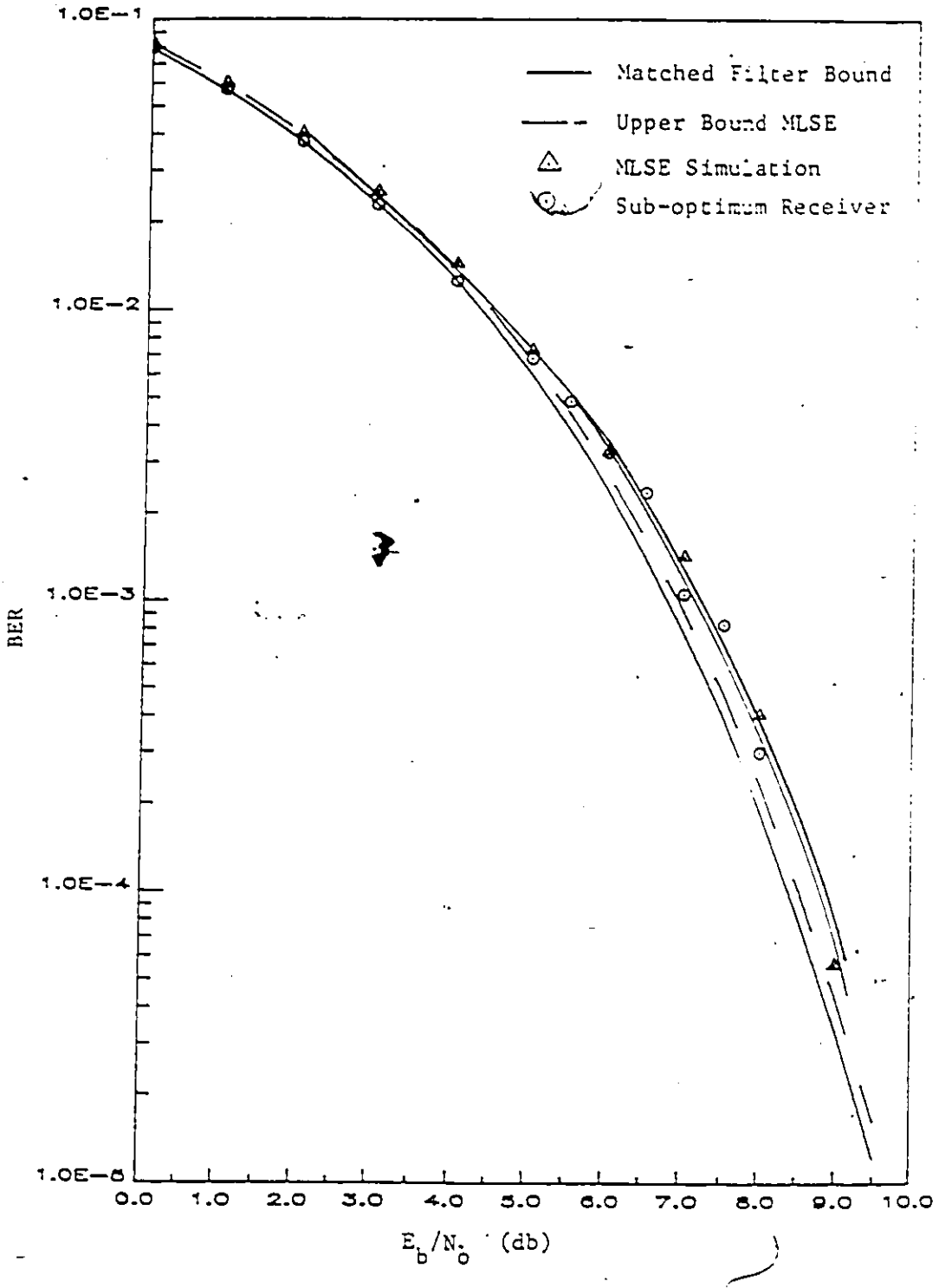

Fig. 4.5 Performance comparison of MLSE and sub-optimum receiver for a fourth-order Chebyshev filter with 2BT = 1.

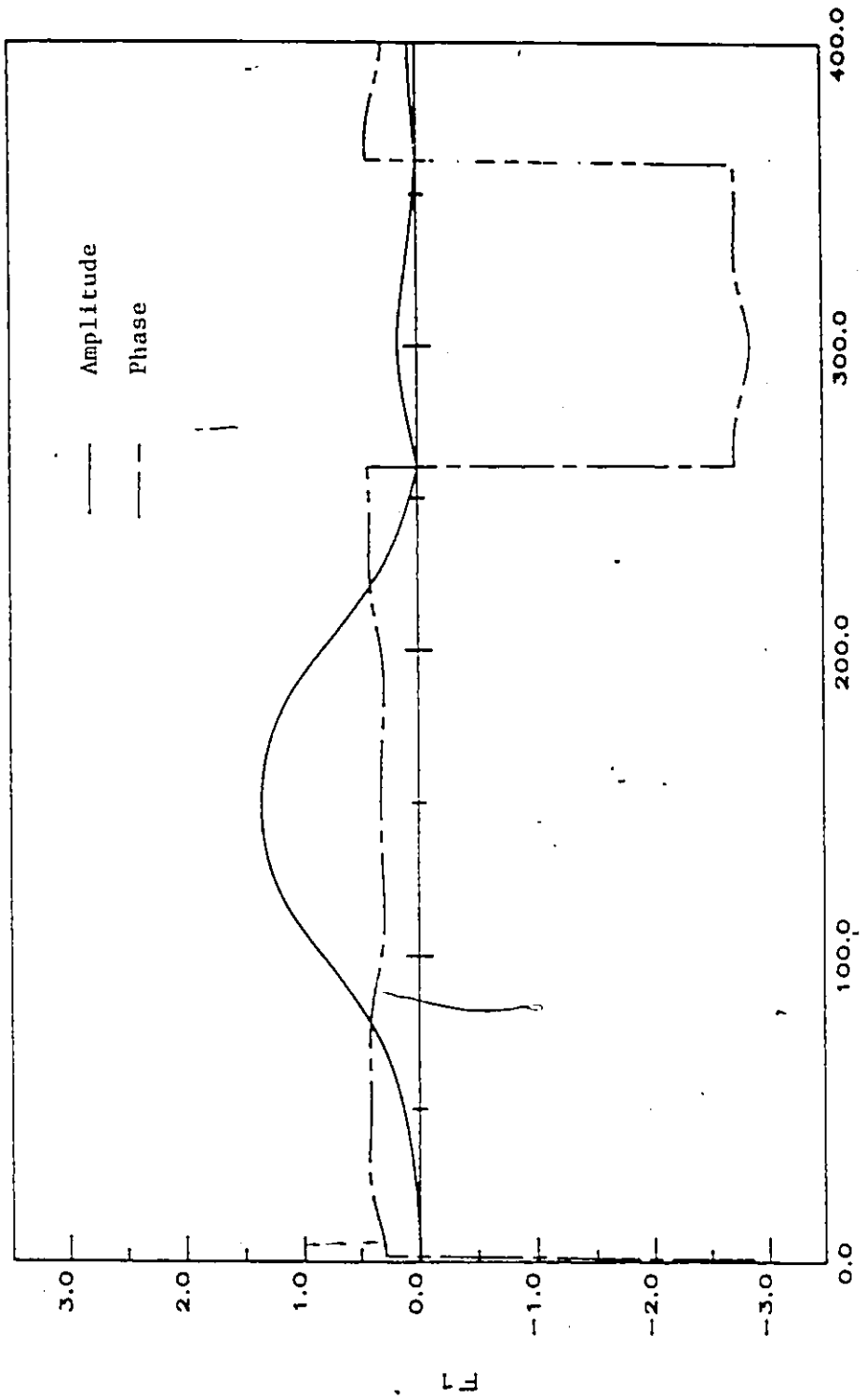

Fig. 4.6 The average generic waveform F1{(t),A} for 3 dB input back-off of the TWTA.

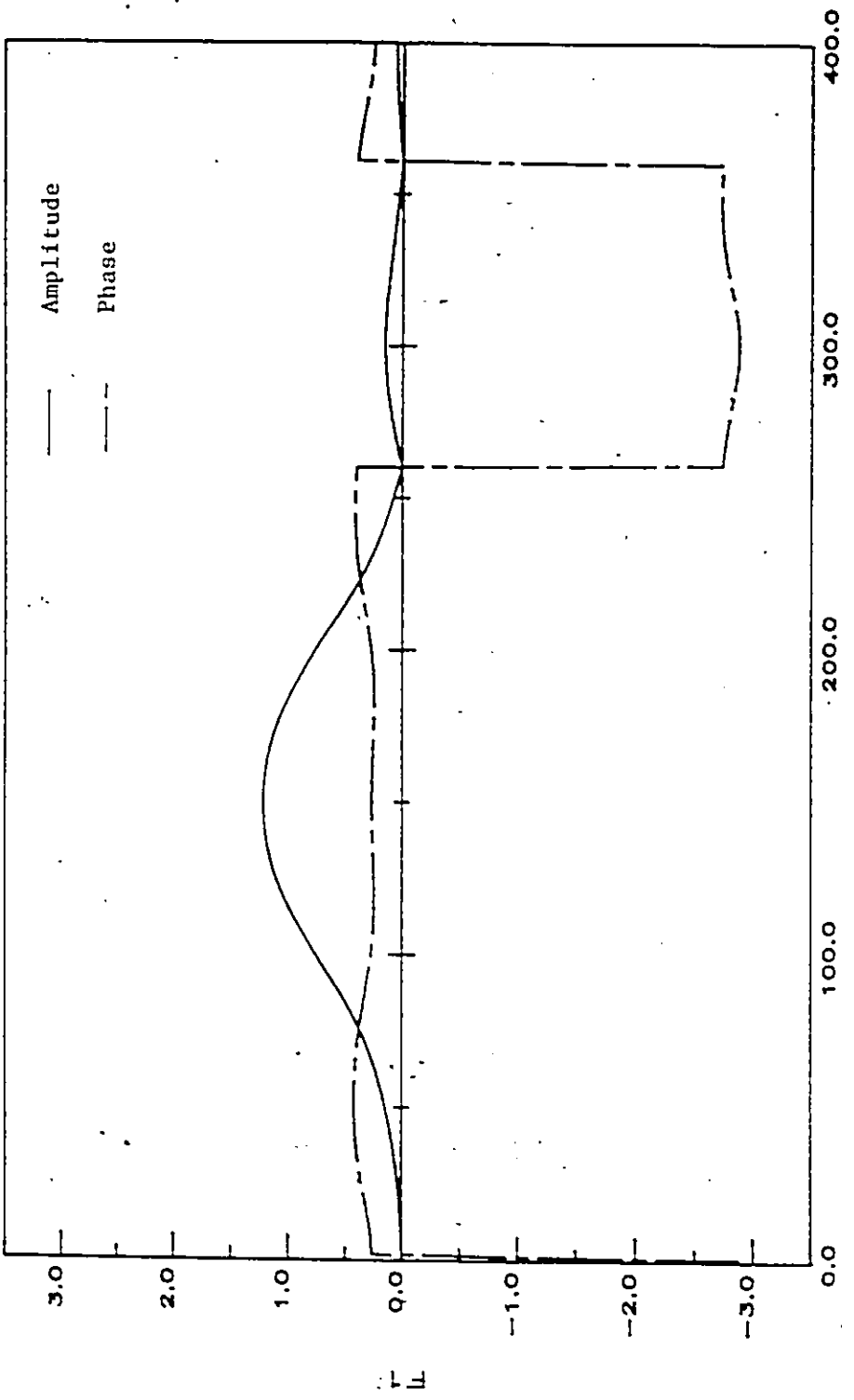

Fig. 4.7 The average generic waveform F1{(t),A} for 6 dB input back-off of the TWTA.

It was found that these waveforms change very little as the input back-off of the TWTA is varied. In Figure 4.6 and 4.7, average F1 for 3 dB and 6 dB input back-offs of the TWTA are shown.

4.3 Sub-optimum Receiver Structure

In this section we develop a sub-optimum receiver structure by using "average" matched filter responses [43,44] in place of the actual filter responses given by $g_{MF}^{(1)}\{(t), p_i\}$ etc. It has been found through both computation and simulation in section 4.2, that in a typical satellite channel (specifically for $v = 3$), at most the first four terms are significant in the expression for the branch metrics of (2.43). Hence the approximate log likelihood ratio can be written from (2.42) and (2.43) as

$$J_l(\{\alpha_i,\beta_i\}) = \sum_i -2\mathrm{Re}\left[(\alpha_i - j\beta_i) + (I)^*_{\phi_i} Z_i^{31}(p_i) + (II)^*_{\phi_i} Z_i^{32}(p_i) + (III)^*_{\phi_i} Z_i^{33}(p_i)\right] \tag{4.2}$$

In (4.1), we could use $Z_i^{1}(A)$, $Z_i^{32}(A)$ and $Z_i^{33}(A)$ instead of $Z_i^{31}(p_i)$, $Z_i^{31}(p_i)$, $Z_i^{32}(p_i)$ and $Z_i^{33}(p_i)$, where the former are "average" matched filters defined as

$$\begin{aligned} g_{MF}^{(1)}\{(t), A\} &= F1^*\{(-t), A\} \\ g_{MF}^{(31)}\{(t), A\} &= F31^*\{(-t), A\} \\ g_{MF}^{(32)}\{(t), A\} &= F32^*\{(-t), A\} \\ g_{MF}^{(33)}\{(t), A\} &= F33^*\{(-t), A\} \end{aligned} \tag{4.3}$$

and the corresponding average filter responses are found by averaging over the I-Q phase histories p_k to obtain

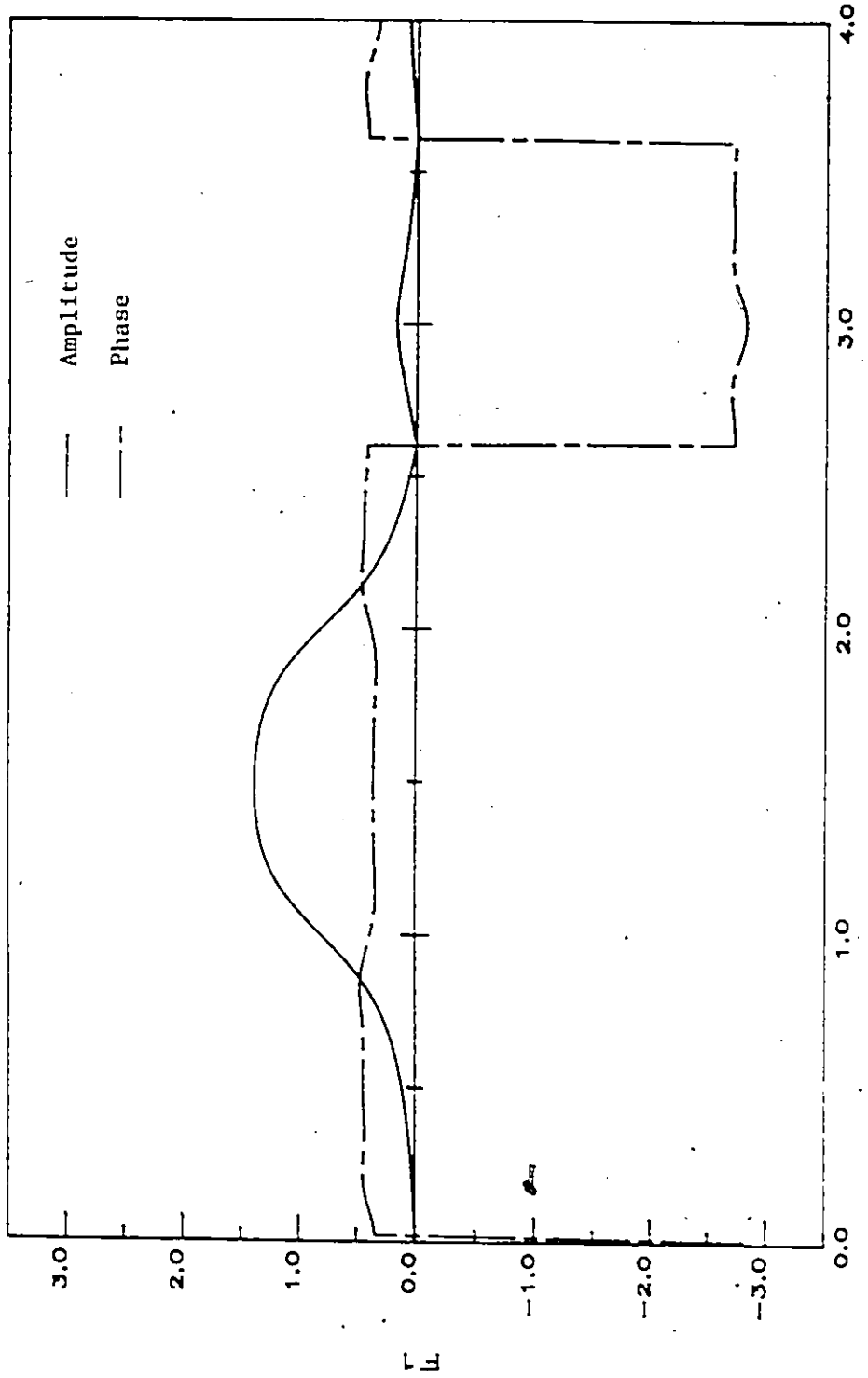

Fig. 4.8 The average generic waveform F1((t),A) for input back-off of 0 dB.

$$F1\{(t), A\} = \frac{1}{16} \sum_{p_k=0}^{15} F1(p_k)$$

$$F31\{(t), A\} = \frac{1}{16} \sum_{p_k=0}^{15} F31(p_k)$$

$$F32\{(t), A\} = \frac{1}{16} \sum_{p_k=0}^{15} F32(p_k)$$

$$F33\{(t), A\} = \frac{1}{16} \sum_{p_k=0}^{15} F33(p_k)$$

The approximate log likelihood ratio can then be written as

$$J_1(\{\alpha_i, \beta_i\}) = \sum_i -2\,\mathrm{Re}[(\alpha_i - j\beta_i) Z_i^1(A) + (I)^*_{\phi_i} Z_i^{31}(A) + (II)^*_{\phi_i} Z_i^{32}(A) + III)^*_{\phi_i} Z_i^{33}(A)] \tag{4.4}$$

The average waveform $F1\{(t), A\}$ for the example considered in section 4.2, is shown in Fig. 4.8. Since $F31(pk) = -F31(15-pk)$, $F32(pk) = -F32(15-pk)$ and $F33(pk) = -F33(15-pk)$, the average waveform $F31\{(t) A\}$, $F32\{(t), A\}$ and $F33\{(t), A\}$ will be zero. Hence the expression for the log likelihood ratio can be simplified to the approximate form

$$J_1(\{\alpha_i, \beta_i\}) = \sum_i -2\,\mathrm{Re}[(\alpha_i - j\beta_i) Z_i^1(A)] \tag{4.5}$$

which depends only on the present data symbol (α_i, β_i). A sub-optimum receiver structure can then be specified, and is seen to consist of the "average" matched filter defined by $g_{MF^{(1)}}\{(t), A\}$ followed by a decision device. We note that this is a symbol-by-symbol receiver. The decision devices outputs the data bits (α_i, β_i) for which $J_1(\alpha_i, \beta_i)$ has minimum value. The resulting sub-optimum receiver is shown in Figure 4.9. The sub-optimum receiver structure developed here represents an enormous simplification compared to the MLSE structure in terms of both memory and computation requirements, since it consists only of a filter followed by a decision device.

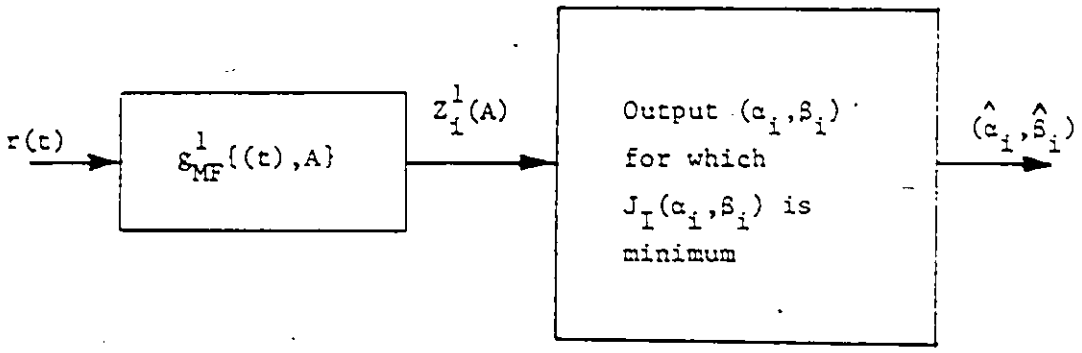

Fig. 4.9 Sub-optimum receiver, defined by eqn. (4.4)

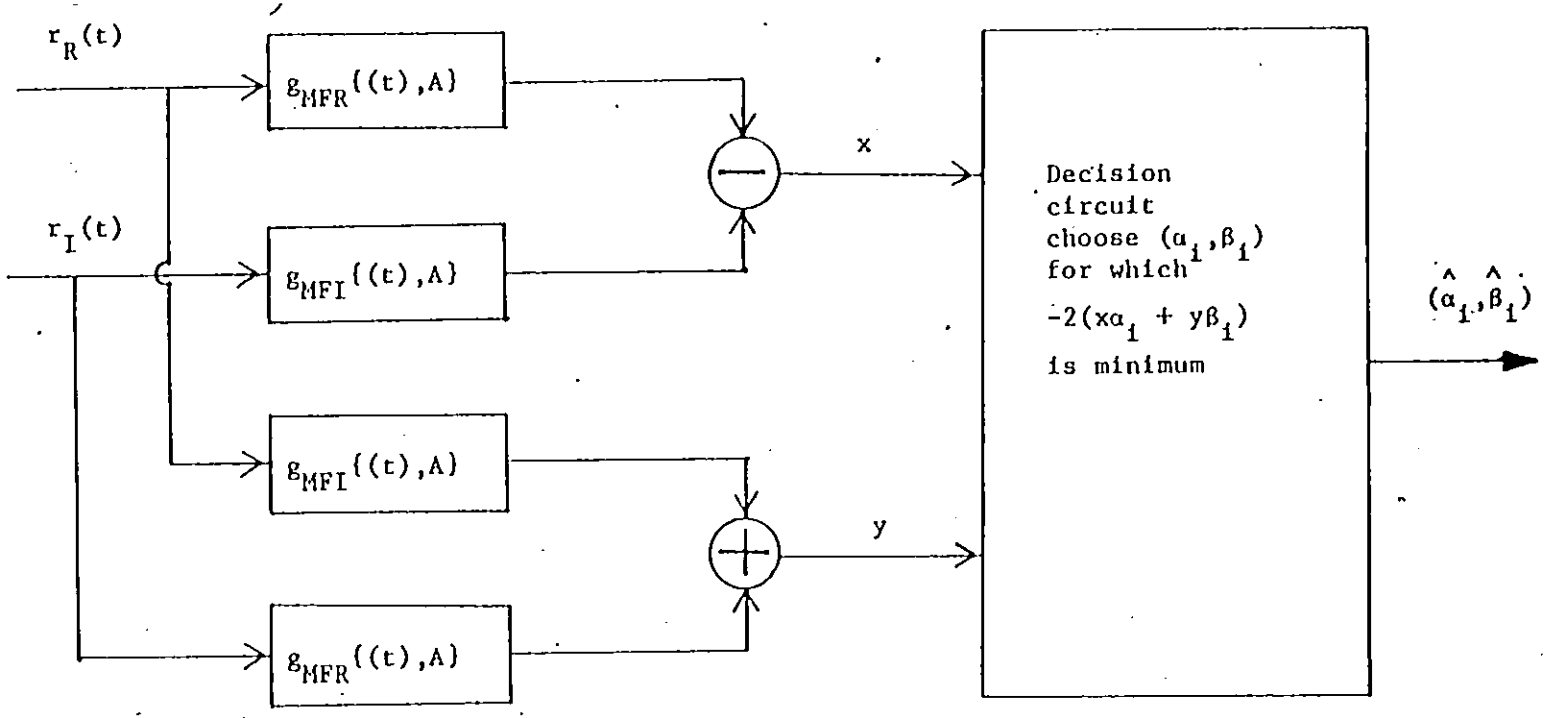

Fig. 4.10 Baseband realization of the sub-optimum receiver structure as defined by eqn. (4.6).

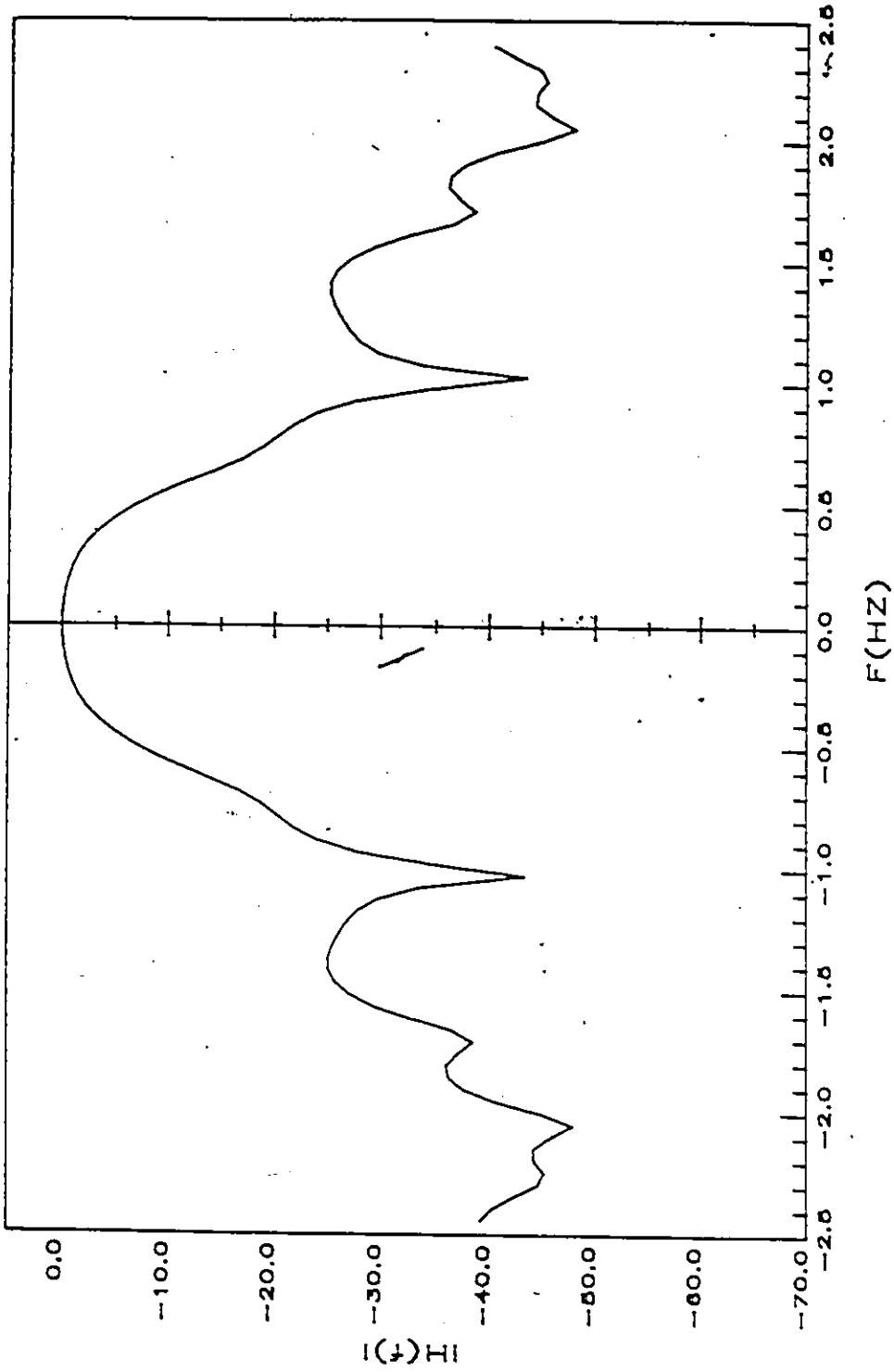

Fig. 4.11 Frequency response of baseband "average" matched filter $g_{MFR}(t)$, A).

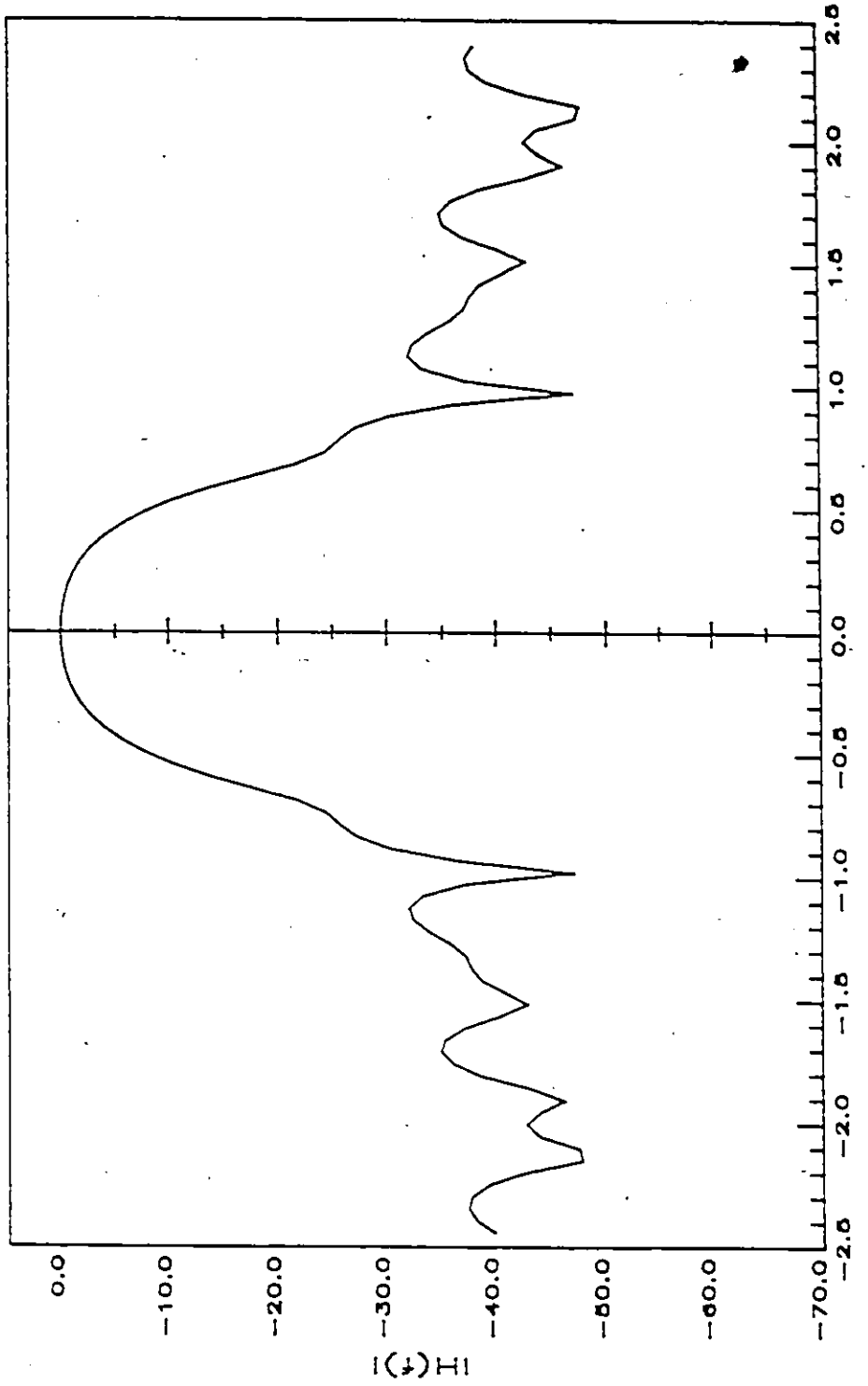

Fig. 4.12 Frequency response of baseband "average" matched filter $g_{MFR}((t), A)$.

Now let us employ complex notation to write

$$r(t) = r_R(t) + j\, r_I(t)$$

$$\text{and} \qquad g^{(1)}_{MF}\{(t), A\} = g_{MFR}\{(t), A\} + j\, g_{MFI}\{(t), A\} \tag{4.6}$$

In terms of these notations, the log likelihood ratio of (4.4) may be written as

$$J_l(\{\alpha_i, \beta_i\}) = -2 \left\{ \alpha_i \left[r_R(t) * g_{MFR}\{(t), A\} - r_I(t) * g_{MFI}[(t), A\} \right] \right.$$

$$\left. + \beta_i \left[r_I(t) * g_{MFR}\{(t), A\} + r_R(t), A] \right] \right\} \tag{4.7}$$

The base-band realization of the receiver suggested by (4.7) is shown in Figure 4.10. Since the impulse responses of the filters $g_{MFR}\{(t), A\}$ and $g_{MFI}\{(t), A\}$ are known, their frequency responses can be computed, and for the example considered in section VI are shown in two-sided baseband form in Figures 4.11 and 4.12 respectively.

4.4 Sub-optimum Receiver: Simulation Results

4.4.1 Example 1

The probability of bit error for the sub-optimum receiver was estimated using computer simulation. The uplink filter is assumed to be a fourth-order Chebyshev filter with 2BT = 1, the same as in section 4.2. Also, as in section 4.2, TWTA characteristics which are typical of those used in the sub-optimum receiver are plotted in Fig. 4.5. It can be seen that the performance of the sub-optimum receiver is essentially as good as that of the MLSE receiver.

4.4.2 Example 2

As a second example of this averaging technique, we considered the bandlimiting to be the cascade of a Nyquist raised cosine filter (roll-off factor $\alpha = 0.3$) and the fourth-order Chebyshev filter both with 2BT = 1, where B is one-sided bandwidth. The sub-optimum

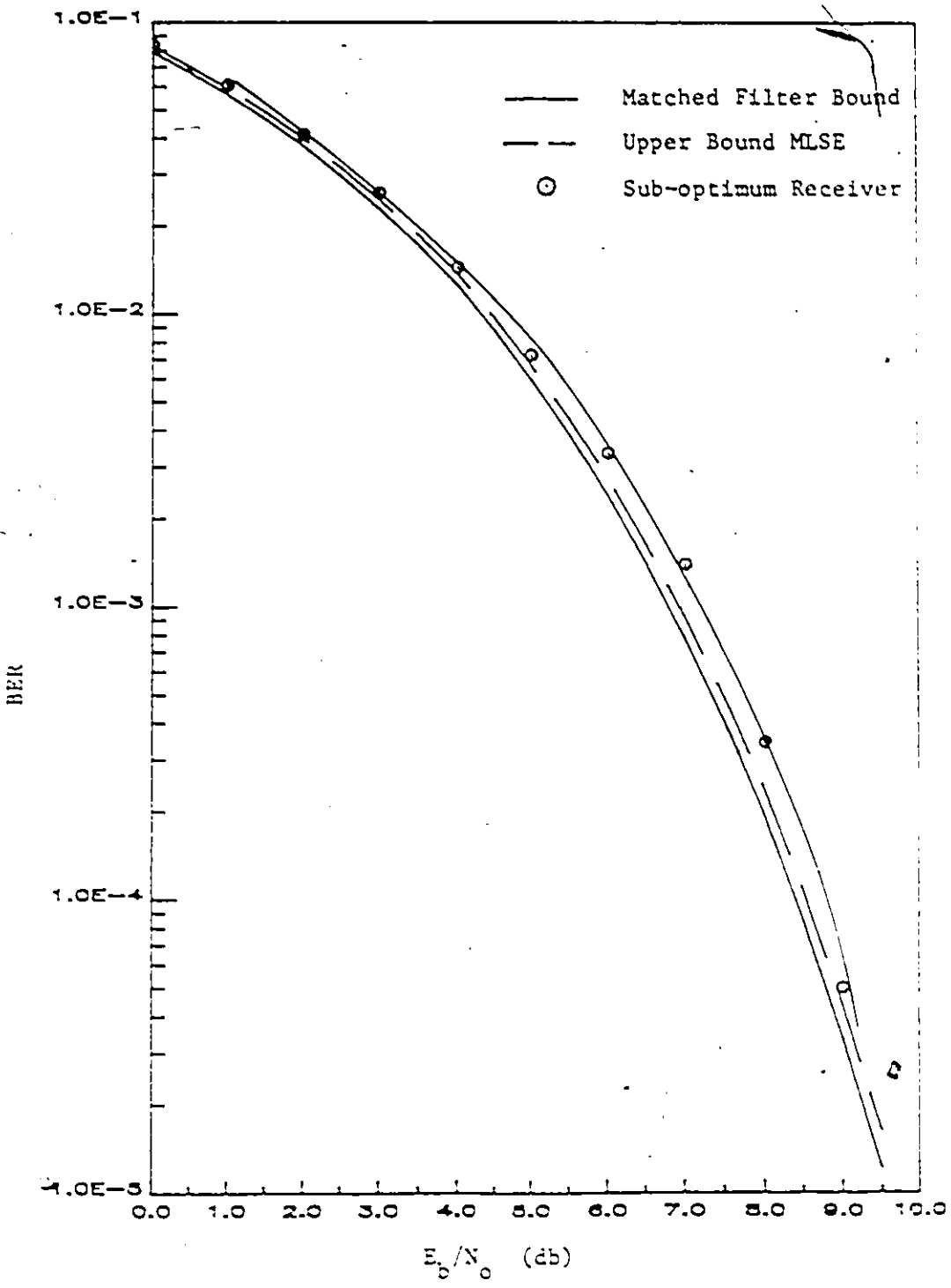

Fig. 4.13 Performance of the sub-optimum receiver when the bandlimiting filter consists of the cascade of a 30% roll-off Nyquist filter and the fourth order Chebyshev filter.

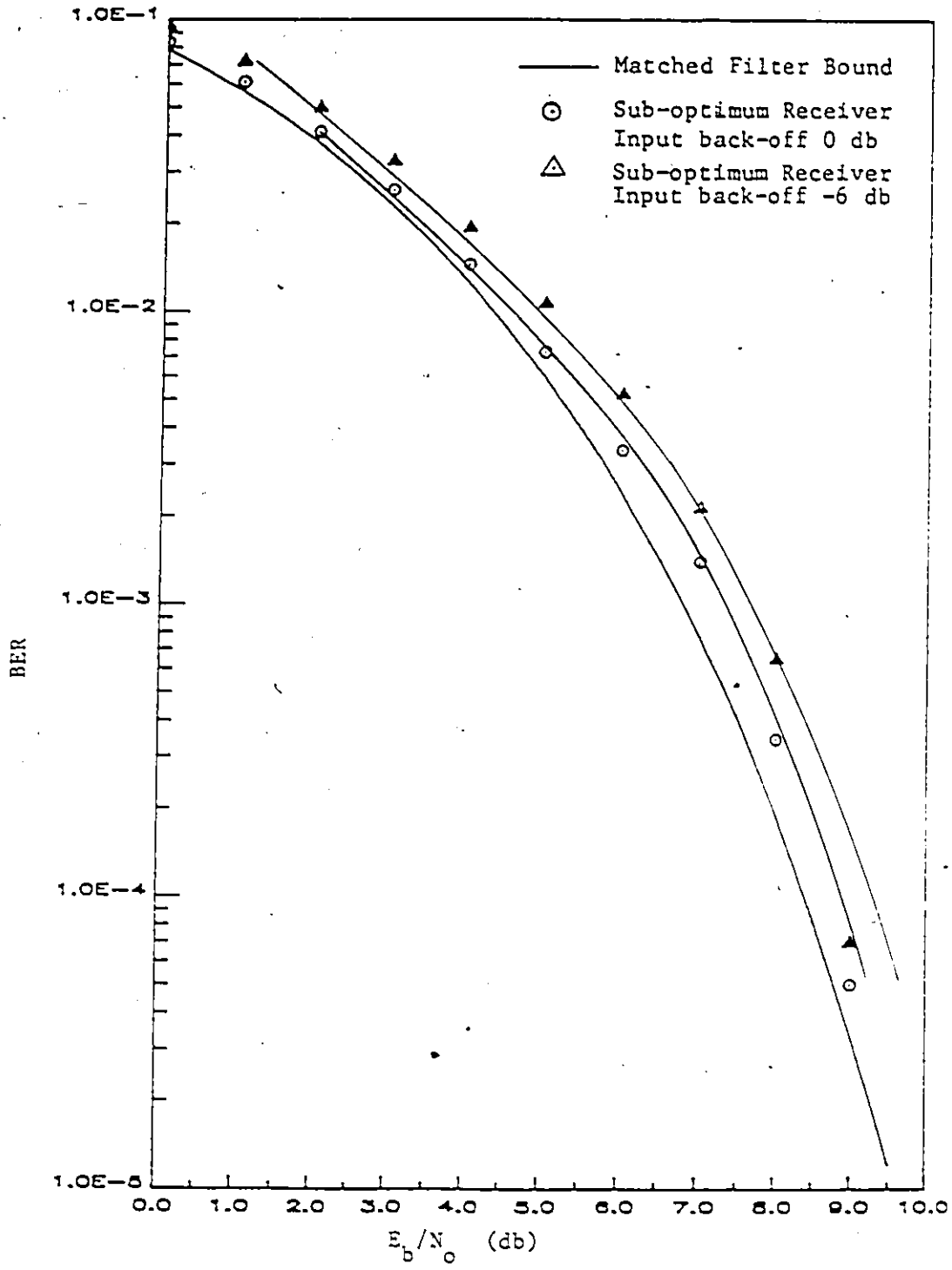

Fig. 4.14 Performance of the sub-optimum receiver when the TWTA is operated at the input back-off of 6 dB.

receiver structure was synthesized and its performance evaluated using computer simulation. The performance for this filter combination is shown in Figure 4.13 and appears to be essentially as good as in the first example.

4.4.3 Sensitivity to TWTA Input Back-off

The "average" filter responses for several TWTA input back-off's were also computed. It was found that these waveforms, as in the MLSE case, do not change significantly up to an input back-off of -6 dB. Therefore, it appears that the performance of the sub-optimum receiver will not be very sensitive to TWT back-off, at least for input back-offs of -6 dB or less, the normal range of operation in most satellite systems. The simulated performance of the receiver of the second example is shown in Figure 4.14 for a 6 dB backoff. The receiver was synthesized assuming saturation, and it can be seen that there is only a 0.3 to 0.5 dB loss in performance, so that while the sub-optimum receiver exhibits some sensitivity to the TWTA operating point, it appears to be a relatively robust structure. This small degradation can be largely removed by re-designing the filters for different values of back off.

4.5 Conclusions

In this Chapter, the performance of the MLSE receiver is estimated using computer simulation and by computing an approximate upper bound on the probability of error, which indicates that the performance of the MLSE receiver should be found to be close to the matched filter lower bound. It is shown that at least for the case of a channel memory extending over $\nu = 3$ symbols, we need to store only 8 waveforms for each of the two significant filter responses. For larger channel memory, this requirement will increase. The computation of maximum matched filter output is achieved by comparing two matched filter

outputs, instead of the 128 comparisons required for an optimum computation for $v = 3$. Our simulation shows that this simplified method of computing the minimum branch metrics (or maximum matched filter outputs), which is analogous to decision feedback processing, give results very close to the optimum computation.

A sub-optimum receiver was then derived by using the average matched filter responses. The performance of the sub-optimum receiver was estimated for two bandlimiting filter combinations by computer simulation, and the performance of each was found to be essentially as good as that of the MLSE receiver. As v, the channel memory, increases, we would expect more terms in the branch metrics of (2.43) to become significant. This would, in turn, require that more of the terms in (2.43) be taken into account in the receiver design, and in any averaging process to obtain a suboptimum structure could result in a receiver that requires more complex signal processing than the simple filtering found here for a channel of memory $v = 3$ symbols. This additional complexity could manifest itself as either a requirement for more complicated filtering or as a requirement to actually use a Viterbi detector.

CHAPTER 5

RECEIVERS FOR THE NONLINEAR CHANNEL INCLUDING PRE- AND POST-NONLINEARITY FILTERING

5.1 Introduction

In Chapter 2, and all the references given therein, the channel models do not include down link filtering following the nonlinearity. However, most real systems have significant filtering on the downlink path, which should be taken into account in a receiver design. In this chapter, we develop an optimum receiver structure and estimate its performance for QPSK signalling over bandlimited, non-linear satellite channels which include downlink filtering. We show that the optimum receiver for the above-channel model can be implemented in the form of a bank of matched filters followed by a Viterbi Processor employing a suitable metric as an extension to the work in Chapter 2. An approximate upperbound on the probability of error is also developed. Further we develop a sub-optimum receiver structure which approximates in some sense the optimum receiver and allows for a significantly simpler implementation in the form of a complex filter followed by decision circuitry. The performance of both receiver structures is estimated using computer simulation, and it is shown that the performance of the sub-optimum receiver is close to that of the optimum receiver.

5.2 The System Model

The satellite channel model including downlink filtering is shown in Fig. 5.1. In this channel model there is a filter introduced following the TWTA. Let $h_1(t)$ and $h_2(t)$ be the

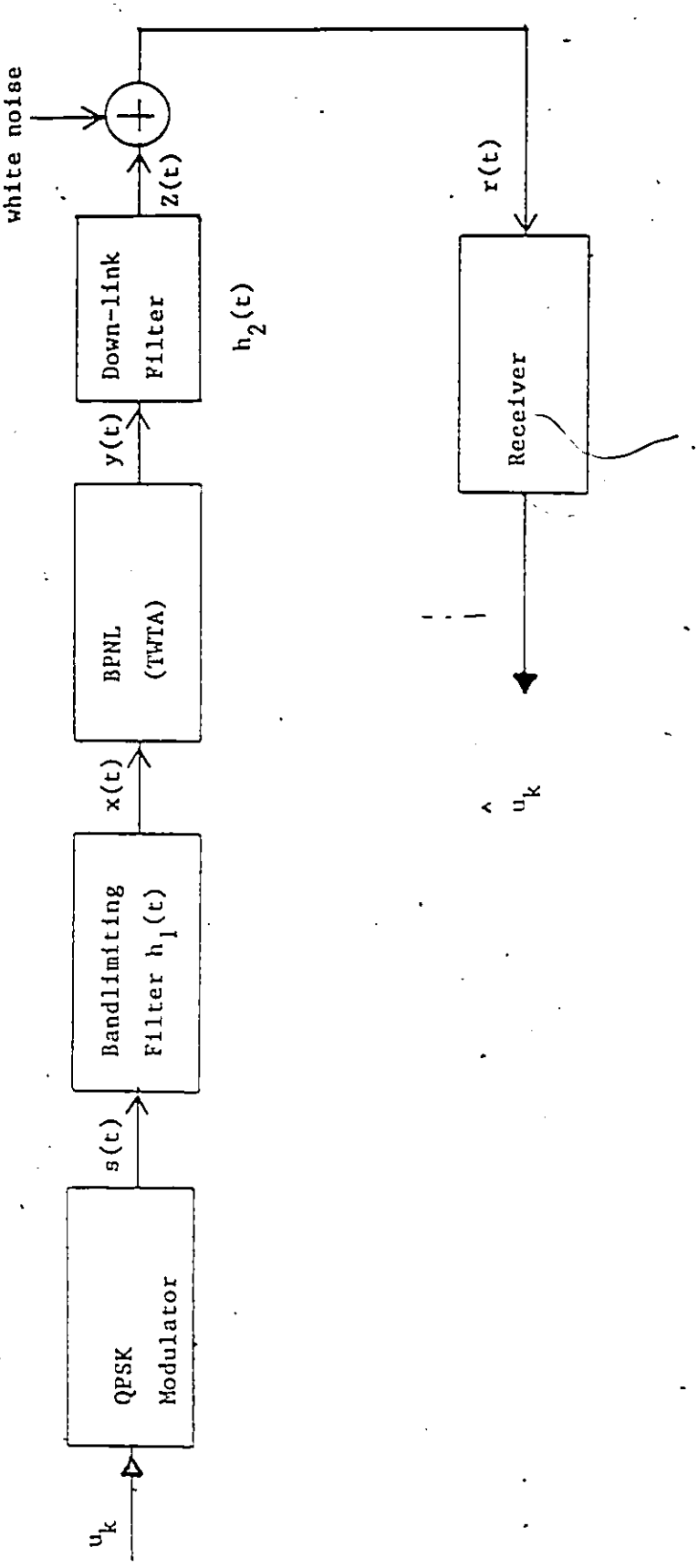

Fig. 5.1 The satellite channel model including pre- and post-nonlinearity filtering.

impulse responses of the uplink and downlink filters respectively. In most satellite systems, an uplink channel memory of $v = 3$, is a reasonable approximation to the actual impulse-response duration [32]. Therefore in the remainder of the chapter, we will assume $v = 3$. Extension to larger values of v is straightforward. Using the same notation as in Chapter 2, we can write an expression for the output of the bandpass nonlinearity for $v = 3$, as

$$y(t) = \mathrm{Re}\Big\{\exp(j\omega_d t)\sum_k \{\exp(j\phi_k) f^{(1)}\{(t-kT), p_k\} + \exp j(\phi_k + \phi_{k-1} + \phi_{k-2})$$
$$f^{(31)}\{(t-kT), p_k\} + \exp j(\phi_k + \phi_{k-2} + \phi_{k-3}) f^{(32)}\{(t-kT), p_k\}$$
$$+ \exp j(\phi_k + \phi_{k-1} + \phi_{k-3}) f^{(33)}\{(t-kT), p_k\}\}\Big\} \tag{5.1}$$

where we have defined the combined baseband waveforms

$$f^{(1)}\{(t-kT), p_k\} = f_0^{(1)}\{(t-kT), p_k\} + f_1^{(1)}\{(t-(k+1)T), p_{k+1}\}$$
$$+ f_2^{(1)}\{(t-(k+2)T), p_{k+2}\} + f_3^{(1)}\{(t-(k+3)T), p_{k+3}\}$$
$$f^{(31)}\{(t-kT), p_k\} = f_{0,1,2}^{(3)}\{(t-kT), p_k\} + f_{1,2,3}^{(3)}\{(t-(k+1)T), p_{k+1}\}$$
$$f^{(32)}\{(t-kT), p_k\} = f_{0,2,3}^{(3)}\{(t-kT), p_k\} \tag{5.2}$$

and

$$f^{(33)}\{(t-kT), p_k\} = f_{0,1,3}^{(3)}\{(t-kT), p_k\}$$

It should be noted that y(t) is a function of the Inphase (I)−quadrature (Q) phase histories, where by I-Q phase history we mean, to which channel (in-phase or quadrature) the present and previous data phases, given by ϕ_{k-i}, where $i = 0 \ldots v$, belong. The I-Q phase history is denoted by the binary value of the number p_k, with a zero meaning I channel and one meaning Q channel. For example, $f_0^{(1)}\{(t),3\}$ denotes a constituent waveform for a transmitted phase sequence given by IIQQ (binary equivalent of 3 is 0011).

Let $h_2(t) = k(t) \exp j\eta(t)$ to be the impulse response of the downlink filter, where k(t) is the amplitude response and $\eta(t)$ is the phase response. The complex envelope of the output of the downlink filter can then be written as

$$z(t, \{\alpha_i, \beta_i\}) =$$

$$\sum_k [W^{(1)}\{(t-kT), p_k\} \exp j\,\phi_k + W^{(31)}\{(t-kT), p_k\} \exp j\,(\phi_k + \phi_{k-1} + \phi_{k-2})$$

$$+ W^{(32)}\{(t-kT), p_k\} \exp j\,(\phi_k + \phi_{k-2} + \phi_{k-3})$$

$$+ W^{(33)}\{(t-kT), p_k\} \exp j\,(\phi_k + \phi_{k-1} + \phi_{k-3})] \qquad (5.3)$$

where

$$W^{(1)}\{(t-kT), p_k\} = f^{(1)}\{(t-kT), p_k\} * h_2(t)$$

$$W^{(31)}\{(t-kT), p_k\} = f^{(31)}\{(t-kT), p_k\} * h_2(t) \qquad (5.4)$$

$$W^{(32)}\{(t-kT), p_k\} = f^{(32)}\{(t-kT), p_k\} * h_2(t)$$

$$W^{(33)}\{(t-kT), p_k\} = f^{(33)}\{(t-kT), p_k\} * h_2(t)\ ,$$

* denoting convolution.

The duration of k(t) is assumed to be L'T secs, where L' is an integer. Defining the memory of the downlink filter as $v' = L' - 1$, it is clear that the duration of the waveforms $W^{(1)}\{(t-kT), k_k\}$ and $W^{(31)}\{(t-kT), p_k\}$ will be $(v+v'+1)T$ s and $(v'+v'-1)T$ s respectively. Furthermore, the duration of $W^{(32)}\{(t-kT), p_k\}$ and $W^{(33)}\{(t-kT), p_k\}$ will be $(v+v'-2)T$ s. The waveforms $W^{(1)}\{(t), p\}$, etc., are calculated by convolving the constituent waveforms $f^{(1)}\{(t), p\}$ etc. with $h_2(t)$, denoted by * in (5.4).

5.3 Structure of the Maximum Likelihood Receiver

The objective of the receiver is to estimate the transmitted sequence $\{u_i\} = \{\alpha_i, \beta_i\} = \{\cos \phi_i, \sin \phi_i\}$ from the received signal

$$y(t) = z(t; \{u_i\}) + n(t) \quad t \in I \qquad (5.5)$$

where n(t) is the complex envelope of the White Gaussian noise (WGN) added at the front end of the receiver. For the special case of WGN, the likelihood function $\Lambda[\gamma(t); \{a_i, \beta_i\}]$ is given by [36] as

$$\Lambda[\gamma(t); \{a_i, \beta_i\}] = \exp\left\{\mathrm{Re}\left[\frac{1}{N_o}\int_I \gamma(t)\, Z^*(t; \{a_i, \beta_i\})\, dt\right]\right.$$

$$\left. - \frac{1}{2N_o}\int_I |Z(t; \{a_i, \beta_i\})|^2 dt\right\} \tag{5.6}$$

Substituting $Z(t; \{a_i, \beta_i\})$ from (5.3) into (5.6) we get

$$\Lambda[\gamma(t); \{a_i, \beta_i\}] = \exp\left\{\frac{1}{2N_o}\left[2\mathrm{Re}\left(\sum_i \exp(-j\phi_i)\, Z_i^1(p_i)\right.\right.\right.$$

$$\left. + (\mathrm{I})^*_{\phi_i} Z_i^{31}(p_i) + (\mathrm{II})^*_{\phi_i} Z_i^{32}(p_i) + (\mathrm{III})^*_{\phi_i} Z_i^{33}(p_i)\right)$$

$$- \sum_i \sum_k \mathrm{Re}(\exp(j\phi_i)\exp(-j\phi_k)\, S_{i-k}^{1,1} + (\mathrm{I})_{\phi_i} (\mathrm{I})^*_k S_{i-k}^{31,31}$$

$$+ (\mathrm{II})_{\phi_i} (\mathrm{II})^*_{\phi_k} S_{i-k}^{32,32} + (\mathrm{III})_{\phi_i} (\mathrm{III})^*_{\phi_k} S_{i-k}^{33,33}$$

$$+ 2\exp(j\phi_i)(\mathrm{I})^*_{\phi_k} S_{i-k}^{1,31} + 2\exp j\phi_i (\mathrm{II})_{\phi_i} (\mathrm{I})^*_{\phi_k} S_{i-k}^{1,32}$$

$$+ 2\exp(j\phi_i)(\mathrm{III})^*_{\phi_k} S_{i-k}^{1,33} + 2(\mathrm{I})_{\phi_i} (\mathrm{II})^*_{\phi_k} S_{i-k}^{31,32}$$

$$\left.\left. + 2(\mathrm{I})_{\phi_i} (\mathrm{III})^*_{\phi_k} S_{i-k}^{31,33} + 2(\mathrm{II})_{\phi_i} (\mathrm{III})^*_{\phi_k} S_{i-k}^{32,33}\right)\right]\right\} \tag{5.7}$$

where

$$(\mathrm{I})_{\phi_i} = \exp j(\phi_i + \phi_{i-1} + \phi_{i-2})$$

$$(\mathrm{II})_{\phi_i} = \exp j(\phi_i + \phi_{i-2} + \phi_{i-3})$$

$$(\mathrm{III})_{\phi_i} = \exp j(\phi_i + \phi_{i-1} + \phi_{i-3})$$

and $(\cdot)^*$ denotes the complex conjugate. Using the notation $\langle a(t), b(t)\rangle$ to denote the inner product $\int a(t)\, b^*(t)\, dt$, we may write

$$Z_i^{\ell}(p_i) = \langle y(t), W^{(\ell)}\{(t-iT), p_i\}\rangle, \qquad \ell = 1, 31, 32, 33$$

$$S_{i-k}^{1,1} = \langle W^{(1)}\{(t-iT), p_i\}, W^{(1)}\{(t-iT), p_k\}\rangle, \qquad i-k = -(v+v'+1), \ldots, -1, 0$$

$$S_{i-k}^{31,31} = \langle W^{(31)}\{(t-iT), p_i\}, W^{(31)}\{(t-iT), p_k\}\rangle, \qquad i-k = -(v+v'-1), \ldots, -1, 0$$

$$S_{i-k}^{\ell m,\ell n} = \langle W^{(\ell m)}\{(t-iT), p_i\}, W^{(\ell n)}\{(t-iT), p_k\}\rangle, \qquad i-k = -(v+v'-2), \ldots, -1, 0, \ldots, (v+v'-2)$$
$$\ell_m = 32,33 \quad \ell_n = 32,33$$

$$S_{i-k}^{1,31} = \langle W^{(1)}\{(t-iT), p_i\}, W^{(31)}\{(t-iT), p_k\}\rangle, \qquad i-k = -(v+v'+1), \ldots, 0, \ldots, (v+v'-1)$$

$$S_{i-k}^{1,32} = \langle W^{(1)}\{(t-iT), p_i\}, W^{(32)}\{(t-iT), p_k\}\rangle, \qquad i-k = -(v+v'+1), \ldots, -1, 0, \ldots, (v+v'-2)$$

$$S_{i-k}^{1,33} = \langle W^{(1)}\{(t-iT), p_i\}, W^{(33)}\{(t-iT), p_k\}\rangle, \qquad i-k = -(v+v'+1), \ldots, -1, 0, \ldots, (v+v'-2)$$

$$S_{i-k}^{1,\ell'} = \langle W^{(1)}\{(t-iT), p_i\}, W^{(\ell')}\{(t-iT), p_k\}\rangle, \qquad i-k = -(v+v'+1), \ldots, -1, 0, \ldots, (v+v'-2)$$
$$\ell' = 32,33$$

(5.9)

In equation (5.7), the quantities $Z_i^{1}(p_i)$, $Z_i^{31}(p_i)$, $Z_i^{32}(p_i)$ and $Z_i^{33}(p_i)$ can be interpreted as sample values taken at the the symbol rate from the outputs of matched filters with impulse reponse functions,

$$g_{MF}^{(1)}\{(t), p_i\} = W^{(1)}\{(-t), p_i\}$$

$$g_{MF}^{(31)}\{(t), p_i\} = W^{(31)}\{(-t), p_i\} \qquad (5.9)$$

$$g_{MF}^{(32)}\{(t), p_i\} = W^{(32)}\{(-t), p_i\}$$

$$g_{MF}^{(33)}\{(t), p_i\} = W^{(33)}\{(-t), p_i\}$$

respectively. The sequences $\{Z_i^{1}(p_i)\}$, $\{Z_i^{31}(p_i)\}$, $\{Z_i^{32}(p_i)\}$ and $\{Z_i^{33}(p_i)\}$ contain all the information about the received signal. The likelihood ratio can be computed by knowing the matched filter outputs and the quantities $\{S_{i-k}^{1,1}\}$ etc, which may be generated once and stored for use thereafter for any given channel.

The structure of the maximum likelihood receiver can now be specified. It consists of a bank of matched filters $g_{MF}^{(1)}\{(t), p_k\}$, $g_{MF}^{(31)}\{(t), p_k\}$, $g_{MF}^{(32)}\{(t), p_k\}$ and $g_{MF}^{(33)}\{(t), p_k\}$ with output symbol rate samplers, followed by a processor called the maximum likelihood sequence estimator (MLSE). The MLSE determines the most probable sequence $\{\alpha_i, \beta_i\}$ as the one that maximizes (5.7), or equivalently, that assigns a minimum value to the path metric [37] given by

$$J_T(\{\alpha_i, \beta_i\}) = -\ell n\, \Lambda[Y(t);\{\alpha_i, \beta_i\}] \qquad (5.10)$$

Defining [22,35] the state at time KT as $S_k = \{(\alpha_{k-1}, \beta_{k-1}), \cdots (\alpha_{k-(v+v'+1)}, \beta_{k-(v+v'+1)})\}$ and the corresponding state transitions as $\xi_k = (S_{k+1}, S_k)$, it is then possible [35] to write the path metric of equation (5.10) as the sum of the branch metrics,

$$J_T(\{\alpha_i, \beta_i\}) = \sum \lambda(\xi_i) \qquad (5.11)$$

where the branch metrics $\lambda(\xi_i)$ are given by

$$\lambda(\xi_i) = -2\mathrm{Re}\Big\{\Big[(a_i - j\beta_i)Z_i^1(p_i) + (\mathrm{I})^*_{\phi_i} Z_i^{31}(p_i) + (\mathrm{II})^*_{\phi_i} Z_i^{32}(p_i) + (\mathrm{III})^*_{\phi_i} Z_i^{33}(p_i)\Big]$$

$$+ (S_0^{1,1} + S_0^{31,31} + S_0^{32,32} + S_0^{33,33})$$

$$+2\Big[(a_i + j\beta_i)\sum_{\ell=-(v+v'+1)}^{-1}(a_{i+\ell} - j\beta_{i+\ell})S_\ell^{1,1} + (\mathrm{I})_{\phi_i}\sum_{\ell=-(v'+2)}^{-1}(\mathrm{I})^*_{\phi_i+\ell} S_\ell^{31,31}$$

$$+ (\mathrm{II})_{\phi_i}\sum_{\ell=-(v+v'-2)}^{-1}(\mathrm{II})^*_{\phi_i+\ell} S_\ell^{32,32} + (\mathrm{III})_{\phi_i}\sum_{\ell=-(v+v'-2)}^{-1}(\mathrm{III})^*_{\phi_i+\ell} S_\ell^{33,33}$$

$$+ (\mathrm{I})_{\phi_i}\sum_{\ell=-(v+v'+1)}^{0}(a_{i+\ell} - j\beta_{i+\ell}) S_\ell^{1,31} + (\mathrm{I})_{\phi_i}\sum_{\ell=1}^{v'+2}(a_{i-\ell} - j\beta_{i-\ell}) S_\ell^{1,31}$$

$$+ (\mathrm{II})_{\phi_i}\sum_{\ell=-(v+v'+1)}^{0}(a_{i+\ell} - j\beta_{i+\ell}) S_\ell^{1,32} + (\mathrm{II})_{\phi_i}\sum_{\ell=1}^{v'+v-2}(a_{i-\ell} - j\beta_{i-\ell}) S_\ell^{1,32}$$

$$+ (\mathrm{III})_{\phi_i}\sum_{\ell=-(v+v'+1)}^{0}(\mathrm{II})^*_{\phi_i+\ell} S_\ell^{32,33} + (\mathrm{III})_{\phi_i}\sum_{1}^{v'+v-2}(\mathrm{II})_{\phi_i-\ell} S_\ell^{32,33}$$

$$+ (\mathrm{II})_{\phi_i}\sum_{\ell=-(v+v'+1)}^{0}(\mathrm{I})^*_{\phi_i+\ell} S_\ell^{31,32} + (\mathrm{II})_{\phi_i}\sum_{\ell=1}^{(v'+v-2)}(\mathrm{II})^*_{\phi_i-\ell} S_\ell^{31,32}$$

$$+ (\mathrm{III})_{\phi_i}\sum_{\ell=-(v+v'-1)}(\mathrm{III})^*_{\phi_i+\ell} S_\ell^{31,33} + (\mathrm{III})_{\phi_i}\sum_{\ell=1}^{(v'+v-2)}(\mathrm{I})^*_{\phi_i-\ell} S_\ell^{31,33}\Big]\Big\} \qquad (5.12)$$

Since the channel memory $(v+v'+1)$ is finite, the channel itself may be viewed as a finite-state machine driven by the information source. This implies that the receiver can be implemented in the form of a Viterbi detector. The Viterbi processor for our case will require $M^{v+v'+1}$ states unlike the uplink filtering model in Chapter 2, where we have M^v states only. For QSPK with $M = 4$, the number of states is usually too large for any useful implementation. Also the computation of the quantities $S_{\ell-k}^{1,1}$ etc. is tedious, since they are dependent on the p_k's and hence a large number of these quantities must be stored. However,

our simulation experience, as described later, has shown that in the situations of interest, neglecting these quantities has negligible effect on the value of the branch metrics given by (5.12). That means we can synthesize the Viterbi processor by taking into account only the first four terms of the branch metric, (5.12). This observation leads to considerable simplification in receiver structure because we then need only M^{v} states in the Viterbi processor as compared to $M^{v+v'+1}$. It should be mentioned here that the complexity of the receiver increases rapidly as the uplink channel memory v is increased, however, the increase in downlink filter memory v' does not increase the number of filters, it essentially affects only the complexity of the matched filter responses.

A block diagram of the receiver structure for an uplink channel memory of v = 3 and a downlink filter memory of v' = 3 is shown in Fig. 5.2. As explained in Chapter 2, for an uplink channel memory of v = 3, there are 128 responses corresponding to $f^{(1)}\{(t), p_k\}$, 32 responses to $f^{(31)}\{(t), p_k\}$, and 16 responses each to $f^{(32)}\{(t), p_k\}$ and $f^{(33)}\{(t), p_k\}$. For purposes of simulation, these waveforms may be generated as in Chapter 4, by storing the generic uplink waveforms defined as

$$\begin{aligned} F^{1}(p_k) &= f^{(1)}\{(t-kT), p_k\} \quad \text{where } p_k = p_{k+1} = p_{k+2} = p_{k+3} \\ F^{31}(p_k) &= f^{(31)}\{(t-kT), p_k\} \quad \text{where } p_k = p_{k+1} \\ F^{32}(p_k) &= f^{(32)}\{(t-kT), p_k\} \\ F^{33}(p_k) &= f^{(33)}\{(t-kT), p_k\} \end{aligned} \tag{5.13}$$

It is now possible to generate any of the responses $f^{(1)}\{(t), p_i\}$ etc., as a suitable combinations of segments of the generic waveforms defined in (5.13). Once we have the responses $f^{(1)}\{(t), p_i\}$, etc. generated, it is straightforward to compute the matched responses $g_{MF}{}^{(1)}\{(t), p_i\}$ etc., by (5.4) and (5.9).

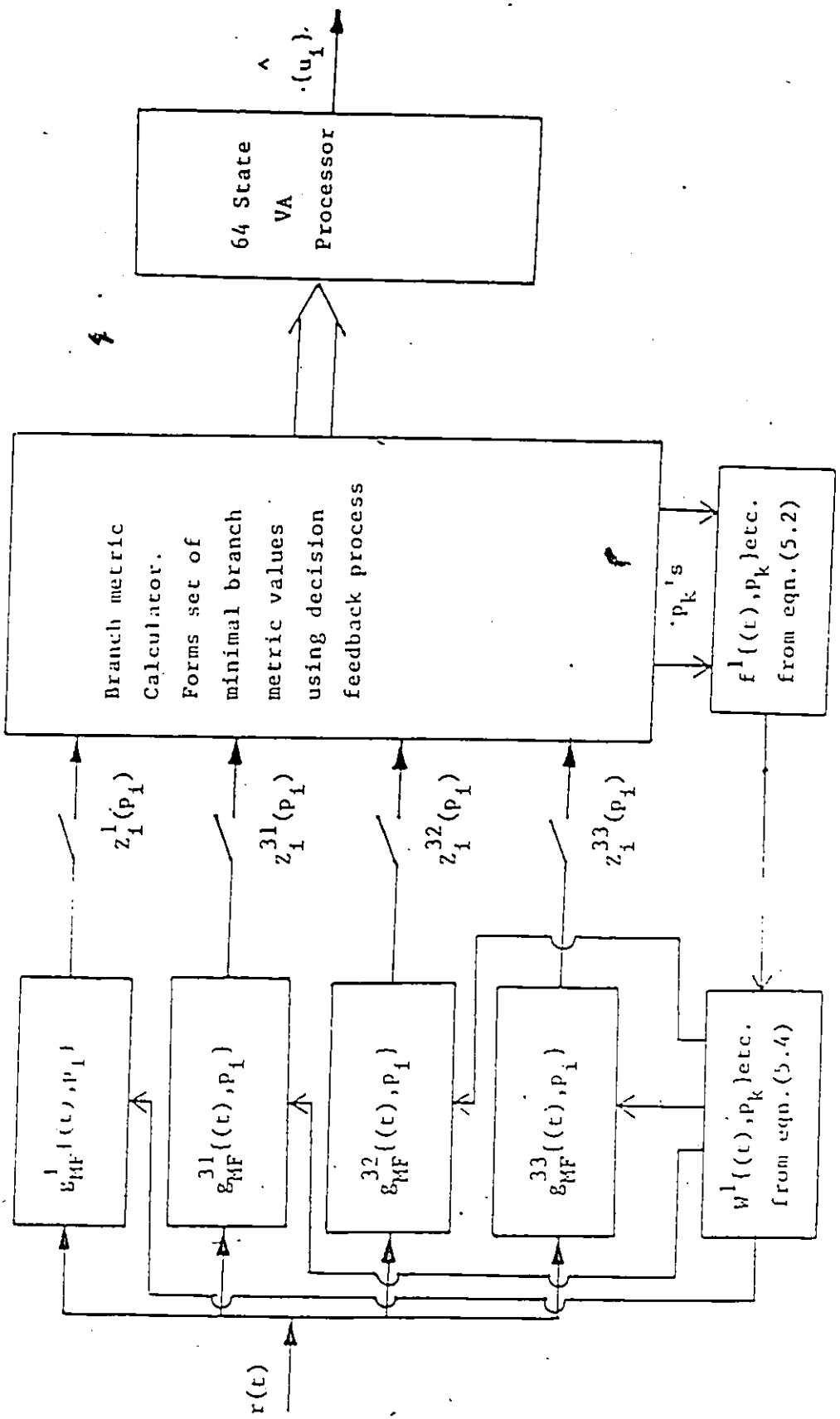

Fig. 5.2 Structure of the approximate MLSR as simulated for an uplink channel memory of $v = 3$, and downlink memory $v' = 3$.

5.4 Error Performance

Following arguments as in Chapter 3, an upper bound on the error performance of the receiver at moderate to high signal-to-noise ratio can be written as

$$P_e \le K Q\left[\frac{d\min}{\sqrt{2N_o}}\right] \tag{5.14}$$

where

$$K = \sum_{\varepsilon \in E d\min} \left[\frac{1}{M^{W_H(\varepsilon)}}\right] W_H(\varepsilon)$$

and

$$E d\min = \{\varepsilon \in E \mid \bar{d}(\varepsilon) = d\min\}$$

An error event ε is said to extend from K_1 to K_2 if the estimated state sequence $\{\hat{S}_i\}$ is equal to the correct state sequence $\{S_i\}$ at time k_1 and k_2, but nowhere in between. In terms of an error sequence $\{e_k\} = \{\hat{u}_k\} - \{u_k\}$, ε is defined as

$$\varepsilon = [\{e_K\} = \ldots 0, 0, \ldots e_{K_1}, \ldots, e_{K_1+\eta_e-\nu_1}, 0, 0, \ldots, \quad \text{with } e_{K_1}, e_{K_1+\eta_e-\nu_1} \neq 0]$$

where $n_e \triangleq K_2 - K_1 - 1$ is defined as the length of the error event, $W_H(\varepsilon)$ is the Hamming weight of the error event ε, and $M = 4$ in the case of QPSK. The total channel memory ν_1 in our case is $(\nu + \nu' + 1)$.

The average distance $\bar{d}(\varepsilon)$ can be found as a solution to the transcendental equation

$$Q[(2N_o)^{-1/2}\,\bar{d}(\varepsilon)] = \frac{1}{\mathrm{card}(S_\varepsilon)} \sum_{\{S_i\}} Q\left[(2N_o)^{-1/2}\, d\left(\varepsilon; \{S_i\}_{K_1}^{K_1+\eta_e+1}\right)\right] \tag{5.15}$$

where the distance $d(\varepsilon; \{S_i\}_{K_1}^{K_1+\eta_e+1})$ for our case is given by

$$d\left(\varepsilon; \{S_i\}_{K_1}^{K_1+\eta_e+1}\right) = \int \left| Z\left(t; \{u_i\}_{K_1-\nu_1}^{K_1+\eta_e+1} + \{e_i\}_{K_1-\nu_1}^{K_1+\eta_e+1}\right) - Z\left(t; \{u_i\}_{K_1-\nu_1}^{K_1+\eta_e}\right)\right|^2 dt \tag{5.16}$$

with

$$\{u_i\} \overset{1-1}{\longleftrightarrow} \{S_i\} \in S_\varepsilon$$

and S_ε = the set of allowable error state sequence segments.

In particular, if single error events of the form $\varepsilon_o = [\{e_k\} = 0 \ldots, e_{k_1}, 0, \ldots]$ with $e_{k_1} \neq 0$, are dominant, the bound on probability of symbol error P_e is given by

$$P_e \leq Q\left[\frac{d_o}{\sqrt{2N_o}}\right] \tag{5.17}$$

where

$$d_c = \overline{d(\varepsilon_o)}$$

5.5 Receiver Performance

In this section we apply our results to evaluating, the performance of the MLSR structure, shown in Fig. 5.2, through computer simulation. In the satellite channel model, we assume that the bandlimiting in the uplink is introduced by the cascade of a Nyquist raised cosine filter (rolloff factor = 0.3) and a fourth-order Chebyshev filter both with 2BT = 1, where B is one sided bandwidth [39]. The TWTA characteristics are typical of those used in an INTELSAT IV Satellite [34]. The downlink filter is also assumed to be a fourth order Chebyshev filter with 2BT = 1. The uplink channel memory v, and downlink filter memory v' are both assumed to be 3.

To compute the minimum branch metric value for each transition thereby eliminating parallel trellis branches in an optimum way, we must compare the 128 branch metric values given by the first four terms of (5.12). Thus an optimum computation of minimum branch metric is too complex for any practical implementation. To circumvent this, a simplified procedure, similar to that described in Chapter 4 is used. The procedure is analogous to decision feedback processing, and works as follows.

An initial combination of p_k's corresponding to maximum matched filter output is determined and stored. The initial sequence of p_k's can be found by exhaustive search, by single sample detection, or possibly just arbitrarily set. Suppose for example at any instant of time, the p_k's are $p_k = 2$, $P_{k+1} = 4$, $p_{k+2} = 9$, and $p_{k+3} = 2$, as shown in Fig. 5.3. Then at

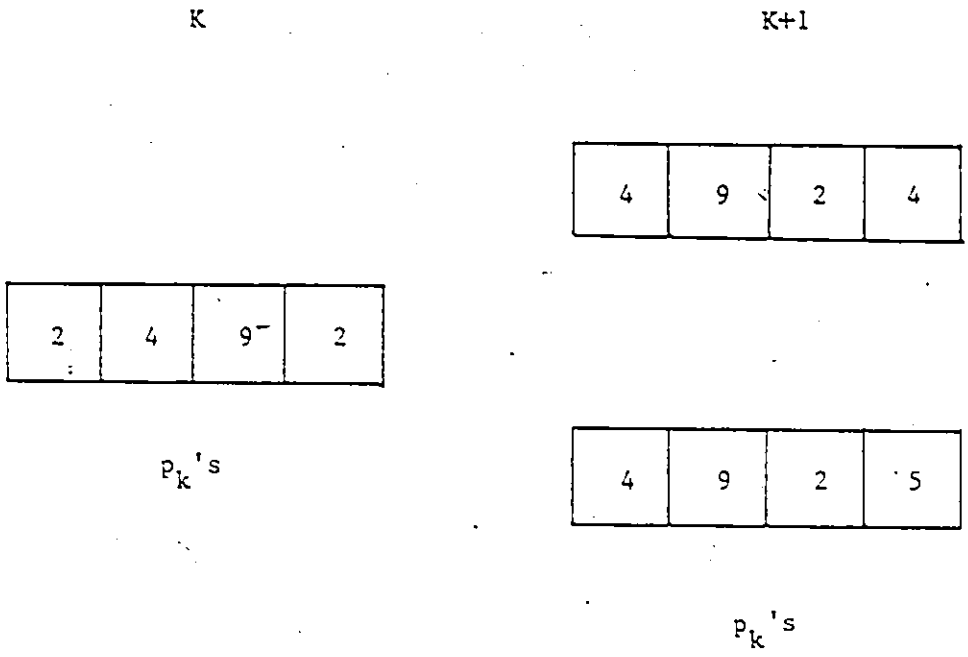

Fig. 5.3 Estimation of p_k's using simplified procedure.

the next instant of time, as shown in Fig. 5.3, the values of the p_k's will be $p_{k+1} = 4$, $p_{k+2} = 9$, $p_{k+3} = 2$ and $p_{k+4} = 4$ or 5. Hence by storing the present values of the p_k's, we are able to estimate the p_k's at the next sampling instant. The required minimum metric value is then obtained as the minimum of only two metric values. We, therefore, only need to store the present values of the p_k's and then keep on updating them. It can be seen that this simplified procedure for computing the minimum branch metric results in a significant reduction in computation, since for each transition we need to compare only two matched filter outputs compared to the 128 comparisons required in the optimum case. It might be mentioned here that although the simplified procedure is not theoretically equivalent to the optimum computation of the minimum branch metric, our simulation results show that the performance using the simplified procedure is essentially as good as that of the optimum computation.

The error performance of the MLSR at low to moderate signal-to-noise ratio has been estimated using computer simulation. For the purpose of simulation, the minimum branch metric was computed using the simplified procedure as explained above. A 64 state Viterbi detector with a decision depth of 20 was used and the initial sequence of p_k's was arbitrarily set. This was found to cause a short initial transient or burst of errors. The resulting simulated probability of bit error is shown in Fig. 5.4. For comparison purposes, the matched filter bound attained in an additive white gaussian noise channel is also plotted in Fig. 5.4. In addition, it was found by simulation that single error events were dominant at moderate-to-high SNR. Hence the probability of error was estimated using the approximate bound of equation (5.17). It can be seen from our results in Fig. 5.4, that there is about 0.7 dB of degradation at $P_{be} = 10^{-4}$ compared to the matched filter bound, and that equation (5.17) provides a fairly good estimate of error rate. In addition, it is likely that some of the

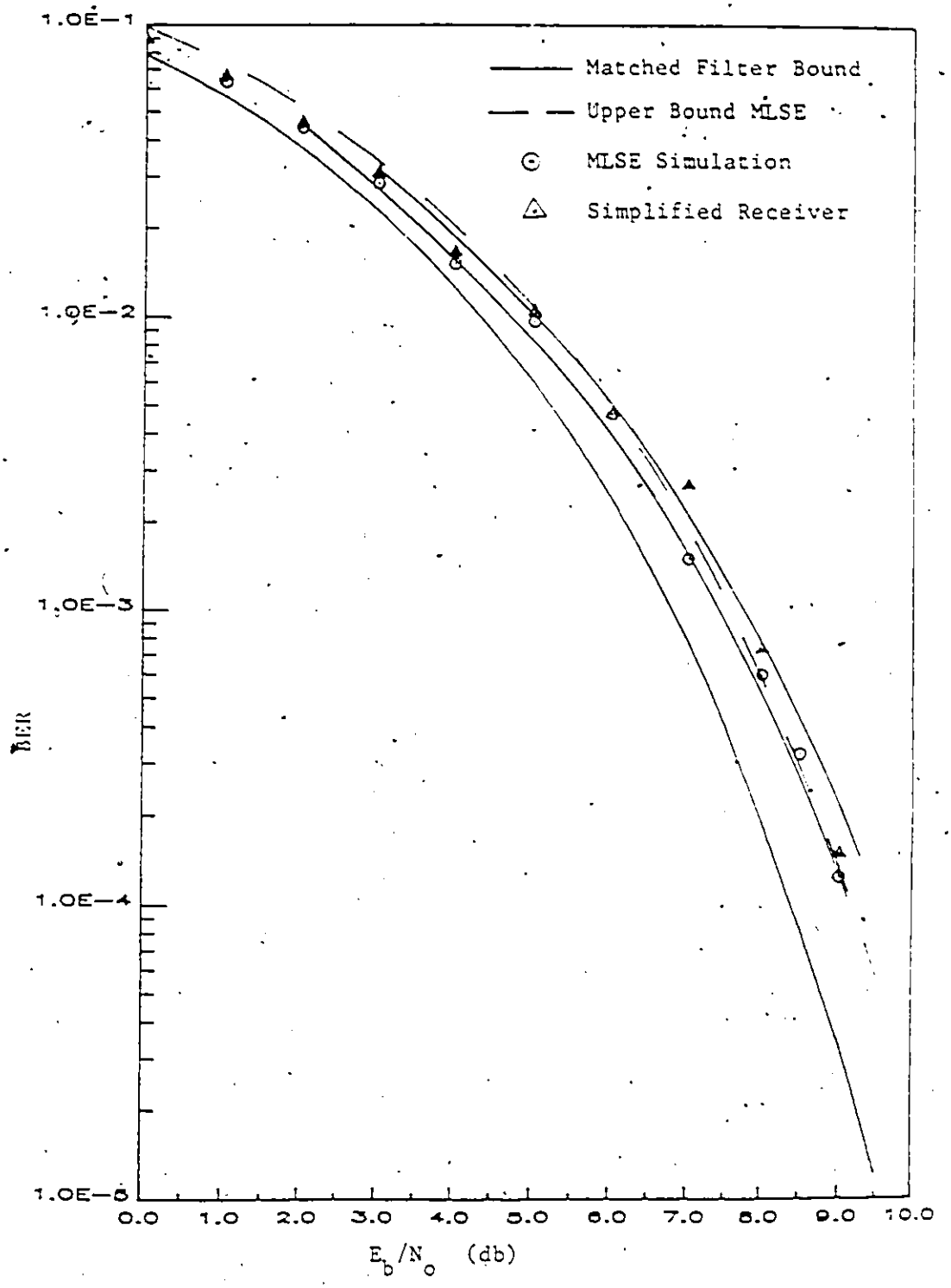

Fig. 5.4. Performance comparison of the MLSE and the simplified receiver structure for the down-link filtering channel.

remaining degradation could be removed by including the neglected quantities in the metric computation.

5.6 Simplified Receiver

In this section we develop a simplified receiver structure by using average matched filter responses instead of the actual matched filter responses $g_{MF}^{(1)}\{(t), p_i\}$ etc.* As explained in section 5.5, it has been found through computation and simulation, that in a typical satellite channel (uplink memory $v = 3$), at most the first four terms are significant in the expression of the branch metric (5.12). Hence the approximate log likelihood ratio can be written from (5.11) and (5.12) as

$$J_1(\{\alpha_i, \beta_i\}) = \sum_i -2\mathrm{Re}[(\alpha_i - j\beta_i)Z_i^1(p_i) + (I)_{\phi_i}^{*} Z_i^{31}(p_i) + (II)_{\phi_i}^{*} Z_i^{32}(p_i) + (III)_{\phi_i}^{*} Z_i^{33}(p_i)] \quad (5.18)$$

One approach to further receiver simplification is to use average matched filter outputs $Z_i^1(A)$, $Z_i^{31}(A)$, $Z_i^{(32)}(A)$ and $Z_i^{33}(A)$ instead of actual matched filter outputs $Z_i^1(p_i)$ etc. The average matched filter responses may be defined as

$$\begin{aligned} g_{MF}^{(1)}\{(t), A\} &= W^{(1)}\{(-t), A\} \\ g_{MF}^{(31)}\{(t), A\} &= W^{(31)}\{(-t), A\} \\ g_{MF}^{(32)}\{(t), A\} &= W^{(32)}\{(-t), A\} \\ g_{MF}^{(33)}\{(t), A\} &= W^{(33)}\{(-t), A\} \end{aligned} \quad (5.19)$$

where the corresponding average filter responses are found by averaging over the I-Q phase histories p_k to obtain

---

* The idea of averaged matched filters has been used in [43,44].

$$W^{(1)}\{(-t), A\} = \frac{1}{128} \sum_{\text{over all } p_k\text{'s}} f^{(1)}\{(t), p_k\} * h_2(t)$$

$$W^{(31)}\{(-t), A\} = \frac{1}{32} \sum_{\text{over all } p_k\text{'s}} f^{(31)}\{(t), p_k\} * h_2(t)$$

$$W^{(32)}\{(-t), A\} = \frac{1}{16} \sum_{\text{over all } p_k\text{'s}} f^{(32)}\{(t), p_k\} * h_2(t) \qquad (5.20)$$

$$W^{(33)}\{(-t), A\} = \frac{1}{16} \sum_{\text{over all } p_k\text{'s}} f^{(33)}\{(t), p_k\} * h_2(t)$$

The average matched filter responses $W^{(1)}\{(t), A\}$ etc., in (5.20), can also be written in terms of the generic waveforms defined in (5.13), as

$$W^{(1)}\{(t), A\} = \frac{1}{16} \sum_{p_k=0}^{15} F1(p_k) * h_2(t)$$

$$W^{(31)}\{(t), A\} = \frac{1}{16} \sum_{p_k=0}^{15} F31(p_k) * h_2(t) \qquad (5.21)$$

$$W^{(32)}\{(t), A\} = \frac{1}{16} \sum_{p_k=0}^{15} F32(p_k) * h_2(t)$$

$$W^{(33)}\{(t), A\} = \frac{1}{16} \sum_{p_k=0}^{15} F33(p_k) * h_2(t)$$

The generic waveform $F1(p_k)$ for the example considered in section V was computed in Chapter 4. Furthermore, it was found that $F31(p_k) = -F31(15-p_k)$, $F32(p_k) = -F32(15-p_k)$ and $F33(p_k) = -F33(15-p_k)$, so the average filter responses $W^{(31)}\{(t), A\}$, $W^{(32)}\{(t), A\}$ and $W^{(33)}\{(t), S\}$ will be zero. Hence the approximate expression for the log likelihood ratio (5.18), can be reduced to

$$J_1(\{\alpha_i, \beta_i\}) \simeq \sum_i -2\mathrm{Re}[(\alpha_i - j, \beta_i) Z_i^1(A)] \qquad (5.22)$$

The third order matched filter responses $Z_i^{31}(A)$ etc, for a severe ISI channel (say v = 5), will still average out to zero. However, the fifth order matched filter responses for such channels may not average to zero, nevertheless, it can be shown that for satellite channels these fifth order responses will be insignificant. Hence it appears possible to simplify the likelihood ratio to the form of (5.22), even for severe ISI channels.

A sub-optimum receiver structure, based on (5.22) can now be specified. It consists of the "average" matched filter $g_{MF^{(1)}}\{(t), A\}$ followed by a decision device. The decision device outputs the data bits (α_i, β_i) for which $J_I(\alpha_i\, \beta_i)$ has minimum value. The resulting sub-optimum receiver is shown in Fig. 5.5. It is quite similar to the receiver developed in Chapter 4. The sub-optimum receiver developed in either case is very simple compared to the MLSR, since it consists only of a filter followed by a decision circuit.

A complex base-band realization of this receiver can be derived by re-writing the log-likelihood ratio of (5.22), in the following form:

$$J_I(\{\alpha_i, \beta_i\}) = \sum - 2\{\alpha_i[Y_R(t) * g_{MFR}\{(t), A\} - Y_I(t) * g_{MFI}\{(t) A\}] + \beta_i[Y_I(t) * g_{MFR}\{(t), A\} + Y_R(t) * g_{MFI}\{(t) A\}]\} \tag{5.23}$$

where

$$Y(t) = Y_R(t) + j\, Y_I(t)$$

and

$$g^{(1)}_{MFR}\{(t), A\} = g_{MFR}\{(t), A\} + j\, g_{MFI}\{(t) A\}$$

The base-band realization of the receiver suggested by (5.23) is shown in Fig. 5.6. Since the impulse responses of the filters $g_{MFR}\{(t), A\}$ and $g_{MFI}\{(t), A\}$ are known, their frequency responses can be computed, and for the example considered in section 5.5 are shown in two sided baseband form in Figs 5.7 and 5.8 respectively.

The probability of bit error for this sub-optimum receiver was estimated using

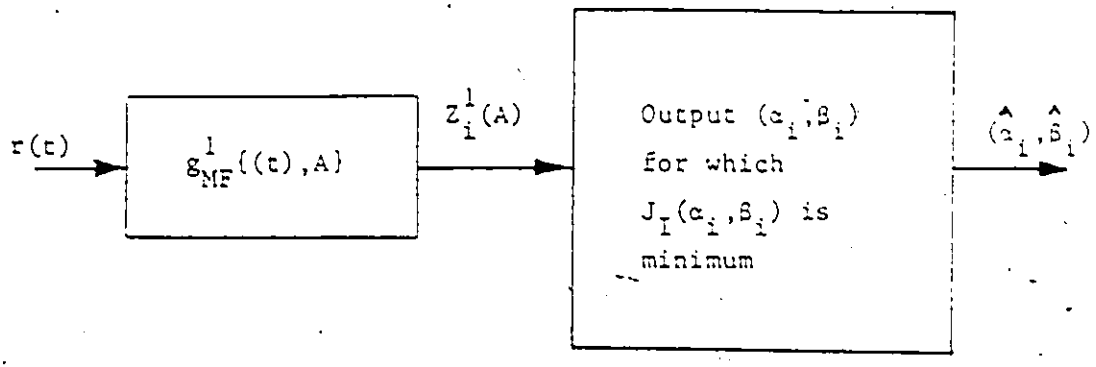

Fig. 5.5 Sub-optimum receiver, defined by eqn. (5.22)

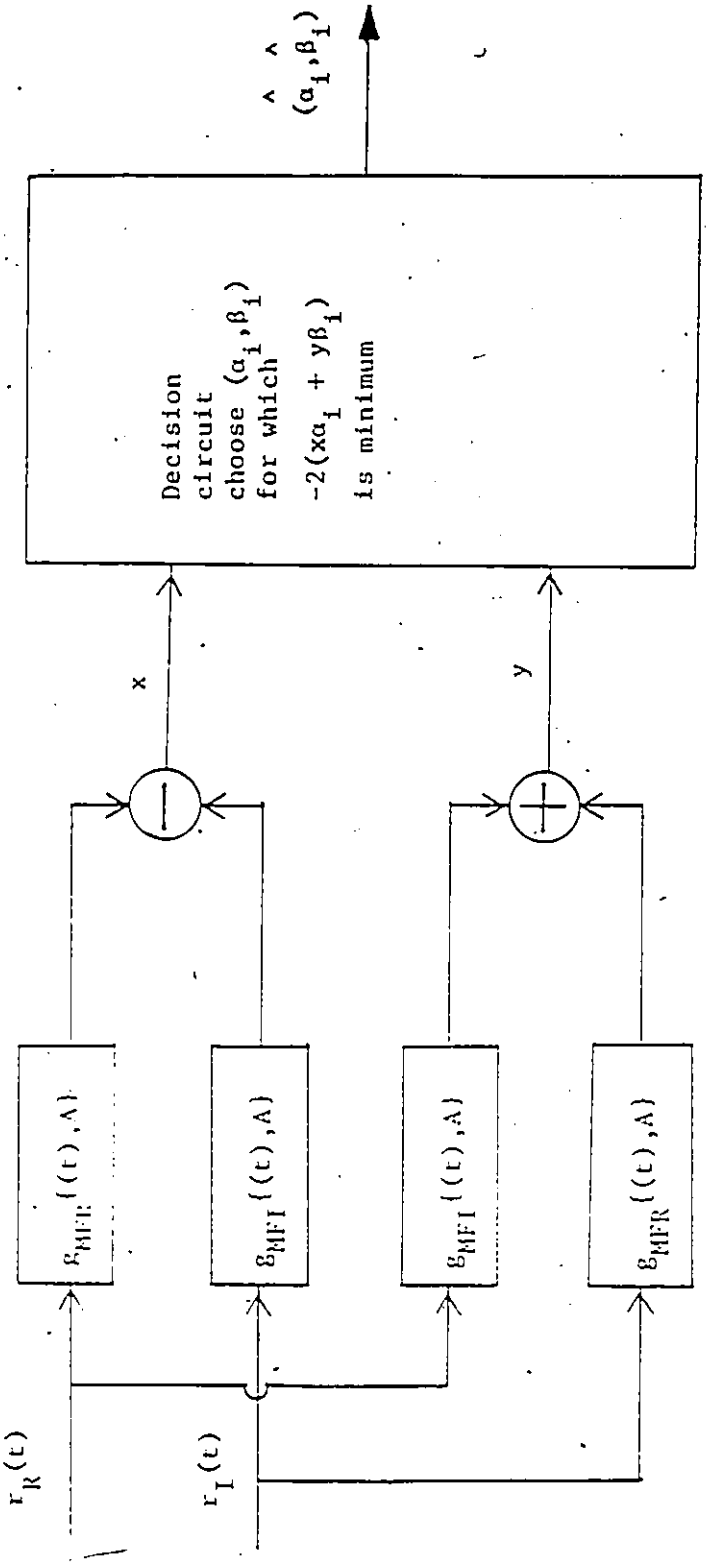

Fig. 5.6 Baseband realization of the sub-optimum receiver structure defined by eqn. (5.23).

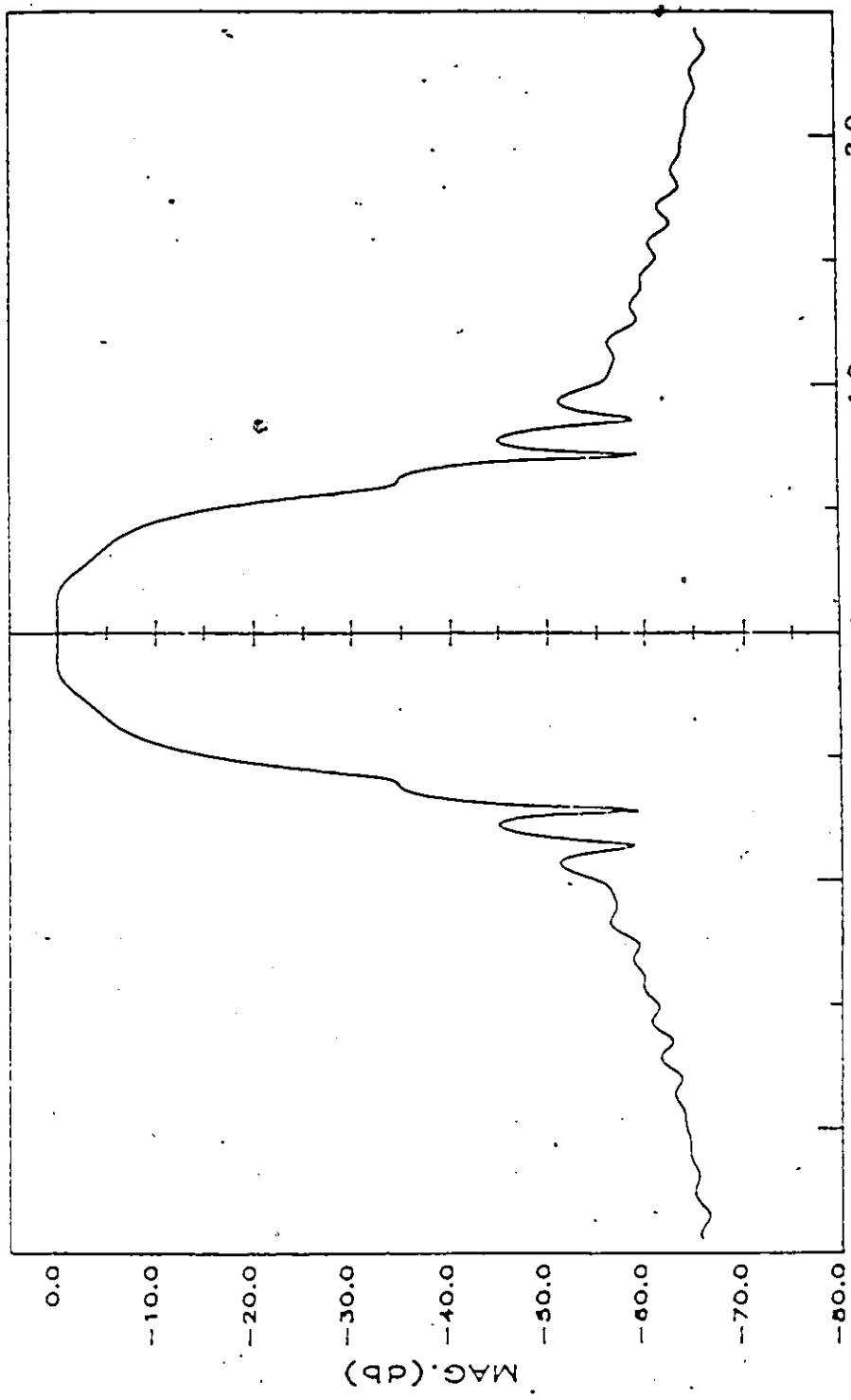

Fig. 5.7 . Frequency response of the imaginary component of the baseband average matched filter.

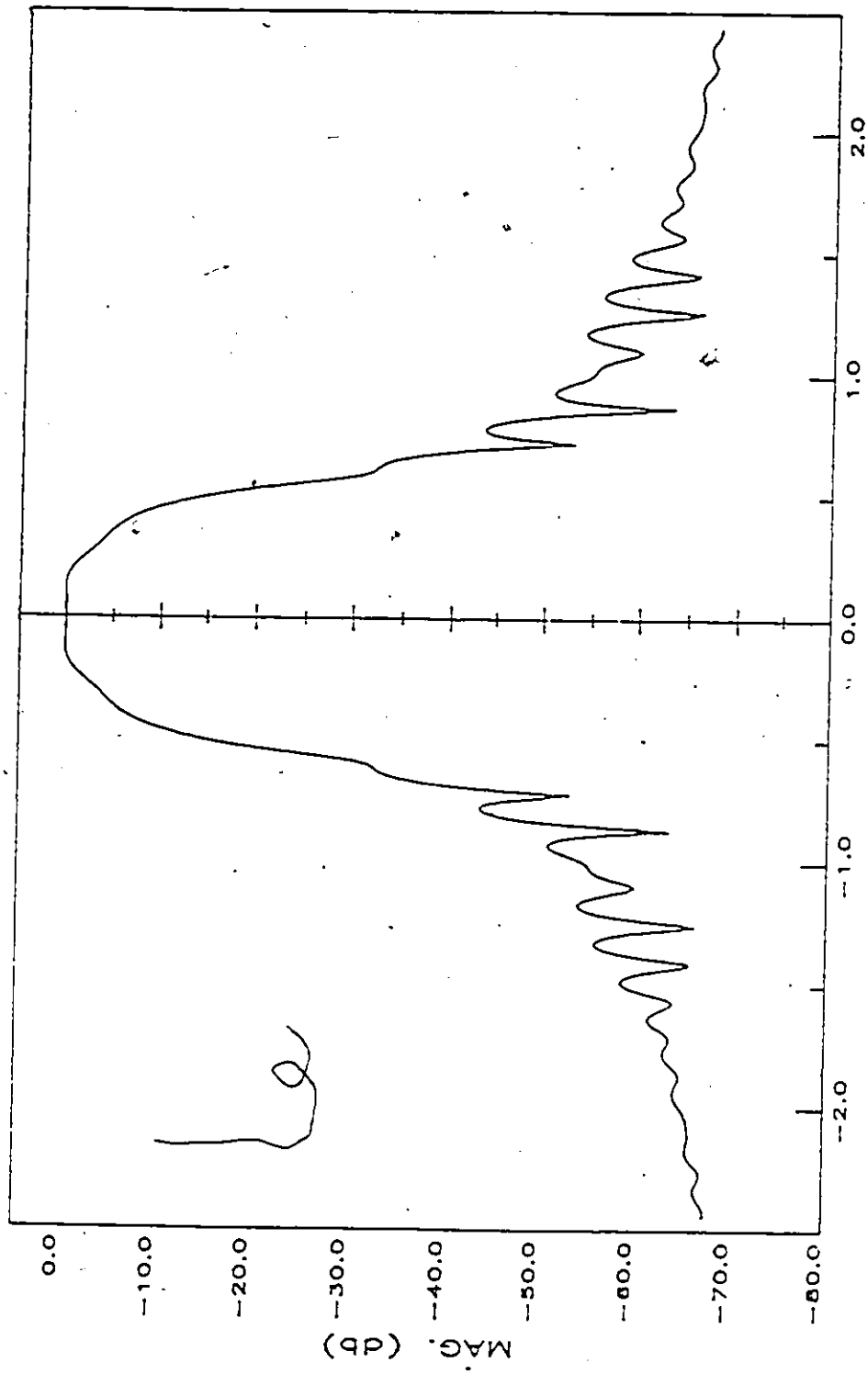

Fig. 5.8 Frequency response of the real component of the baseband average matched filter.

computer simulation and is plotted in Fig. 5.4. It can be seen that the performance of the sub-optimum receiver is close to that of the MLSE receiver with no noticeable degradation. In addition, as in Chapter 4, we have found its performance to be robust to changes in the operating point of the TWT nonlinearity.

5.7 Conclusions

In this chapter we have derived a receiver structure based on the MLSE concept for the reception of QPSK signals transmitted over bandlimited, non-linear channels, which include the effects of filtering following the BPNL. The likelihood ratio consists of two types of terms, (a) terms dependent on data bits that are determined only by uplink channel memory v, (b) terms dependent on data bits determined by total channel memory $(v+v'+1)$. For the combination of filters and BPNL assumed, it is possible to approximate the likelihood ratio with terms which are dependent primarily on the uplink channel memory v. Hence the complexity of the approximate MLSE receiver and structure is, in fact, decided by the uplink channel memory v.

Performance of the approximate MLSE receiver is estimated using computer simulation and by computing an approximate upperbound on the probability of error, which indicates that the performance of this receiver is not far from the matched filter bound. A sub-optimum receiver was then derived using the average matched filter responses. The performance of the sub-optimum receiver was estimated by computer simulation, and the performance was found to be virtually as good as that of the approximate MLSE receiver.

CHAPTER 6

CONCLUSIONS AND SUGGESTIONS FOR FUTURE WORK

6.1 Conclusions

In this thesis we have investigated a maximum likelihood sequence receiver for QPSK signals transmitted over a bandlimited, non-linear channel. In addition, a sub-optimum receiver structure was suggested which approximates the MLSE receiver. We also investigated the MLSE receiver structure and its simplification, for QPSK transmission over the bandlimited, non-linear channel including post-nonlinearity filtering. In brief, this thesis examined the problem of digital communication by QPSK signalling over bandlimited, non-linear satellite channels, and the following objectives have been achieved:

(i) An explicit expression for the output of the BPNL for a QSPK signal was obtained with p_k(I−Q path history) as a parameter. A similar expression was earlier developed in [30], for the BPSK signal, which corresponds to $p_k = 0$ in our representation. Since QPSK is one of the most commonly used modulation schemes for satellite communication, we feel that our representation will be quite useful, at least for moderate value of satellite channel memory v.

(ii) A maximum likelihood sequence receiver structure for QPSK signalling over bandlimited, non-linear channels, has been derived. It was shown that the requirement of large memory and computation could be enormously reduced, by estimating the p_k's using a simplified procedure referred to as decision feedback processing. The results obtained through computer simulation using the above procedure, and by computing upper bound on probability of error, were found to be close to optimum.

(iii) It was also shown that the sub-optimum receiver structure which approximates the MLSE receiver, consisted of a complex average matched filter followed by a decision device. The performance of the sub-optimum receiver was evaluated using computer simulation for two filter combinations. Its performance for each filter combination was found to be very close to that which could be attained using MLSE receivers. Our simulation results also showed that the sub-optimum receiver structure was relatively insensitive to TWT back-off, at least for input back-offs of -6 dB or less, the normal range of operation in most satellite systems.

(iv) Finally, we extended our results to include a channel model with post-nonlinearity filtering. It was shown that the complexity of the MLSE receiver was in fact largely decided by the uplink channel memory. The performance of the MLSE receiver was estimated using computer simulation and by computing an upper bound. The sub-optimum receiver, which approximated the MLSE receiver, was evaluated using computer simulation. Our results showed that the performance of the sub-optimum receiver was essentially as good as that of the MLSE receiver.

6.2 Suggestions for Future Work

It would be both worthwhile and of interest to study the performance degradation of the receivers developed in this thesis due to Adjacent and Co-channel interference. It looks difficult to incorporate these effects analytically, however, one could use computer simulation to study their effect on performance degradation.

Another useful problem to look at is to extend the work in this thesis to include other modulation methods such as FFSK (Fast Frequency Shift Keying). These modulation methods are increasingly becoming attractive for satellite communications, because of their

efficient spectral properties. The major difficulty lies in characterizing the output of the BPNL as a function of some parameter, such as p_k in the expression for QPSK.

In this thesis we have neglected the uplink noise, which is usually very small for large earth terminals. Since the smaller terminals are becoming more and more popular, it may be useful to consider the uplink noise in the channel model. The problem here is to expand the output of BPNL in terms of some kernel function such that the expectation of these functions over uplink noise samples could be easily computed. It appears that such an approach could be employed using some of the concepts developed by Biglieri et al. [45].

APPENDIX A

Here we show that equation (3.8)

$$J_I\left(\{u_i\}_{K_1-v}^{K_1+n_c} + \{e_i\}_{K_1}^{K_1+n_\epsilon-v}\right) \le J_I\left(\{u_i\}_{K_1-v}^{K_1+n_c}\right) \tag{A1}$$

is equivalent to (3.9).

From (2.37), (2.38) and (A1) we get

$$2\,\mathrm{Re} < n(t),\, y(t;\{u_i\}+\{e_i\}) - y(t;\{u_i\}) > \;\ge\; \|y(t;\{u_i\}+\{e_i\}) - y(t;\{u_i\})\|^2 \tag{A2}$$

where

$$< a(t),\, b(t) > = \int_I a(t)\, b(t)^*\, dt$$

and thus

$$\|a(t)\| = < a(t),\, a^*(t) >$$

Now

$$y(t);\{u_i\}+\{e_i\}) - y(t;\{u_i\})$$

$$= \sum_i \Big[e^{j(\phi_i+e_i)} f^{(1)}\{(t-iT), A\} + (I)_{\phi_i+e_i} f^{(31)}\{(t-iT), A\}$$

$$+ (II)_{\phi_i+e_i} f^{(32)}\{(t-iT), A\} + (III)_{\phi_i+e_i} f^{(33)}\{(t-iT), A\} \Big|$$

$$- \Big[e^{j\phi_i} f^{(1)}\{(t-iT), A\} + (I)_{\phi_i} f^{(31)}\{(t-iT), A\}$$

$$+ (II)_{\phi_i} f^{(32)}\{(t-iT), A\} + (III)_{\phi_i} f^{(33)}\{(t-iT), A\} \Big| \tag{A3}$$

from (2.34).

In (A3), we have used average waveforms ($f^{(1)}\{(t-iT), A\}$ etc, which is defined as the average of waveforms $f^{(1)}\{(t-iT), p_i\}$ etc., over all possible I-Q path history p_i.

Substituting (A3) in (A2), we obtain

$$2\,\mathrm{Re}\left[\sum_i \left(\gamma_i^1 n_i^1 + \gamma_i^2 n_i^{31} + \gamma_i^3 n_i^{32} + \gamma_i^4 n_i^{33}\right)\right] \geq d^2\left(\varepsilon; \{S_i\}_{K_1}^{K_1+n_\epsilon+1}\right) \tag{A4}$$

where

$$n_i^1 = \langle n(t), f^{(1)}\{(t-iT), A\}\rangle ,$$

$$n_i^{31} = \langle n(t), f^{(3)}\{(t-iT), A\}\rangle ,$$

$$n_i^{32} = \langle n(t), f^{(3)}\{(t-iT), A\}\rangle ,$$

$$n_i^{33} = \langle n(t), f^{(33)}\{(t-iT), A\}\rangle ,$$

$$d^2\left(\varepsilon; \{S_i\}_{K_1}^{K_1+n_\epsilon+1}\right) = \mathrm{Re}\left\{\sum_i \sum_k \left[\left(\gamma_i^1 \gamma_i^{1*} S_{i-k}^{1,1} + \gamma_i^2 \gamma_k^2 S_{i-k}^{31,31}\right]\right.\right.$$

$$+ 2\left(\gamma_i^2 \gamma_i^{1*} S_{i-k}^{1,31} + \gamma_i^1 \gamma_k^{3*} S_{i-k}^{1,32} + \gamma_i^1 \gamma_i^{4*} S_{i-k}^{1,33} + \gamma_i^2 \gamma_k^{3*} S_{i-k}^{31,32}\right.$$

$$\left.\left.\left. + \gamma_i^{2*} \gamma_k^4 S_{i-k}^{31,33} + \gamma_i^{3*} \gamma_k^4 S_{i-k}^{32,33}\delta_{i,k}\right) + \left[\gamma_i^{3*} \gamma_k^3 S_o^{32,33}\delta_{i,k} + \gamma_i^{4*} \gamma_k^4 S_o^{33,33}\delta_{i,k}\right]\right]\right\}$$

and

$$\gamma_i^1 = e^{j(\phi_i + e_i)} - e^{j\phi_i},\ \gamma_i^2 = (I)_{\phi_i + e_i} - (I)_{\phi_i}$$

$$\gamma^3 = (II)_{\phi_i + e_i} - (II)_{\phi_i},\ \gamma_i^4 = (III)_{\phi_i + e_i} - (III)_{\phi_i}$$

APPENDIX B

In this appendix a step by step procedure for obtaining the complex filter responses of the sub-optimum receivers, derived in Chapter 2 and 5, is given. We will first consider the satellite channel model shown in Fig. 1.5. It is assumed that the impulse response of the uplink filter is available to us. It is also assumed that the BPNL transfer characteristic $G(v)\exp[j\alpha(v)]$ can be approximated [34] by a Bessel function expansion with complex coefficients,

$$G(v)\exp j\alpha(v) = 2\sum_{k=1}^{N} b_k J_1\left[(2K-1)\frac{\pi v}{R}\right] \tag{B1}$$

where R is range of interest. Since this problem is fully addressed in [34, 47], therefore we will assume here that the complex coefficients b_k's are available to us.

As mentioned in Chapter 2, the channel memory $v = 3$, is a reasonable approximation to most real satellite channels, and so we will assume $v = 3$. However, it is straightforward to extend these results for other values of channel memory v. the first step is to compute generic waveforms defined as

$$\begin{aligned}
F1(p_k) &= f^{(1)}\{(t-kT), p_k\}, \\
&\qquad \text{where } p_k = p_{k+1} = p_{k+2} = p_{k+3} \\
F31(p_k) &= f^{(31)}\{(t-kT), p_k\}, \\
&\qquad \text{where } p_k = p_{k+1} \\
F32(p_k) &= f^{(32)}\{(t-kT), p_k\} \\
F33(p_k) &= f^{(33)}\{(t-kT), p_k\}
\end{aligned} \tag{B2}$$

where the combined baseband waveforms are given by

$$f^{(1)}\{(t-kT), p_k\} = f_0^{(1)}\{(t-kT), p_k\} + f_1^{(1)}\{(t-(k+1)T), p_{k+1}\}$$
$$+ f_2^{(1)}\{(t-(k+2)T), p_{k+2}\} + f_3^{(1)}\{(t-(k+3)T), p_{k+3}\}$$
$$f^{(31)}\{(t-kT), p_k\} = f_{0,1,2}^{(3)}\{(t-kT), p_k\} + f_{1,2,3}^{(3)}\{(t-(k+1)T), p_{k+1}\}$$
$$f^{(32)}\{(t-kT), p_k\} = f_{0,2,3}^{(3)}\{(t-kT), p_k\} \qquad \text{(B3)}$$

and

$$f^{(33)}\{(t-kT), p_k\} = f_{0,1,3}^{(3)}\{(t-kT), p_k\}$$

The first order baseband waveforms

$$f_q^{(1)}\left\{(t-kT), p_k\right\}$$

are defined as

$$f_q^{(1)}\left\{(t-kT), p_k\right\} = \sum_{n_o} \cdots\cdots \sum_{n_v} \prod_{i=0}^{v} \exp(jm_i\phi_{k-i})\, f_n(t-kT) \qquad q \in (0, 1, \cdots v)$$

so that the condition $\sum_{i=0}^{v} n_i = 1,$

implies $n_i = \begin{cases} \text{odd integer} & i=q \\ 0 \text{ or even} & \text{otherwise} \end{cases}$

and let $m_i = \begin{cases} n_i - 1 & \text{if } n_i \text{ is odd} \\ n_i & \text{otherwise} \end{cases}$. (B4)

The superscript in $f_q^{(\cdot)}$ denotes the number of indices n_i in each term of the summation that are constrained to be odd. Similarly third order baseband waveforms $f_{q,r,s}^{(3)}\{(t-kT), p_k\}$ are defined as

$$f_q^{(3)}\left\{(t-kT), p_k\right\} = \sum_{n_o} \cdots\cdots \sum_{n_v} \prod_{i=0}^{v} \exp(jm_i\phi_{k-i}) f_n(t-kT) \qquad q,r,s \in (0, 1, \cdots v)$$

so that the condition $\sum_{i=0}^{v} n_i = 1,$

implies $$n_i = \begin{cases} \text{odd integer} & i = q,r,s \\ 0 \text{ or even} & \text{otherwise} \end{cases}$$

and let $$m_i = \begin{cases} n_i - 1 & \text{if } n_i \text{ is odd} \\ n_i & \text{otherwise} \end{cases}$$

(B5)

To compute the generic waveforms defined in (B2) and (B3), we need to evaluate the interpulse product $f_n(t)$. By combining (2.18) and (2.28), we can compute $f_n(t)$ as

$$f_n(t) = 2 \exp j\left[\sum_{i=0}^{v} n_i \psi_i(t)\right] \sum_{k=1}^{N} b_k \prod_{i=0}^{v} J_{n_i}\left[(2K-1)\frac{\pi}{R} h_i(t)\right] \qquad \text{(B6)}$$

It was found sufficient to compute pulse products up to order 9. (B2) through (B6) are the main equations needed for computing the generic waveforms.

Let us investigate the relationship among the generic waveforms for different values of p_k (I-Q path history). As mentioned in Chapter 4, for a channel memory of $v = 3$, we will have 16 waveforms each for F1, F31, F32 and F33. The variation in generic waveforms is due to the exponential weighting function

$$\prod_{i=0}^{v} \exp j\phi_{K-i} m_i$$

which is dependent on p_k. Its value for $p_k = 1$ (I, I ,I, Q), will be

$$(-1)^{\frac{m3}{2}}$$

where $$m_0 + m_1 + m_2 + m_3 = 0 \qquad \text{(B7)}$$

Now let us compute this weighting function for $p_k = 14$ (Q, Q, Q, I), which will be

$$= (-1)^{\frac{m_o + m_1 + m_2}{2}}$$

$$= (-1)^{\frac{m3}{2}} \qquad \text{(from (B7))}$$

and hence we obtain

$$F1(p_k) = F(15 - p_k) \tag{B8}$$

Similarly, we can establish the following relationship among the third order generic waveforms F31, F32 and F33 for different values of p_k.

$$F31(p_k) = -F31(15 - p_k)$$

$$F32(p_k) = -F32(15 - p_k)$$

$$F33(p_k) = -F33(15 - p_k) \tag{B9}$$

Because of the relationship (B8) and (B9), we need to compute only 8 of the 16 waveforms. Next, we compute the average filter responses by averaging over the I-Q phase histories p_k to obtain

$$F1\{(t), A\} = \frac{1}{16} \sum_{p_k=0}^{15} F1(p_k) \tag{B10}$$

The third order waveforms will average out to zero because of (B9).

Finally the complex matched filter response is obtained as

$$g_{MF}^{(1)}\{(t), A\} = F1^*\{(-t), A\} \tag{B11}$$

In Chapter 5, we derived a sub-optimum receiver for the satellite channel model shown in Figure 5.1, which includes post-nonlinearity filtering. It is assumed that the impulse response of the downlink filter is available to us. The complex average waveforms for this channel can be obtained from (5.21) as

$$W^{(1)}\{(t), A\} = \frac{1}{16} \sum_{p_k=0}^{15} F1(p_k) * h_2(t) \tag{B12}$$

and subsequently the complex matched filter response of the sub-optimum receiver can be computed by using the following relation.

$$g_{MF}^{(1)}\{(t), A\} = W^{(1)*}\{(-t), A\} \tag{B13}$$

REFERENCES

[1] D.G. Gabbard and P. Kaul, "Time division multiple access", Eascon Rec., pp. 179-188, 1974.

[2] T. Muratani, "Satellite-switched time-domain multiple access", Eascon Rec., pp. 189-196, 1974.

[3] Puente, J.G. and Schmidt, W.G. and Werth, A.M., "Multiple-access techniques for commercial satellites", IEEE Proceedings, Vol. 59, No. 2, pp. 218-229, February 1971.

[4] Gould, R.G. and Lum, Y.F., Communications satellite systems: An overview of the technology, IEEE Press, 1975.

[5] Dalgleish, D.I. and Reed, A.G., "Some comparisons of the traffic-carrying capacity of communication satellites using digital techniques with the capacity of satellites using frequency modulation", Intelsat/IEE International Conf. on Digital Satellite Communications, pp. 226-240, Nov. 1969.

[6] Cook, W.L., "Interactive computer simulation of satellite transmission systems", in Proc. 5th Annu. Pittsburg Conf. Modeling, Simulation, Apr. 1974, pp. 867-872.

[7] Chakraborty, D. Noguchi, T., Campanella, S.J. and Wolejsza, C.J., "Digital modem design for nonlinear satellite channels", presented at the 4th Int. Conf. Digital Satellite Communication, Montreal, P.Q., Canada, Oct. 1978.

[8] Chakraborty, D. and Woljsza, C.J., "A survey of modem design and performance in digital satellite communications", IEEE Journal on selected areas in communications, Vol. SAC-1, No.1, pp. 5-20, January 1983.

[9] Spilker, J.J., Jr., Digital Communications by Satellite, Prentice-Hall, 1977.

[10] Nyquist, H., "Certain Topics in Telegraphy Transmission Theory", Trans. AIEE, Vol. 47, pp. 617-644, Feb. 1928.

[11] Chalk, H.H., The optimum pulse-shape for pulse communication", Proc. IEE, Vol. 97, Pt. III, pp. 88-92, March 1950.

[12] Tufts, D.W., "Nyquist's Problem - The Joint Optimization of Transmitter and Receiver in Pulse Amplitude Modulation", Proc. IEEE, Vol. 53, pp. 248-259, March 1965.

[13] Smith, J.W., "The Joint Optimization of Transmitted signal and Receiving Filter for Data Transmission Systems", BSTJ, Vol. 44, pp. 2363-2392, Dec. 1965.

[14] Lucky, R.W., Saltz, J. and Weldon, E.J., "Principles of Data Communications", McGraw-Hill Book Company, New York, 1968.

[15] Berger, T. and Tufts, D.W., "Optimum Pulse Amplitude Modulation. Part I: Transmitter-Receiver Design and Bounds from Information Theory", IEEE Trans. on Information Theory, Vol. IT-12, pp. 196-208, April 1962.

[16] Aaron, M.K. and Tufts, D.W., "Intersymbol Interference and Error Probability", IEEE Trans. of Information Theory, Vol. IT-12, pp. 26-34, Jan. 1965.

[17] Austin, M.E., "Decision feedback equalization for digital communication over dispersive channels", MIT/R.L.E. Tech. Rep. 461, Aug. 1967.

[18] George, D.A., "Match filters for interfering signals", IEEE Trans. Inform. Theory, Vol. IT-11, Jan. 1965.

[19] Taylor, D.P., "The estimate feedback equalizer: A sub-optimum nonlinear receiver", IEEE Trans. Commun., Vol. COM-21, pp. 979-990, Sept. 1973.

[20] Ekanayake, N. and Taylor, D.P., "A Decision Feedback Receiver Structure for Bandlimited Non-linear Channels, IEEE Trans. Commun., Vol. COM-29, No. 5, pp. 539-548, May 1981.

[21] Viterbi, A.J., "Error Bounds for Convolutional Codes and an Asymptotically Optimum Decoding Algorithm", IEEE Trans. Information Theory, IT-13, pp. 260-269, April 1967.

[22] Forney, G.D., "Maximum-Likelihood Sequence Estimation of Digital Sequences in the Presence of Intersymbol Interference", IEEE Trans. Information Theory, IT-18, pp. 363-378, May 1972.

[23] Kobayashi, H., "Applications of Probabilistic Decoding to Digital Magnetic Recording Systems", IBM J. Res. Develop., Vol. 15, pp. 64-74, Jan. 1971.

[24] Kobayashi, H., "Correlative Level Coding and Maximum Likelihood Decoding", IEEE Trans. on Information Theory, Vol. IT-17, Sept. 1971, pp. 586-594.

[25] Omura, J.K., "Optimal Receiver Design for Convolutional Codes and Channels with Memory via Control Theoretical Concepts", Information Sciences, Vol. 3, pp. 243-266, July 1971.

[26] Magee, F.R., Jr., and Proakis, J.G., "Adaptive Maximum-Likelihood Sequence Estimation for Digital Signallin in the Presence of Intersymbol Interference", IEEE Trans. on Information Theory, Vol. IT-19, Jan. 1973, pp. 120- 124.

[27] Falconer, D.D. and Magee, F.R., Jr., "Adaptive Channel Memory Truncation for Maximum-Likelihood Sequence Estimation", BSTJ, Vol. 9, Nov. 1973, pp. 1541-1562.

[28] Qureshi, S.V.H. and Newhall, E.E., "An Adaptive Receiver for Data Transmission over Time Dispersive Channels", IEEE Trans. on Information Theory, Vol. IT-19, No. 4, July 1973, pp. 448-457.

[29] Lawless, W.J. and Schwartz, M., "Binary Signalling over Channels Containing Quadratic Non-linearities", IEEE Trans. Comm., Vol. COM-22, pp. 288-299, March 1974.

[30] Mesiya, M.F., Mclane, P.J. and Campbell, L.L., "Maximum Likelihood Sequence Estimation of Binary Sequences Transmitted over Bandlimited Channels", IEEE Trans. Comm., Vol. COM-25, pp. 633-643, July 1977.

[31] Divsalar, D. and Omura, J.K., "Performance of Mismatched Viterbi Receiver on Satellite Channels", ICC'78, Boston, MA, June 1978.

[32] Furuya, Y., Akashi, F. and Mirakami, S., "A Practical Approach Toward Maximum Likelihood Sequence Estimation for Band-limited Non-linear Channels", Fifth Conference on Satellite Communications, Genoa, Italy, March 23-26, 1981.

[33] Chakraborthy, D. and Kappes, J.M., "Experimental evaluation of adaptive threshold detection with estimated sequence processor performance", Comsat Technical Review, Vol. 12, No. 2, Fall 1982.

[34] Fuenzalida, J.C., Shimbo, O. and Cook, W.L., "Time-domain Analysis of Intermodulation Effects Caused by Nonlinear Amplifiers", COMSAT Tech. Review, Vol. 3, pp. 89-143, Spring 1973.

[35] Forney, G.D., "The Viterbi Algorithm", Proc. IEEE, Vol. 61, pp. 268-278, March 1973.

[36] Helstrom, C.W., Statistical Theory of Signal Detection, Second Edition, New York: Pergamon Press, 1968.

[37] Ungerboeck, G., "Adaptive Maximum Likelihood Receiver for Carrier Modulated Data Transmission Systems", IEEE Trans, on Comm., Vol. COM-22, pp. 624-636, May 1974.

[38] Foschini, G.J., "Performance Bound for Maximum Likelihood Reception of Digital Data", IEEE Trans. on Information Theory, Vol. IT-21, pp. 47-50, Jan. 1975.

[39] Shimbo, O., Fang, R.J. and Celebiler, M., "Performance of M-any PSK systems in Gaussian noise and Intersymbol Interference", IEEE Trans. on Inform. Theory, Vol. IT-19, No. 1, January 1973.

[40] Churchill, R.V., Fourier Series and Boundary Value Problems, Second Edition, New York: McGraw-Hill, 1969.

[41] Ekanayake, N., Digital Transmission through Satellite Channels: Performance Analysis and Receiver Sythesis, Ph.D. Thesis, McMaster University, September 1979.

[42] Papoulis, A., Systems and transforms with applications in optics, McGraw-Hill, 1968.

[43] Osborne, W.P. and Luntz, M.B., "Coherent and Non-Coherent Detection of CPFSK", IEEE Trans. on Comm., Vol. COM-22, pp. 1023-1036, Aug. 1984.

[44] Svensson, A. and Sundberg, C.E., "Performance of generalized AMF receivers for Continuous phase modulation", IEE Proceedings-F, Communications, Radar and Signal Processing, Vol. 132, Part F, No. 7, pp. 541-547, Dec. 1985.

[45] Benedetto, S., Biglieri, E. and Daffara, R., "Modelling and Performance Evaluation of Non-linear Satellite Links - A Volterra Series Approach", IEEE Trans. on AES, Vol. AES-15, No. 4, pp. 494-507, July 1979.

[46] Benedetto, S., Biglieri, E., "Nonlinear Equalization of Digital Satellite Channels", IEEE Journal on Selected Areas in Communications, Vol. SAC-1, No. 1, pp. 57-62, January 1983.

[47] Kaye, A.R., George, D.A. and Eric, M.J., "Analysis and Compensation of Bandpass Nonlinearities for Communications", IEEE Trans. on Comm., Vol. COM-20, pp. 365-372, Oct. 1972.

[48] Dubey, V.K. and Taylor, D.P., "Maximum Likelihood Sequence Detection for QPSK on Nonlinear, Bandlimited Channels", accepted for publication in IEEE Trans. Comm.

[49] Dubey, V.K. and Taylor, D.P., "Further Results on Receivers for the Nonlinear Channel including Pre- and Post-Nonlinearity Filtering", Submitted to IEEE Trans. Comm.